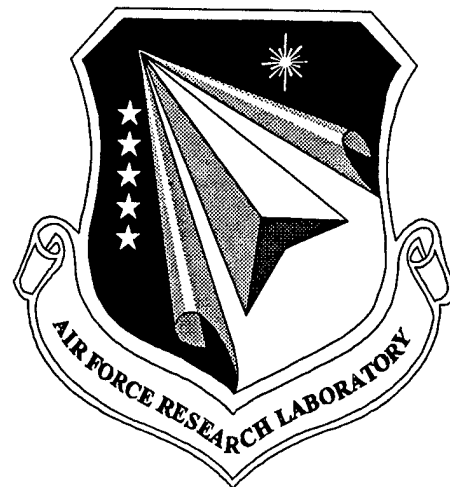


**AFRL-PR-WP-TR-1999-2038**

**ADVANCED AIRBREATHING  
HYDROCARBON-FUELED  
AERO-ENGINE CONCEPTS**



**G.D. STREBY  
T. MATHUR  
T.H. CHEN  
W. EAKINS**

**TAITECH, INC.  
3675 HARMELING DRIVE  
BEAVERCREEK, OHIO 45440**

**JULY 1999**

**FINAL REPORT FOR MAY 1996 – JUL 1998**

**APPROVED FOR PUBLIC RELEASE; DISTRIBUTION UNLIMITED**

**PROPULSION DIRECTORATE  
AIR FORCE RESEARCH LABORATORY  
AIR FORCE MATERIEL COMMAND  
WRIGHT-PATTERSON AIR FORCE BASE OH 45433-7251**

**DTIC QUALITY INSPECTED 4**

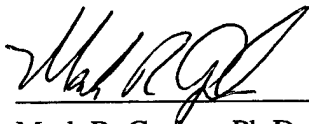
**20000201 036**

## NOTICE

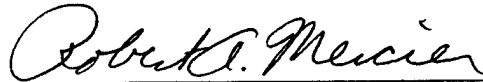
WHEN GOVERNMENT DRAWINGS, SPECIFICATIONS, OR OTHER DATA ARE USED FOR ANY PURPOSE OTHER THAN IN CONNECTION WITH A DEFINITE GOVERNMENT-RELATED PROCUREMENT, THE UNITED STATES GOVERNMENT INCURS NO RESPONSIBILITY OR ANY OBLIGATION WHATSOEVER. THE FACT THAT THE GOVERNMENT FORMULATED OR IN ANY WAY SUPPLIED THE SAID DRAWINGS, SPECIFICATIONS, OR OTHER DATA, IS NOT TO BE REGARDED BY IMPLICATION, OR OTHERWISE IN ANY MANNER CONSTRUED, AS LICENSING THE HOLDER, OR ANY OTHER PERSON OR CORPORATION; OR CONVEYING ANY RIGHTS OR PERMISSION TO MANUFACTURE, USE, OR SELL ANY PATENTED INVENTION THAT MAY IN ANY WAY BE RELATED THERETO.

THIS REPORT IS RELEASABLE TO THE NATIONAL TECHNICAL INFORMATION SERVICE (NTIS). AT NTIS, IT WILL BE AVAILABLE TO THE GENERAL PUBLIC, INCLUDING FOREIGN NATIONS.

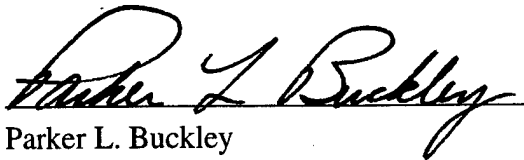
THIS TECHNICAL REPORT HAS BEEN REVIEWED AND IS APPROVED FOR PUBLICATION.



Mark R. Gruber, Ph.D.  
Aerospace Engineer  
High Speed Systems Development Branch



Robert A. Mercier  
Chief  
High Speed Systems Development Branch



Parker L. Buckley  
Deputy  
Propulsion Sciences and Advanced Concepts Division

IF YOUR ADDRESS HAS CHANGED, IF YOU WISH TO BE REMOVED FROM OUR MAILING LIST, OR IF THE ADDRESSEE IS NO LONGER EMPLOYED BY YOUR ORGANIZATION PLEASE NOTIFY AFRL/PRSS WRIGHT-PATTERSON AFB OH 45433 TO HELP MAINTAIN A CURRENT MAILING LIST.

Copies of this report should no be returned unless return is required by security considerations, contractual obligations, or notice on a specific document.

REPORT DOCUMENTATION PAGE			Form Approved OMB No. 0704-0188	
Public reporting burden for this collection of information is estimated to average 1 hour per response, including the time for reviewing instructions, searching existing data sources, gathering and maintaining the data needed, and completing and reviewing the collection of information. Send comments regarding this burden estimate or any other aspect of this collection of information, including suggestions for reducing this burden, to Washington Headquarters Services, Directorate for Information Operations and Reports, 1215 Jefferson Davis Highway, Suite 1204, Arlington, VA 22202-4302, and to the Office of Management and Budget, Paperwork Reduction Project (0704-0188), Washington, DC 20503.				
1. AGENCY USE ONLY (Leave blank)		2. REPORT DATE JULY 1999		3. REPORT TYPE AND DATES COVERED FINAL REPORT FOR MAY 1996 - JUL 1998
4. TITLE AND SUBTITLE ADVANCED AIRBREATHING HYDROCARBON-FUELED AERO-ENGINE CONCEPTS			5. FUNDING NUMBERS C F33615-96-C-2670 PE 62269 PR 1025 TA 05 WU 04	
6. AUTHOR(S)  G.D. STREBY, T. MATHUR, T.H. CHEN, AND W. EAKINS				
7. PERFORMING ORGANIZATION NAME(S) AND ADDRESS(ES) TAITECH, INC. 3675 HARMELING DRIVE BEAVERCREEK, OHIO 45440			8. PERFORMING ORGANIZATION REPORT NUMBER	
9. SPONSORING/MONITORING AGENCY NAME(S) AND ADDRESS(ES) PROPULSION DIRECTORATE AIR FORCE RESEARCH LABORATORY AIR FORCE MATERIEL COMMAND WRIGHT-PATTERSON AFB, OH 45433-7750 POC: JEFF DONBAR, AFRL/PRSS, 937-255-2175			10. SPONSORING/MONITORING AGENCY REPORT NUMBER  AFRL-PR-WP-TR-1999-2038	
11. SUPPLEMENTARY NOTES				
12a. DISTRIBUTION AVAILABILITY STATEMENT  APPROVED FOR PUBLIC RELEASE; DISTRIBUTION UNLIMITED.			12b. DISTRIBUTION CODE	
13. ABSTRACT (Maximum 200 words) An advanced long-duration, high-enthalpy direct-connect water-cooled supersonic combustion research facility has been designed and manufactured; initial calibrations have been performed. This facility provides the AFRL/PRS division with in-house capability to conduct long-duration scramjet combustor research and development. Simulations of flight Mach numbers to 7+ at flight dynamic pressures to 2000 psf are achievable using four separate facility nozzles (M = 1.8, 2.2, 2.6, and 3.0). These efforts are directed at developing advanced propulsion systems for future Air Force high-speed flight vehicles. In less than twenty-four months, concepts and ideas for a scramjet test facility were analyzed and developed, and components were designed, fabricated, and installed to build an operational scramjet test facility. Components were assembled in Test Cell 22 at AFRL Bldg. 18E. The majority of the components (vitiator, inlet transition, facility nozzle, isolator sections, and fixed and traversing probes) are water-cooled. The combustor test section provides a wide parametric space for evaluating fuel injection and flameholding concepts. The AFRL/PRSS Scramjet Test Facility is fully operational and a series of preliminary calibration tests have been completed to fully document the flow characteristics at the combustor inlet for a wide range of flight Mach numbers and dynamic pressures. Data from these tests are presented herein.				
14. SUBJECT TERMS Combustor, Scramjet, Hypersonics			15. NUMBER OF PAGES 88	
			16. PRICE CODE	
17. SECURITY CLASSIFICATION OF REPORT  UNCLASSIFIED	18. SECURITY CLASSIFICATION OF THIS PAGE  UNCLASSIFIED	19. SECURITY CLASSIFICATION OF ABSTRACT  UNCLASSIFIED	20. LIMITATION OF ABSTRACT  SAR	

## Table of Contents

List of Figures .....	iv
List of Tables .....	x
1. Introduction .....	1
2. Analysis and Design Effort .....	5
3. Testing and Simulation Capabilities.....	7
4. Flow Channel Design.....	9
4.1 Kaiser-Marquart SUE® Burner/Vitiator .....	11
4.2 Instrumentation Section.....	12
4.3 Traversing Probes.....	13
4.4 Inlet Transition Flange.....	15
4.5 Supersonic Nozzle Section.....	15
4.6 Isolator Sections.....	18
4.7 Calibration Section.....	19
4.8 Heat Sink Variable Geometry Combustor Section.....	19
4.9 Combustor to Calorimeter Transition Section.....	21
4.10 Calorimeter Section.....	21
4.11 Facility Exhaust Elbow.....	23
5. Fabrication Effort.....	24
6. Instrumentation.....	26
7. Preliminary Calibration Experiments.....	28
7.1 Nozzle/Isolator.....	31
7.2 Combustor.....	33
8. Related Follow-On Contract Work.....	36
9. Expert Consultant Services.....	38
10. Future Plans.....	39
References.....	40
Appendix A .....	41

## List of Figures

<u>Figure</u>	<u>Page</u>
1. Test Cell 22 Scramjet Facility Schematic	42
2. Scramjet Test Rig Facility Map	43
3. Kaiser-Marquardt SUE® Burner/Vitiation Schematic Diagram	44
4. Kaiser-Marquardt SUE® Burner/Vitiation Mounted on Test Cell 22 Thrust Stand	45
5. Schematic Diagram of Instrumentation Section	46
6. Photograph of Instrumentation Section Showing Traversing Probe Port and Plug	47
7. Instrumentation Section Inner Oxygen-Free Copper Liner with Milled Passages	47
8. Schematic Diagram of Water Cooled Traversing Probe And Housing	48
9. Photograph of Traversing Probe Internal and External Components	49
10. Photograph of Traversing Probes Showing Instrumentation Tips	49
11. Traversing Probe Housing Assembly	50
12. Traversing Probe Assembly Mounted on Calibration Section	51
13. Schematic Diagram of Inlet Transition Flange	52
14. Photograph of Inlet Transition Flange Oxygen-Free Copper Machined Insert	53
15. Photograph of Assembled Inlet Transition Flange	53
16. Inlet Transition Flange Assembly Showing Water Cooling Lines and Manifolds	54
17. Schematic Diagram of Nozzle Section Showing Flow Channel Dimensions	55

## List of Figures (continued)

<u>Figure</u>	<u>Page</u>
18. Mach 1.8 Nozzle Section Beryllium Copper Top Wall Showing Machined and Drilled Coolant Passages	56
19. Mach 1.8 Nozzle Section Beryllium Copper Top Wall Showing Coolant Passages and Side Plate	56
20. Nozzle Section Side Wall	57
21. Mach 1.8 Nozzle Section Showing Top and Bottom Wall Contours	57
22. Nozzle Section Showing Side Wall Instrumentation Ports	58
23. Mach 1.8 Nozzle Section Showing Water Cooling Lines and Manifolds	58
24. Mach 1.8 and 2.2 Nozzle Contours	59
25. Mach 2.6 and 3.0 Nozzle Contours	60
26. Schematic Diagram of Isolator Sections	61
27. Photograph of Isolator Section Side Wall Oxygen-Free Copper Inner Wall Plate	62
28. Photograph of Finished Isolator Section Side Walls	62
29. Assembled Isolator Section Showing Pressure Instrumentation Ports	63
30. Isolator Section with Water Cooling Lines and Manifolds	63
31. Photograph of Mach 1.8 Nozzle Section and Two Isolator Sections Mounted On Test Cell 22 Thrust Stand	64
32. Facility Calibration Section Showing Traversing Probe Mounting Bosses	64

## List of Figures (continued)

<u>Figure</u>	<u>Page</u>
33. Schematic Diagram of Scramjet Test Rig Heat-Sink Combustor Section	65
34. Photograph of Scramjet Heat-Sink Combustor Section (Flow from Right to Left) Showing the Three Side Wall Sections and Instrumentation Ports	66
35. Fuel Injection/Flame-Holder Insert	66
36. Fuel Injection/Flame-Holder Insert Mounted In Bottom Wall of Heat-Sink Combustor Forward Section (Side Wall Insert Removed)	67
37. Heat-Sink Combustor Side Wall Frames and Inserts	67
38. Heat-Sink Combustor/Calorimeter Transition Section	68
39. Facility Calorimeter Section Mounted on Exhaust Elbow	68
40. Calorimeter Thermocouple Array	69
41. Calorimeter Aero-Grid	70
42. PSI Pressure Measurement Terminal Box	71
43. Thermocouple Reference Junction Boxes	71
44. Nozzle-Isolator Pressure Distribution at $M_0=4$ , $Q_0=1000$ psf ( $p_e/p_i=0.88$ )	72
45. Isolator Exit Pitot Pressure Distribution at $M_0=4$ , $Q_0=1000$ psf ( $p_e/p_i=0.88$ )	72
46. Nozzle-Isolator Pressure Distribution at $M_0=4$ , $Q_0=1000$ psf ( $p_e/p_i=2.74$ )	72
47. Isolator Exit Pitot Pressure Distribution at $M_0=4$ , $Q_0=1000$ psf ( $p_e/p_i=2.74$ )	72
48. Nozzle-Isolator Pressure Distribution at $M_0=4$ , $Q_0=1000$ psf ( $p_e/p_i=3.46$ )	72
49. Isolator Exit Pitot Pressure Distribution at $M_0=4$ , $Q_0=1000$ psf ( $p_e/p_i=3.46$ )	72

# List of Figures (continued)

<u>Figure</u>	<u>Page</u>
50. Nozzle-Isolator Pressure Distribution at $M_0=4$ , $Q_0= 2000$ psf ( $p_e/p_i=0.86$ )	73
51. Isolator Exit Pitot Pressure Distribution at $M_0=4$ , $Q_0=2000$ psf ( $p_e/p_i=0.86$ )	73
52. Nozzle-Isolator Pressure Distribution at $M_0=4$ , $Q_0= 2000$ psf ( $p_e/p_i=2.72$ )	73
53. Isolator Exit Pitot Pressure Distribution at $M_0=4$ , $Q_0=2000$ psf ( $p_e/p_i=2.72$ )	73
54. Nozzle-Isolator Pressure Distribution at $M_0=4$ , $Q_0= 2000$ psf ( $p_e/p_i=3.40$ )	73
55. Isolator Exit Pitot Pressure Distribution at $M_0=4$ , $Q_0=2000$ psf ( $p_e/p_i=3.40$ )	73
56. Nozzle-Isolator Pressure Distribution at $M_0=5$ , $Q_0= 1000$ psf ( $p_e/p_i=0.87$ )	74
57. Isolator Exit Pitot Pressure Distribution at $M_0=5$ , $Q_0= 1000$ psf ( $p_e/p_i=0.87$ )	74
58. Nozzle-Isolator Pressure Distribution at $M_0=5$ , $Q_0= 1000$ psf ( $p_e/p_i=2.68$ )	74
59. Isolator Exit Pitot Pressure Distribution at $M_0=5$ , $Q_0= 1000$ psf ( $p_e/p_i=2.68$ )	74
60. Nozzle-Isolator Pressure Distribution at $M_0=5$ , $Q_0= 1000$ psf ( $p_e/p_i=3.39$ )	74
61. Isolator Exit Pitot Pressure Distribution at $M_0=5$ , $Q_0= 1000$ psf ( $p_e/p_i=3.39$ )	74
62. Nozzle-Isolator Pressure Distribution at $M_0=5$ , $Q_0= 2000$ psf ( $p_e/p_i=0.87$ )	75
63. Isolator Exit Pitot Pressure Distribution at $M_0=5$ , $Q_0= 2000$ psf ( $p_e/p_i=0.87$ )	75



# List of Figures (continued)

<u>Figure</u>	<u>Page</u>
64. Nozzle-Isolator Pressure Distribution at $M_0=5$ , $Q_0= 2000$ psf ( $p_e/p_i=2.80$ )	75
65. Isolator Exit Pitot Pressure Distribution at $M_0=5$ , $Q_0= 2000$ psf ( $p_e/p_i=2.80$ )	75
66. Nozzle-Isolator Pressure Distribution at $M_0=5$ , $Q_0= 2000$ psf ( $p_e/p_i=3.22$ )	75
67. Isolator Exit Pitot Pressure Distribution at $M_0=5$ , $Q_0= 2000$ psf ( $p_e/p_i=3.22$ )	75
68. Nozzle-Isolator Pressure Distribution at $M_0=6$ , $Q_0= 1000$ psf ( $p_e/p_i=0.88$ )	76
69. Isolator Exit Pitot Pressure Distribution at $M_0=6$ , $Q_0= 1000$ psf ( $p_e/p_i=0.88$ )	76
70. Nozzle-Isolator Pressure Distribution at $M_0=6$ , $Q_0= 1000$ psf ( $p_e/p_i=2.55$ )	76
71. Isolator Exit Pitot Pressure Distribution at $M_0=6$ , $Q_0= 1000$ psf ( $p_e/p_i=2.55$ )	76
72. Nozzle-Isolator Pressure Distribution at $M_0=6$ , $Q_0= 1000$ psf ( $p_e/p_i=3.24$ )	76
73. Isolator Exit Pitot Pressure Distribution at $M_0=6$ , $Q_0= 1000$ psf ( $p_e/p_i=3.24$ )	76
74. Nozzle-Isolator Pressure Distribution at $M_0=6$ , $Q_0= 2000$ psf ( $p_e/p_i=0.87$ )	77
75. Isolator Exit Pitot Pressure Distribution at $M_0=6$ , $Q_0= 2000$ psf ( $p_e/p_i=0.87$ )	77
76. Nozzle-Isolator Pressure Distribution at $M_0=6$ , $Q_0= 2000$ psf ( $p_e/p_i=2.48$ )	77
77. Isolator Exit Pitot Pressure Distribution at $M_0=6$ , $Q_0= 2000$ psf ( $p_e/p_i=2.48$ )	77
78. Nozzle-Isolator Pressure Distribution at $M_0=6$ , $Q_0= 2000$ psf ( $p_e/p_i=3.40$ )	77

# List of Figures (continued)

<u>Figure</u>	<u>Page</u>
79. Isolator Exit Pitot Pressure Distribution at $M_0=6$ , $Q_0= 2000$ psf ( $p_e/p_i=3.40$ )	77
80. Baseline Combustor-Pressure Distribution at $p_0=112$ psia, $T_0=540^\circ\text{R}$	78
81. Baseline Combustor-Shadowgraph at $p_0=112$ psia, $T_0=540^\circ\text{R}$	78
82. Baseline Combustor with Cavity-Pressure Distribution at $p_0=112$ psia, $T_0=540^\circ\text{R}$	78
83. Baseline Combustor with Cavity-Shadowgraph at $p_0=112$ psia, $T_0=540^\circ\text{R}$	78
84. Combustor with Cavity ( $\text{N}_2$ Injection, $p_{\text{jet}}= 87\text{psia}$ ) Pressure Distribution at $p_0=112$ psia, $T_0=540^\circ\text{R}$	78
85. Combustor with Cavity ( $\text{N}_2$ Injection, $p_{\text{jet}}= 87\text{psia}$ ) -Shadowgraph at $p_0=112$ psia, $T_0=540^\circ\text{R}$	78

## List of Tables

<u>Tables</u>	<u>Page</u>
1. Simulation Conditions	8
2. Scramjet Simulation - Using M=1.8 Facility Nozzle	29
3. Scramjet Simulation - Using M=1.8 Facility Nozzle	29
4. Scramjet Simulation - Using M=2.2 Facility Nozzle	30
5. Scramjet Simulation - Using M=2.2 Facility Nozzle	30

## 1.0 Introduction

This report presents activities that were performed under Air Force contract F33615-96-C-2670, "Advanced Air-breathing Hydrocarbon-Fueled Aero-Engine Concepts," during the period 30 May 1996 to 31 July 1998. Taitech, Inc. provided scientific, engineering and technical support services to the Air Force Research Laboratory Propulsion Directorate, High Speed Development Branch (AFRL/PRSS).

Taitech, Inc. personnel contributing to this effort included; Research Team: Dr. T. Chen, Dr. T. Mathur, and Mr. G.D. Streby, P.E. (Project Engineer); Design Staff: Mr. W. Eakins, Mr. G. Haines, and Mr. P. Saunders; Technical Support Staff: Messrs. M. Cox and W. Haendiges, and the Taitech, Inc. administrative staff. In addition, Taitech, Inc. would like to acknowledge the technical support provided by Mr. C. Smith of ISSI and Mr. J. Bryant of AFRL/PRSS in many technical efforts that were required during this project.

Work efforts reported herein were completed at the Scramjet Test Facility in Test Cell 22, Building 18E, Area B, Wright Patterson AFB, Ohio. This project was undertaken to develop a modern, well characterized and documented direct-connect scramjet test facility in Test Cell 22. This facility will allow the Air Force the opportunity to develop and study unique concepts in supersonic combustion ignition, fuel injection, and flameholding. Further, there is a strong need for the Air Force to develop in-house facilities, expertise, and qualified personnel in the areas of high-speed propulsion systems testing and analysis. This will give in-house government scientists the ability to intelligently purchase contracted work and will also enable them to develop technological breakthroughs at a local level.

This contract provided scientific, engineering, design, and specialized consulting services and technical support to Test Cell 22 and other advanced propulsion facilities of the

Air Force Research Laboratory, Propulsion Sciences and Advanced Concepts Division. These other facilities include the Thrust Stand Facility in Test Cell 18 and the Cold Flow Facility in Test Cell 19.

The objective of this contract was to provide the engineering, design and development support necessary to develop advanced aerodynamic scramjet propulsion test capabilities for the Air Force Research Laboratory, Propulsion Directorate, High Speed Development Branch (AFRL/PRSS) Test Cell 22 facility. Improvements made to Test Cell 22 provide the Air Force with the capability to conduct long-duration (steady-state), continuous-flow, direct-connect supersonic combustion research and development at simulated supersonic and hypersonic flight conditions up to Mach 7+. These capabilities are necessary to conduct advanced research and development of future scramjet propulsion system configurations and components. Scramjet technology development will be advanced through studies of combustor configurations and investigations of special fuels and fuel injection and ignition techniques, and through the performance of parametric studies to determine the operational matrix required for reliable scramjet operation. Contract efforts included the engineering analysis of supersonic facility concepts and designs; the development of complete design drawing packages; the fabrication and installation of large and complex scramjet hardware components; and the complete operational checkout of all hardware, instrumentation, control, data acquisition and support systems to achieve a fully operational scramjet facility.

The goals of the current effort include support of the HyTech program (i.e., development of a Mach 4-8 hydrocarbon-fueled scramjet missile) and exploration of alternative piloting/fuel injection concepts. To meet these ends, the facility was designed and developed to perform long-duration, steady-state direct-connect combustor tests, with the eventual ability to simulate

a full flight vehicle trajectory in a single test run. Great care is being taken to accurately characterize and document all aspects of this facility. Modern measurement techniques and instrumentation are being incorporated for evaluation of scramjet performance parameters such as thrust-based, chemical-based, and calorimeter-based combustion efficiency.

The Test Cell 22 Scramjet Facility flow path is made up of a number of specially designed components, in addition to a modified Kaiser-Marquardt Sudden Expansion (SUE®) Burner/Vitiator. Attached to the exit of the SUE® Burner/Vitiator is an instrumentation section, an inlet transition flange, a supersonic nozzle section, isolator sections, a calibration section and a variable configuration non-cooled combustor section. A flow analysis and gas sampling transition section and steam calorimeter are downstream of the combustor section and are supported by the facility exhaust system elbow. A schematic drawing of the complete Test Cell 22 Scramjet Test Rig configuration is presented in Fig. 1, Appendix A.

The Test Cell 22 Scramjet Facility is being used to conduct experimental tests of new and advanced scramjet combustor configurations, fuels, and fuel injection techniques. The Scramjet Test Facility also has design features for conducting experiments using advanced laser and optical diagnostic methods for the study of supersonic flow mixing and combustion characteristics. Facility nozzle calibration and preliminary flow characteristic tests have been conducted. The results of those tests are presented in this report (see Section 7). In the course of the design, construction, and preliminary testing of the Scramjet Facility, a large body of documentation has been developed. A complete set of design drawings for the components are available, they are referenced below. Three volumes of photographs of the facility components, Advanced Airbreathing Hydrocarbon-Fueled Aero-Engine Concepts, Photographic Information, Volumes I-III, have been archived at Taitech, Inc. A selection of

photographs is presented in Appendix A. In addition, three technical papers have been prepared and published, and are referenced below (Refs. 4-6).

## 2.0 Analysis and Design Effort

The primary objective of this program was to provide a scramjet test facility capable of conducting long-duration (steady-state) operation. Long-duration operation is necessary for comprehensive studies of supersonic fuel injection, fuel mixing, and combustion phenomena related to scramjet technology. Achieving long-duration testing capabilities required the design of actively water-cooled hardware. Water-cooling is the most reasonable and cost effective design method for protecting components from the extreme thermal environments encountered in simulation of high-energy supersonic flows. However, incorporating the capability to water-cool facility components does greatly increase the cost and complexity of the design.

Water-cooling of Scramjet Test Facility components is accomplished by forcing a thin film of high velocity water to flow near the heated surfaces of the flow channel. The interior flow channel walls that are exposed to the high-energy flows are made from solid copper to improve the efficiency of the water-cooling. Oxygen-free hard copper is utilized in the instrumentation, inlet transition, and isolator sections of the Scramjet Test Facility. In the nozzle section the interior flow path walls are made of beryllium copper. Beryllium copper provides higher strength than oxygen-free copper at elevated temperatures. Increased material strength is necessary in the supersonic nozzle due to high thermal stresses and heat transfer loads encountered in the nozzle throat area.

The copper walls are fused to stainless steel weldments using a silver brazing process. The stainless steel weldments provide strength to support the loads imposed upon the interior flow path walls and to maintain the exterior structural integrity. The stainless steel also provides protection against possible corrosion by the water coolant. The choice of brazing



process for joining the copper walls to the stainless steel depends upon the type of copper to be fused.

The Scramjet Test Facility design incorporates both circular and rectangular water-cooling passages, selected according to the design requirements of individual sections. Water-cooling passages are designed to withstand both the internal water pressure and the external flow channel surface pressures produced by flow conditions. Small water-cooling passages were machined or drilled into the back side of the copper walls. The small size of the water-cooling passages (0.156 inch diameter holes or 0.10 inch wide by 0.1 inch deep grooves) increased the water flow velocity and therefore increased the heat transfer coefficient between the copper and the cooling water. The nominal wall thickness of the copper at the cooling passage is 0.1 inches and the centerline-to-centerline spacing of cooling passages is 0.25 inches. The lengths of the cooling passages are kept as short as possible to reduce the pressure drop losses of the water and to prevent excessive heating of the water coolant.

### 3.0 Testing and Simulation Capabilities

The Research Air Facility supplies Test Cell 22 and the Scramjet Facility with up to 30 lbm/sec of continuous airflow at 750 psia and a maximum temperature of 1660°R with 3.5 psia continuous exhaust. The facility and test hardware is mounted on a thrust stand capable of measuring 10,000 lbf thrust load with a 10,000 lbf maximum load limit. The test cell has liquid and gaseous fuel systems available, currently including pumped JP-4, MCH, ethylene, and hydrogen. Liquid and gaseous oxygen systems are also available to provide make-up oxygen and for use with igniters and torches. A re-circulating tower cooling water system provides 2500 gpm at 70 psia, and raw dump water at 350 psia is also available.

The JHU/APL Ramjet Performance Analysis (RJPA)<sup>1,2</sup> code inlet/diffuser model was used to relate the actual flight conditions of a hypersonic vehicle (and the corresponding combustor inlet conditions) to the test cell operational capabilities, in order to generate the facility map shown in Fig. 2. The facility map indicates the range of flight conditions (altitude, Mach number, and dynamic pressure) that can be simulated in the test cell based on the supply air pressure, temperature and mass flow. The facility map assumes that the facility nozzle is operated at its design point (i.e., that the Mach number exactly matches the desired combustor Mach number for the simulation).

The inlet/diffuser calculations from RJPA have also been extended to design the experiments conducted in Test Cell 22. The facility nozzle is the primary determinant of the supersonic combustor inlet conditions. Four facility nozzles with design Mach numbers of 1.8, 2.2, 2.6, and 3.0 are available to provide the range of combustor inlet conditions corresponding to flight Mach numbers between 4 and 8 at dynamic pressures between 500 and 2000 psf (see Table 1 ).

Table 1. Simulation Conditions

$M_0$	$Q_0$	$M_4$	$T_4$	$P_4$	$U_4$
4	500	1.962	959	4.75	2960
4	1000	1.962	941	9.62	2928
4	2000	1.962	935	18.39	2915
5	500	2.385	1154	4.84	3925
5	1000	2.385	1130	9.67	3889
5	2000	2.385	1108	19.57	3849
6	500	2.787	1339	4.83	4923
6	1000	2.787	1313	9.53	4877
6	2000	2.787	1286	19.35	4831
7	500	3.166	1536	4.74	5972
7	1000	3.166	1490	9.34	5882
7	2000	3.166	1459	18.7	5826

$M_0$  = Flight Mach Number

$Q_0$  = Flight Dynamic Pressure (psf)

$M_4$  = Mach Number at Combustor Inlet

$T_4$  = Static Temperature at Combustor Inlet ( $^{\circ}\text{R}$ )

$P_4$  = Static Pressure at Combustor Inlet (psia)

$U_4$  = Flow Velocity at Combustor Inlet (ft/s)

#### **4.0 Flow Channel Design**

The facility air supply can be heated and conditioned to 4000°R before it enters the scramjet nozzle using an extensively modified Kaiser-Marquardt SUE® Burner/Vitiator. The air flow is then accelerated to supersonic velocities.

The design of the internal supersonic flow path is very important to the overall operation of the Scramjet Combustor. The nozzle contour must be very accurate to produce an efficient and clean supersonic flow and must also compensate for boundary layer growth. The design must also minimize joints and sharp edges that can generate unwanted shocks and disturbances in the flow path. Therefore, internal surfaces must form a smooth and continuous flow path with only a minimum number of joints exposed to the flow. The flow path must also be designed to withstand internal pressure and thermal loads imposed by high energy supersonic flows.

The schematic in Fig. 1 shows the Scramjet Test Facility with flow from left to right. Supply air is fed to the modified Kaiser-Marquardt SUE® Burner/Vitiator, which is water-cooled and is capable of sustaining temperatures to 4000°R. It has an H<sub>2</sub>/air igniter and can be fueled with either liquid or gaseous fuels. The burner/vitiator is followed by a water-cooled instrumentation section that has two ports for temperature and/or total pressure measurements with two traversing probes, wall static pressure/gas sampling ports, and four thermocouple ports in each of the upstream and downstream flanges. A water-cooled transition flange compresses the vitiated air flow from axisymmetric (10 inch ID) to two-dimensional (2.25 x 7 inch) as it enters the facility nozzle.

The test rig has four available interchangeable water-cooled nozzles to expand the air to supersonic conditions at the exit, simulating desired combustor inlet flow conditions. The

nozzle section has 23 static pressure taps on its side wall for documenting the axial pressure profile from the nozzle inlet to the exit. Two removable isolator sections downstream of the nozzle (water cooled, each 12 inches long with a total of 120 static pressure taps distributed across the top and bottom walls) are used to contain the pre-combustion pressure rise.

Immediately following the isolator sections is a variable-geometry heat-sink combustor with a flexible upper wall, which permits combustor exit-to-inlet area ratios of up to four. The upper wall has four independent sections, currently set to provide an area ratio of approximately 2.5. The combustor also has removable inserts on all four walls, allowing optical access and installation of a wide variety of instrumentation. The replaceable inserts provide a wide parametric design space for testing of fuel injection and flameholding concepts.

A baseline fuel injector/flameholder is available for initial fuel injection and combustion experiments in the new combustor. This device has four low-angle (15 degrees) injectors across the span of the tunnel and upstream of a cavity-based flameholder (See Section 4.8). Each fuel injector has its own static pressure tap and the four injectors are fed from a common manifold. Changing the length-to-depth ratio, the distance downstream from the fuel injectors, and the aft ramp angle varies geometry of the cavity. The cavity may also be fueled through its bottom wall. Ports are available for ignition sources, pressure taps, thermocouples, and gas sampling measurements.

A calorimeter instrumentation section that houses water sprays, rakes, and probes connects the combustor to a calorimeter instrumented with thermocouples and heat-flux gages. The calorimeter exit connects to an exhaust elbow, through which the flow exits the test cell to an exhaust system.

The test hardware also includes a carbon steel uncooled calibration section that can be attached at the exit of the facility nozzle or at the exit of either isolator. This section has ports for traversing probes, allowing spanwise and transverse total temperature and Pitot pressure surveys at the nozzle and/or isolator exit planes.

The entire rig is secured to a thrust stand for direct measurements of the thrust produced. This measurement, combined with wall static pressure measurements and a performance analysis code, yields an estimation of the combustion efficiency. Additionally, the energy losses through the various water-cooled components, coupled with the temperature measurements from the steam calorimeter, allow calculation of combustion efficiency.<sup>3</sup> Thus, multiple independent measurements of this vital performance parameter may be obtained in the new facility.

At the beginning of this project, the only components in Test Cell 22 were the Kaiser-Marquardt SUE® Heater/Vitiator and the facility exhaust elbow. All of the additional Scramjet Test Facility components listed above were designed, fabricated, and installed under this contract effort to complete the baseline Test Cell 22 Scramjet Test Facility. Presented in the following paragraphs are detailed descriptions of the engineering, design, and fabrication of the various Scramjet Test Facility flow path components.

#### 4.1 Kaiser-Marquardt SUE® Burner/Vitiator

The Kaiser-Marquardt SUE® Burner/Vitiator model 360-5000 is mounted to an air supply manifold on the Test Cell 22 Thrust Stand. The air supply manifold provides flexible connections from the air supply system to the thrust stand. The modified Kaiser-Marquardt SUE® Burner/Vitiator provides heated inlet air to the scramjet combustor up to a maximum temperature of 4000°R at a maximum pressure rating of 350 psia. The vitiator is water-cooled

for long duration operation. Gaseous oxygen is introduced upstream of the heater to make up (restore) the oxygen content in the vitiated air stream. A schematic diagram of the Kaiser-Marquardt SUE® Burner/Vitiator is shown in Fig. 3. A photograph of the unit is shown in Fig. 4.

#### 4.2 Instrumentation Section

The first component after the Kaiser-Marquardt SUE® Heater/Vitiator in the Scramjet Test Facility flow path is an instrumentation section, where the flow conditions of the heated/vitiated air supply are measured before the air stream enters the supersonic nozzle. The instrumentation section is equipped to measure total pressures and temperatures and can be used to conduct gas sampling analysis of the gas flow. Total (stagnation) measurements in the section are made using water-cooled probes that can be used to survey two radial profiles located at ninety degrees to each other. The probes can traverse approximately 80% of the 10-inch inside diameter of the instrumentation section.

The instrumentation section is a heavy walled stainless steel pipe section with flanges mounted at each end. A schematic diagram is shown in Fig. 5 and a picture in Fig. 6. The instrumentation section is 18 inches long, with a nominal inside diameter of 10 inches. The end flanges are 10 inch, 600# class, 304 stainless steel slip-on flanges that are nickel brazed to the pipe section. The internal wall liner is made of oxygen-free copper. The copper liner is shrink-fitted into the pipe section and then silver brazed. The oxygen-free copper liner is shown in Fig. 7.

The instrumentation section end flanges and pipe section are water-cooled. Water-cooling supply and return manifolds are welded to the top and bottom of the pipe section. The water manifolds and machined cavities in the flanges direct cooling water from water supply

lines to water-cooling passages that go around the circumference of the inner copper liner. Cooling water is then collected in the return manifold and cavities and directed to the water return lines. The interior oxygen-free copper liner is specially designed with milled passages in its outer surface to cool the entire internal surface of the instrumentation section from flange face to flange face. The copper liner is brazed to the flanges and the outer shell to make a solid water-tight unit.

The two flanges of the instrumentation section have ports for making gas sampling, static pressure, and static temperature measurements. Two pressure ports are located 180 degrees apart and four ports for temperature measurement are positioned 90 degrees apart around the perimeter of each flange. Two additional ports that are open to the interior of the instrumentation section are located on each side of the instrumentation section at 45 degrees from the vertical centerline. These two ports permit the mounting of water-cooled traversing probes to measure total pressures and temperatures across radial lines in the instrumentation section. The instrumentation section is detailed in Air Force drawings: D029-PF96, D030-PF96, D031-PF96 and D033-PF96.

#### 4.3 Traversing Probes

The traversing probes are designed to measure and document total pressure and temperature of the incoming air supply. A schematic diagram of the traversing probe is shown in Fig. 8. The traversing probes are water-cooled and are driven in and out of the flow by electric actuators that are remotely programmed and controlled. The probes are 1.50 inches wide by 0.5 inches thick and can be introduced 8 inches into the flow stream. The interior body of the probes is made of 304 stainless steel and has machined cooling and instrumentation



passages. Traversing probe components are shown in Fig. 9. The outer shell of the probe is made of thin oxygen-free copper that is silver brazed to the stainless steel body.

There are seven ports spaced at 1-inch increments along the leading edge of the probe for pressure and/or temperature measurement. Stainless steel tubing from each of the ports is routed from the center of the probe body through the drive tube to external instrumentation interfaces. Tube extensions attach to each instrumentation port. These tube extensions are open for pressure measurement or closed for temperature measurement. They are made from dense Magnesia ceramic and are cemented into the probe housing with high temperature ceramic cement. The tube extensions project into the flow approximately 0.625 inches. Assembled probes are shown in Fig. 10.

The instrumentation probes are housed in high-pressure stainless steel housings mounted onto the outer surface of the instrumentation section. A probe housing assembly is shown in Fig. 11. The probe is driven in and out of the flow stream by electric drive actuators mounted on the housings. An integral drive tube from the end of the probe goes through the probe support housing and attaches to the actuator unit. Instrumentation lines from the probe tips are also routed through the drive tube to the exterior of the flow path. The electric actuator is housed in a sheet metal enclosure that can be purged with air or nitrogen to prevent accumulation of hydrogen or other flammable gases that may be used during testing. A complete traversing probe assembly is shown in Fig. 12.

The traversing probes are detailed in Air Force drawings F034-PF96, F035-PF96, F036-PF96 and D042-PF96.

#### 4.4 Inlet Transition Flange

At the downstream end of the instrumentation section is the inlet transition flange. The inlet transition flange is a modified 304 stainless steel, 10 inch, 600# class blind flange. The inlet transition flange transitions the flow from a circular flow path through the instrumentation section to the rectangular flow path of the supersonic nozzle. The center of the blind flange is machined out and has mounted in it a water-cooled, oxygen-free copper transition insert. A schematic diagram of the inlet transition flange is presented in Fig. 13. Transition of the flow path is accomplished through an elliptical contoured copper insert. The copper insert has EDM-cut cooling passages on all four back surfaces. The water-cooled copper transition piece is shown in Fig. 14. The insert is silver brazed into the modified blind flange. Cooling water supply and return lines are placed around the circumference of the flange. Cooling water enters and exits at the corners of the copper insert.

A photograph of the inlet transition flange assembly is shown in Fig. 15. A picture of the inlet transition flange assembly showing coolant lines is presented in Fig. 16. The inlet transition flange is detailed in Air Force drawing F027-PF96 (9 shts.).

#### 4.5 Supersonic Nozzle Section

The supersonic nozzle section is a water-cooled two-dimensional contoured half-height nozzle. The flow side-walls are made of beryllium copper for greater strength and are brazed to 0.5-inch thick 304 stainless steel weldments. The weldments are ribbed for strength and provide water supply and return connections. The weldments are also flanged at the ends to provide for attachment to other components of the Scramjet Test Facility flow path.

The supersonic nozzle section is made up of four wall sections that are bolted together to form the two-dimensional flow path. The side-walls are flat along the flow path length

while the top and bottom walls form the inlet and nozzle throat contours. The width of the flow path is 7 inches along its entire length. The inlet and exit heights of the supersonic nozzle section are both 2.25 inches. The length of the supersonic nozzle section is 17 inches.

The design of the supersonic nozzle section allows for the top wall to be removed and replaced for different Mach number flows. The top wall contour determines the throat of the half-height nozzle contour. The location of the nozzle throat varies along the length of the nozzle depending upon the Mach number selected. The bottom wall is contoured at the inlet to form the bottom half of the inlet to the nozzle throat. This permits the bottom wall to be used with all nozzle throat contours.

Water-cooling passages in the top and bottom walls are formed by gun drilling 0.156 inch diameter holes across the 7 inch width of the walls. Water is fed into these passages through passages in the stainless steel weldment and cavities machined into the top of the copper wall. The side-walls have milled grooves running vertically on the back sides of the copper side-walls and are also supplied with cooling water through passages in the stainless steel weldment. Figure 17 is a drawing of the supersonic nozzle section showing the flow channel dimensions. The Mach 1.8 supersonic nozzle section beryllium copper top wall is shown in Figs. 18 and 19. A nozzle side-wall section is shown in Fig. 20 and three sides of the Mach 1.8 nozzle assembly are shown in Fig. 21. Figure 22 shows the side-wall of the nozzle section with instrumentation ports. The completed Mach 1.8 nozzle section with water-cooling lines and manifolds is shown in Fig. 23. The Mach 1.8 supersonic nozzle section is detailed in Air Force drawing F028-PF96 (16 shts.).

#### 4.5.1 Nozzle Contours

The nozzle throat contours of the individual half-height nozzle top walls are modified supersonic contours generated using a method-of-characteristics (MOC) based computer program ,“NOZCS2,” developed at the Gas Dynamics laboratory at the University of Illinois at Urbana-Champaign.<sup>4</sup> This program generates the design of continuous slope supersonic nozzles. Contours were calculated for Mach numbers 1.8, 2.2, 2.6,3.0 and 4.0, for a  $\gamma = 1.3$ , which closely matches the flow properties of the vitiated air in Test Cell 22. The nozzle contours are for a half-height nozzle exit height of 2.25 inches.

The “NOZCS2” program was used to generate nozzle contours for each of the desired Mach numbers. Nozzle contours were then modified to compensate for the expected boundary layer growth through the nozzle. Boundary layer displacement thickness was calculated along the length of the nozzle for the range of expected flow conditions. These displacements were then used to generate new nozzle contours that compensated for the boundary layer growth and still had a nozzle exit height of 2.25 inches. The boundary layer growth was assumed to start at the nozzle throat.

The Mach 1.8 and 2.2 nozzle top wall contours are presented in Fig. 24 and the nozzle contours for Mach numbers 2.6 and 3.0 are shown in Fig. 25.

#### 4.5.2 Pressure Ports

The design of the supersonic nozzle section includes 24 pressure ports along the entire length of one side-wall for the measurement of wall static pressures. These pressure ports are approximately at the midpoint of the height of the nozzle contours. Pressure ports are

positioned at 1.0-inch increments from the inlet to the throat. From the throat to the exit, the spacing is 0.5 inches. The Mach 1.8 nozzle side-wall pressure ports are shown in Fig. 22.

Pressure ports are sharp edged 0.032 inch diameter holes drilled perpendicular to the nozzle wall surface that go through the copper and stainless steel wall to pressure fittings on the outside of the wall weldment. Pressure tubing (0.0625 inch OD by 0.0057-inch wall, 304 SS tubing) runs from pressure port fittings to instrumentation connections.

#### 4.6 Isolator Sections

The isolator sections of the Scramjet Facility are similar in design and construction to the nozzle section, except that all walls are flat surfaces. All interior surfaces are water-cooled oxygen free copper brazed to 304 stainless steel weldments. There are two isolator sections each 12.125 inches long. They are located between the nozzle section exit and the combustor entrance. The function of the isolator sections is to contain any shock-train that may be generated due to combustion heat release in the combustor. The side-walls and the top wall are parallel to the flow direction, but the bottom wall diverges at an angle of 0.75 degrees. This divergence compensates for the expected boundary layer growth through the isolator sections. A schematic diagram of the isolator sections is shown in Fig. 26.

The Scramjet Test Facility flow path is designed to operate with no isolators, or with one or two isolators. There are 60 static pressure ports in each isolator, 30 each in the top and bottom walls. Fig. 27 is a picture of an isolator section oxygen-free copper inner wall showing the milled cooling passages before brazing to the stainless steel weldment. Isolator section side-walls are shown in Fig. 28. Figure 29 shows a completely assembled isolator section. Figure 30 shows an isolator section with water manifolds and coolant lines. Shown in Fig. 31

is the Mach 1.8 nozzle and two isolator sections mounted onto the Test Cell 22 Thrust Stand. The isolator sections are completely detailed in Air Force drawing F032-PF96 (21 Sheets).

#### 4.7 Calibration Section

A calibration section is provided for the characterization and documentation of flow conditions exiting the nozzle and isolator sections of the scramjet test rig. The calibration section is fabricated from carbon steel and attaches to the exit of the facility nozzle or to the exit of either isolator section. The calibration section is designed to accommodate the water-cooled traversing probe assemblies for making pressure and temperature surveys or profiles of the supersonic flow conditions. Horizontal flow surveys can be made across the 7 inch width of the flow channel at two different vertical locations. Vertical flow surveys can also be made along the vertical centerline of the flow channel across the flow using a traversing probe or a water-cooled boundary-layer probe. The calibration section is shown in Fig. 32.

#### 4.8 Heat-Sink Variable Geometry Combustor Section

The scramjet combustor section is a non-cooled 304 stainless steel welded and bolted structure that provides an extended variable geometry flow path. The combustor section mounts either directly to the facility nozzle or to the facility in combination with one or both of the two isolator sections. The exhaust from the combustor section flows either directly or through a transition section into the calorimeter.

In the future, a water-cooled combustor will be installed to provide longer duration running times, but the fabrication time and cost did not fit into the program schedule for this contract. A preliminary design of a water-cooled combustor has been completed and is being evaluated. A heat-sink combustor was designed and fabricated to provide the capability to conduct fuel injection and mixing evaluation studies in the interim. The heat-sink combustor

also provides additional information regarding heating loads that will aid in the final design and fabrication of a completely water-cooled combustor. A water-cooled combustor will be designed, fabricated, and installed during the follow-on phase of the program. A drawing of the heat-sink combustor is presented in Fig. 33. A picture of the heat-sink combustor showing the instrumentation side-wall inserts is shown in Fig. 34.

The top wall of the heat-sink combustor section is made of five hinged sections that can be pivoted about each top wall section joint. Each section of the top wall has  $\pm 5.0$  degrees of movement in the vertical direction. This permits the upper wall to be positioned at any angle from a horizontal flat surface to approximately 20 degrees in the vertical direction. Each movable section of the top wall has a removable instrumentation insert. These wall inserts are flush with the interior wall surface and have an array of static pressure ports for flow analysis. Each wall insert may be replaced with test hardware or models, fuel-injection modules, or optical windows, depending upon testing requirements.

The bottom wall of the combustor section is made up of three stainless steel straight segments that are bolted together. The bottom wall assembly can translate in the vertical direction a total of 1.0 inch. This allows the bottom wall to be matched to the bottom walls at the exit of the facility nozzle with no isolators or with one or both isolators installed. Each bottom wall segment has a removable wall insert. Each wall insert has an array of instrumentation ports for static pressure and/or temperature measurements. Inserts may be replaced with test hardware or models, fuel injectors, or optical windows, depending upon testing requirements. A fuel injection flame-holder insert configuration is shown in Fig. 35. Figure 36 shows the fuel injection flame-holder insert installed in the forward bottom wall section with the side-wall insert removed.

The side-walls of the heat-sink combustor section are made up of three wall segments. Each wall segment has an array of static pressure ports for measuring the axial static pressure distribution. Each side-wall segment insert can be removed and replaced with optical windows or special test hardware. Side-wall inserts and frames are shown in Fig. 37.

#### 4.9 Combustor to Calorimeter Transition Section

The calorimeter transition section directs the supersonic flow from the combustor section into the calorimeter section. It provides mounting for four water-cooled pressure, temperature, and gas sampling probe rakes, and eight water spray nozzles for quenching the exhaust flow before it enters the calorimeter section. The probe rakes measure and take gas samples from the exhaust flow to determine flow parameters and conduct analysis of the combustion products exiting the heat-sink combustor section. The combustor/calorimeter transition section is shown in Fig. 38.

Downstream of the rakes are eight water spray nozzles for quenching the high temperature gas flow. The high temperature gas flow must be quenched to generate a uniform flow of high temperature steam. The temperature and mass flow of the steam can then be used to calculate the energy of the flow stream. From this information, the efficiency of the combustion process can be determined.

#### 4.10 Calorimeter Section

The Scramjet Test Facility calorimeter section is used to make heat balance measurements for determining the combustion efficiency of various combustor configurations. Through an arrangement between the Air Force and the Applied Physics Laboratory at The Johns Hopkins University, the Applied Physics Laboratory designed, fabricated, and delivered



the Scramjet Test Facility calorimeter section to Test Cell 22. The calorimeter section shown in Fig. 39 is mounted onto the calorimeter mounting plate and the facility exhaust elbow.

The calorimeter section is a 304L stainless steel, 76 inch long, 24 inch diameter schedule 40 pipe section with raised faced flanges welded to each end. It is instrumented with thermocouples and heat flux gages. At the downstream end of the pipe section there is a thermocouple ring with 20 thermocouples arranged around the circumference of the pipe. Figure 40 shows the arrangement of the thermocouple array. Thermocouples are set to varying depths in a special pattern to obtain an area-weighted temperature distribution of the internal flow profile. There are 10 heat flux gages mounted on top of the calorimeter along its length.

The calorimeter section is mounted to a plate that is directly attached to the Test Cell 22 facility exhaust elbow. The upstream end of the calorimeter section is secured to the mounting plate by three tie rods running from the upstream calorimeter flange to flange bolts on the mounting plate. The calorimeter mounting plate is a carbon steel plate 86.5 inches in diameter and 1.25 inches thick, and bolts directly to the facility exhaust elbow.

In the near future, an aero-grid will be installed at the center of the calorimeter section. The aero-grid is a 1.75 inch thick stainless steel flat disk mounted perpendicular to the gas flow. It has over 1,200 small contoured orifices that are sonic nozzles. The sonic nozzles at the center of the aero-grid will become choked by the high velocity core flow, causing the core flow to be more evenly distributed over the entire face of the aero-grid. This will result in a more evenly distributed velocity and temperature profile through the calorimeter. This will help ensure that the thermocouple array at the downstream end of the calorimeter section will encounter a uniform temperature distribution in the flow.

The aero-grid has been designed, but was not fabricated during the period reported here. A drawing of the aero-grid design is shown in Fig. 41.

#### 4.11 Facility Exhaust Elbow

The exhaust elbow is an 86.5 inch diameter, water-cooled, 90 degree steel elbow. It directs the Scramjet Test Facility high-speed, high-temperature gas flow into the facility's exhaust system. The exhaust elbow has water spray bars mounted at its entrance to quench the hot gas flow as it enters the elbow. The exhaust elbow also supports the mounting plate adapter for attaching the calorimeter section, since the calorimeter section must be aligned with, but separate from, the scramjet flow path, for the accurate measurement of loads by the thrust stand.

## **5.0    Fabrication Effort**

The fabrication of the water-cooled components has been a major obstacle in the development of the Scramjet Test Facility. The major hardware components of the Scramjet Test Facility are one-of-a-kind components that are complex and require many fabrication steps. The greatest difficulty encountered has been the high-temperature brazing of the beryllium copper and oxygen-free copper interior walls to the stainless steel weldments. The brazing processes involved the cleaning, plating, and high-temperature brazing of complex components. Both parts to be joined were copper plated and then the copper parts were brazed to the stainless steel weldments. It is very important that joints be designed properly, that the copper plating be clean and smooth, with no splatter or dirt from the plating process, and that the brazing process be performed properly. Some of the braze joints used in the design of the Scramjet Test Facility components were long (up to seventeen inches long) and had narrow joint surfaces. Some of the joint surfaces were on the order of only 0.100 inches wide. This, in addition to the fact that there is a large difference in the thermal conductivity between copper and stainless steel, makes the brazing process extremely challenging.

There were several leaks in some of the first copper-to-stainless steel braze joints. This resulted in delays in the fabrication of the nozzle. Fabrication techniques had to be closely monitored and design changes made to reduce leaks. In addition, special processes had to be developed to repair the leaks that did occur. Because the size of parts being fabricated makes re-brazing of parts with leaks difficult, other techniques had to be employed. Techniques used to make repairs included electron beam welding and TIG brazing processes. When the fabrication processes were closely monitored and parts inspected between fabrication phases,

problems with braze joint leaks were greatly reduced in size and number but not completely eliminated.

The Scramjet Test Facility is made up of more than 10 large and complex components with many more sub-components. During the fabrication phase of this project, as many as eight different machine shops were contracted to fabricate components simultaneously. For fabrication of the largest component, the heat-sink combustor section, two machine shops were contracted to work on different parts of the heat-sink combustor at the same time. This was necessary to complete the fabrication effort for the Scramjet Test Facility within the time frame for the project.

## 6.0 Instrumentation

A CAMAC process I/O system is used for both data acquisition and process control. Two Sun 630MP workstations serve as the data acquisition and facility control systems, processing 416 analog data channels and calculating 96 performance parameters in real-time. The control system handles up to six closed loops, of which three are currently tuned (facility air valves, vitiator fuel valve, and make-up oxygen valve). For the tests described here, the rig was run successfully with all three loops in automatic mode.

The data acquisition system has 416 channels of analog input. The 12-bit ADC has conversion times of 0.7 seconds for all 416 channels, on-board signal processing, data averaging, and 224 thermocouple reference junction points. The ADC also has a 32-channel transient digitizer system (12-bit ADC, maximum scan rate of 250 kHz for four channels), 64 channels of digital I/O, and 40 channels of analog output. The CAMAC crates are connected to the two workstations via a fiber optic SCSI interface. A Pressure Systems Incorporated (PSI) 8400 pressure scanning system, currently configured with 400 channels (32 @ 500 psid, 16 @ 100 psid, 320 @ 50 psid), with real-time display and data reduction, is also available. A typical PSI system interface box is shown in Fig. 42. These interface boxes were designed and constructed in-house. They facilitate quick and easy hardware instrumentation changes through the use of modular, interchangeable rectangular pattern connectors and disconnects. Shown in Fig. 43 are two thermocouple reference junction boxes for the 224 thermocouples.

Four remote video cameras placed around the thrust stand monitor the facility hardware, windows, and traversing probes. An infrared camera system is used for visual thermal health monitoring of the scramjet hardware, especially for the uncooled carbon steel

calibration section and traversing probe supports during nozzle/isolator calibration, and for the heat-sink combustor during combustion tests.

As described previously, the facility nozzle has 23 usable static pressure ports on the side-wall. The isolators have 30 pressure taps each on the top and bottom walls (total of 120 taps). The heat-sink combustor top, bottom, and side-walls are instrumented with nearly 200 static pressure taps. The pressure lines are purged with nitrogen during vitiator startup, purging and shutdown, and during all changes in operating (supply) conditions. The integrity of the pressure lines and the quality of the pressure data were tested under vacuum (2.5 psia) and higher pressure conditions.

The pressure data acquisition and traversing probe are connected by an automated link for boundary-layer surveys. Quick on-line reduction and plotting of pressure data have also been made possible, through the use of customized macros developed specifically for this purpose. Heat transfer equations have been integrated into the data acquisition code for real-time display of heat losses.

Total mass flow through the rig at each test condition is estimated using two independent methods. The first method sums the flow rates of facility air, fuel, and make-up oxygen, measured using an orifice plate and two turbine meters respectively. The second method uses the stagnation pressure and temperature measurements in the instrumentation section, along with the known nozzle throat area, using simple 1-D gas dynamic relations. The close correspondence between these two estimates, generally within 1 to 3%, inspires confidence in the quality and reliability of instrumentation and analysis in the test cell.

## 7.0 Preliminary Calibration Experiments

Initial tests were conducted for facility shakedown, evaluation, and calibration of the scramjet components (Mach 1.8 facility nozzle and isolators) and instrumentation installed on the thrust stand. A butterfly valve installed downstream of the calibration section was used to back-pressure the nozzle-isolator sections to simulate combustor heat-release pressure rise. Stagnation (air supply) conditions ranged from 55 to 112 psia and 530 to 2300°R. The simulated combustor inlet conditions (static temperature and pressure,  $T_4$  and  $p_4$ ) corresponded to flight Mach numbers of 4, 5, and 6 at dynamic pressures of 1000 and 2000 psf. The flight, combustor inlet, and facility stagnation conditions for the various simulations are presented in Tables 2, 3, 4 and 5. The experimental simulation matrix comprised the above cases with wall static and boundary layer surveys at each test point under no back pressure, partial back pressure, and high back pressure conditions. For brevity, only results from the  $M_o = 4$ ,  $Q_o = 1000$  psf ( $T_o = 1700^\circ\text{R}$ ,  $p_o = 55$  psia supply conditions) case, (Figs. 44 through 49) are discussed here; the same discussion applies to the other five simulated conditions shown in Figs. 50 through 79. Air heating was provided by the SUE vitiator (running up to  $\phi = 0.3$ ). The Research Air Facility gas-fired furnace was used to preheat hardware to avoid contamination due to condensation on internal walls.

**Table 2. Scramjet Simulation - Using M=1.8 Facility Nozzle**

Assumption: Match Static Temperature  $t_4$  and Static Pressure  $p_4$  in combustor, as calculated by RJPA

$M_0$	$q_0$	$M_4$	$M_{4sim}$	$A_0/A_4$	$P_4/P_0$	$\eta_{ke}$	$t_4$	$u_4$	$u_{4sim}$	$p_4$	$t_{t4}$	$p_{t4}$	$m_{total}$
8	2000	3.519	1.8	12.772	59.92	0.9751	1631	6828	3435	18.23	2423	101.4	11.34
8	1000	3.521	1.8	12.772	59.92	0.9749	1663	6896	3468	9.15	2471	50.9	5.64
8	500	3.521	1.8	12.772	59.92	0.9743	1738	7043	3546	4.70	2583	26.1	2.83
7	2000	3.165	1.8	10.857	46.97	0.9734	1459	5826	3250	18.70	2169	104.0	12.29
7	1000	3.165	1.8	10.857	46.97	0.9731	1490	5882	3283	9.34	2214	52.0	6.08
7	500	3.166	1.8	10.857	46.97	0.9727	1536	5972	3334	4.74	2283	26.4	3.04
6	2000	2.787	1.8	8.908	35.28	0.9717	1286	4831	3051	19.35	1911	107.7	13.55
6	1000	2.787	1.8	8.908	35.28	0.9714	1313	4877	3082	9.53	1951	53.0	6.60
6	500	2.787	1.8	8.908	35.28	0.9711	1339	4923	3113	4.83	1990	26.9	3.31
5	2000	2.385	1.8	6.925	24.85	0.9706	1108	3849	2832	19.57	1647	108.9	14.76
5	1000	2.385	1.8	6.925	24.85	0.9705	1130	3889	2859	9.67	1678	53.8	7.23
5	500	2.385	1.8	6.925	24.85	0.9700	1154	3925	2890	4.84	1715	26.9	3.58
4	2000	1.962	1.8	4.908	15.68	0.9711	935	2915	2601	18.39	1389	102.3	15.10
4	1000	1.962	1.8	4.908	15.68	0.9704	941	2928	2609	9.62	1398	53.5	7.88
4	500	1.962	1.8	4.908	15.68	0.9704	959	2960	2634	4.75	1424	26.4	3.85

**Table 3. Scramjet Simulation - Using M=1.8 Facility Nozzle**

Assumption: Match Velocity  $u_4$  and Static Pressure  $p_4$  in combustor, as calculated by RJPA

$M_0$	$q_0$	$M_4$	$M_{4sim}$	$A_0/A_4$	$P_4/P_0$	$\eta_{ke}$	$t_4$	$u_4$	$t_{4sim}$	$p_4$	$t_{t4}$	$p_{t4}$	$m_{total}$
8	2000	3.519	1.8	12.772	59.92	0.9751	1631	6828	6444	18.23	9576	101.4	5.70
8	1000	3.521	1.8	12.772	59.92	0.9749	1663	6896	6572	9.15	9765	50.9	2.84
8	500	3.521	1.8	12.772	59.92	0.9743	1738	7043	6856	4.70	10189	26.1	1.42
7	2000	3.165	1.8	10.857	46.97	0.9734	1459	5826	4691	18.70	6970	104.0	6.85
7	1000	3.165	1.8	10.857	46.97	0.9731	1490	5882	4782	9.34	7106	52.0	3.39
7	500	3.166	1.8	10.857	46.97	0.9727	1536	5972	4928	4.74	7324	26.4	1.70
6	2000	2.787	1.8	8.908	35.28	0.9717	1286	4831	3226	19.35	4793	107.7	8.56
6	1000	2.787	1.8	8.908	35.28	0.9714	1313	4877	3287	9.53	4885	53.0	4.17
6	500	2.787	1.8	8.908	35.28	0.9711	1339	4923	3350	4.83	4978	26.9	2.10
5	2000	2.385	1.8	6.925	24.85	0.9706	1108	3849	2048	19.57	3043	108.9	10.86
5	1000	2.385	1.8	6.925	24.85	0.9705	1130	3889	2091	9.67	3107	53.8	5.31
5	500	2.385	1.8	6.925	24.85	0.9700	1154	3925	2129	4.84	3163	26.9	2.64
4	2000	1.962	1.8	4.908	15.68	0.9711	935	2915	1175	18.39	1746	102.3	13.47
4	1000	1.962	1.8	4.908	15.68	0.9704	935	2915	1175	9.62	1746	53.5	7.05
4	500	1.962	1.8	4.908	15.68	0.9704	959	2960	1211	4.75	1799	26.4	3.43



**Table 4. Scramjet Simulation - Using M=2.2 Facility Nozzle**Assumption: Match Static Temperature  $t_4$  and Static Pressure  $p_4$  in combustor, as calculated by RJPA

$M_{\infty A63}$	$q_0$	$M_4$	$M_{4sim}$	$A_0/A_4$	$P_4/P_0$	$\eta_{ke}$	$t_4$	$u_4$	$u_{4sim}$	$p_4$	$t_{t4}$	$p_{t4}$	$m_{total}$
8	2000	3.519	2.2	12.772	59.92	0.9751	1631	6828	4198	18.23	2815	194.1	13.86
8	1000	3.521	2.2	12.772	59.92	0.9749	1663	6896	4239	9.15	2870	97.4	6.89
8	500	3.521	2.2	12.772	59.92	0.9743	1738	7043	4335	4.70	3000	50.0	3.46
7	2000	3.165	2.2	10.857	46.97	0.9734	1459	5826	3972	18.70	2519	199.0	15.02
7	1000	3.165	2.2	10.857	46.97	0.9731	1490	5882	4013	9.34	2571	99.5	7.43
7	500	3.166	2.2	10.857	46.97	0.9727	1536	5972	4075	4.74	2652	50.5	3.71
6	2000	2.787	2.2	8.908	35.28	0.9717	1286	4831	3728	19.35	2220	206.0	16.56
6	1000	2.787	2.2	8.908	35.28	0.9714	1313	4877	3767	9.53	2266	101.5	8.07
6	500	2.787	2.2	8.908	35.28	0.9711	1339	4923	3805	4.83	2311	51.4	4.05
5	2000	2.385	2.2	6.925	24.85	0.9706	1108	3849	3461	19.57	1913	208.3	18.04
5	1000	2.385	2.2	6.925	24.85	0.9705	1130	3889	3494	9.67	1950	103.0	8.83
5	500	2.385	2.2	6.925	24.85	0.9700	1154	3925	3532	4.84	1992	51.6	4.38
4	2000	1.962	2.2	4.908	15.68	0.9711	935	2915	3179	18.39	1613	195.8	18.46
4	1000	1.962	2.2	4.908	15.68	0.9704	941	2928	3189	9.62	1624	102.4	9.63
4	500	1.962	2.2	4.908	15.68	0.9704	959	2960	3219	4.75	1655	50.6	4.71

**Table 5. Scramjet Simulation - Using M=2.2 Facility Nozzle**Assumption: Match Velocity  $u_4$  and Static Pressure  $p_4$  in combustor, as calculated by RJPA

$M_0$	$q_0$	$M_4$	$M_{4sim}$	$A_0/A_4$	$P_4/P_0$	$\eta_{ke}$	$t_4$	$u_4$	$t_{4sim}$	$p_4$	$t_{t4}$	$p_{t4}$	$m_{total}$
8	2000	3.519	2.2	12.772	59.92	0.9751	1631	6828	4314	18.23	7445	194.1	8.52
8	1000	3.521	2.2	12.772	59.92	0.9749	1663	6896	4399	9.15	7593	97.4	4.24
8	500	3.521	2.2	12.772	59.92	0.9743	1738	7043	4590	4.70	7922	50.0	2.13
7	2000	3.165	2.2	10.857	46.97	0.9734	1459	5826	3140	18.70	5420	199.0	10.24
7	1000	3.165	2.2	10.857	46.97	0.9731	1490	5882	3201	9.34	5525	99.5	5.07
7	500	3.166	2.2	10.857	46.97	0.9727	1536	5972	3299	4.74	5694	50.5	2.53
6	2000	2.787	2.2	8.908	35.28	0.9717	1286	4831	2159	19.35	3727	206.0	12.78
6	1000	2.787	2.2	8.908	35.28	0.9714	1313	4877	2201	9.53	3798	101.5	6.24
6	500	2.787	2.2	8.908	35.28	0.9711	1339	4923	2243	4.83	3871	51.4	3.13
5	2000	2.385	2.2	6.925	24.85	0.9706	1108	3849	1371	19.57	2366	208.3	16.22
5	1000	2.385	2.2	6.925	24.85	0.9705	1130	3889	1400	9.67	2416	103.0	7.93
5	500	2.385	2.2	6.925	24.85	0.9700	1154	3925	1425	4.84	2460	51.6	3.94
4	2000	1.962	2.2	4.908	15.68	0.9711	935	2915	786	18.39	1357	195.8	20.13
4	1000	1.962	2.2	4.908	15.68	0.9704	935	2915	786	9.62	1357	102.4	10.53
4	500	1.962	2.2	4.908	15.68	0.9704	959	2960	811	4.75	1399	50.6	5.12

## 7.1 Nozzle / Isolator

With no back pressure, static pressure profiles along the Mach 1.8 nozzle sidewall and the isolator top and bottom walls matched the inviscid predictions at all test conditions (see Figs. 44, 50, 56, 62, 68, and 74). The Mach number at the nozzle exit, computed from the pressure data (static pressure at nozzle exit and facility stagnation pressure), ranged from 1.79 to 1.83 under the various supply temperature conditions. Vitiator combustion efficiencies, based on temperature measurements, were estimated at 92-98% under different operating conditions.

During the back-pressure tests, static pressure profiles along the nozzle side wall and the isolator top and bottom walls were recorded at various valve positions. As shown in Figs. 46, 48, 52, 54, 58, 60, 64, 66, 70, 72, 76, and 78, with increased valve closing (back pressure), the high back pressure moved gradually upstream through the isolator sections. At the highest back-pressure condition tested ( $p_e/p_i = 3.46$ , close to the normal shock pressure rise at  $M = 1.8$ ), the region of pressure rise reached the nozzle exit. The similarity between the isolator top and bottom wall centerline pressure profiles was not significantly affected by increased back pressure.

Boundary layer surveys were made in the carbon steel calibration section at the aft isolator exit plane along the vertical centerline, in conjunction with the nozzle/isolator calibrations discussed previously. High pressure water was used to cool the probe. Occasional purging of the probe tips during the course of a pressure survey was necessary to clear the pressure lines. Pitot pressure profiles obtained using the boundary layer probe are remarkably consistent across the eight probe tips under all flow conditions (see Figs. 45, 51, 57, 63, 69, and 75), indicating the two-dimensional nature of the flow. High quality boundary layer

profiles were obtained under cold, heated, and vitiated conditions. The effect of back pressure on the boundary layer Pitot pressure profiles (as the shock train moves upstream) can be seen in Figs. 47, 49, 53, 55, 59, 61, 65, 67, 71, 73, 77, and 79. At the highest back pressure condition ( $p_e/p_i = 3.46$ ), the flow exiting the aft isolator is purely subsonic. During the course of some surveys, intermittent blockage of one or more of the probe tips degraded the quality and accuracy of data from the affected tips. In these cases, only data from the unaffected tips have been presented in the final figures.

Initial tests with water flowrates at design conditions showed no appreciable temperature rise in the cooling water return lines. Systematic throttling of the cooling water flows across the different components was required to obtain adequate water temperature elevations across the water supply and return manifolds (approximately 20°F) for reliable heat balance calculations.

At the highest heat load condition ( $M_o = 6$ ,  $Q_o = 2000$  psf), the facility nozzle cooling water flow rate had to be reduced to approximately 100 gpm to obtain the desired bulk temperature rise. Subsequently, the forward and aft isolator water flow rates were each reduced to 40 gpm. Heat fluxes through the transition section, nozzle, forward and aft isolators were then estimated at 60, 230, 100, and 100 BTU/sec, respectively. Similarly, at the lowest heat load condition ( $M_o = 4$ ,  $Q_o = 1000$  psf), the nozzle and isolator flow rates were 30, 15, and 15 gpm, respectively. The calculated heat fluxes were then 30, 90, 40, and 40 BTU/sec through the transition section, nozzle, forward and aft isolators.

The above tests were also performed with back pressure, and the associated effect on wall heat load was examined. The total heat transfer rate increased (relative to the

corresponding no back pressure cases) due to subsonic flow regions downstream of the shock train in the forward and/or aft isolators.

Thermocouples in the instrumentation section and traversing temperature probes in the calibration section are used to provide total temperature estimates for the flow entering and exiting the rig, and are used to assess the reliability of the heat balance calculations. The heat lost by the flow stream across the rig can then be compared with the total energy gained by the cooling water across these sections.

## 7.2 Combustor

Tests were conducted for shakedown and preliminary evaluation of the heat-sink combustor and related instrumentation. The Mach 1.8 facility nozzle was used for all of these tests. The combustor's flexible top wall sections are currently set for an area ratio of about 2.55. Stagnation (air supply) conditions ranged from 55 to 112 psia and 530 to 2000°R. The Research Air Facility furnace was used to preheat hardware and thermally cycle the combustor walls; the SUE vitiator was also used for these tests.

Visualizations of several cases were performed using a pulsed shadowgraph system. A Xenon nanopulser (10 ns pulse duration) was placed at the focal point of a parabolic mirror (8 inch diameter, 48 inch focal length). The resulting collimated beam of light passed through quartz windows into the forward section of the combustor. An identical parabolic mirror then focused the light into a PixelVision CCD camera used for image acquisition. For precise alignment of the optical train, an He-Ne laser was used. A Pentium PC controlled the camera, which was set to trigger the nanopulser and collect a single pulse of light. Thus, the flow entering the combustor was frozen and effectively instantaneous shadowgraph images were

obtained. The resulting images cover approximately 6 inches in the axial direction and the entire height of the forward combustor section.

As shown in Fig. 80, pressure data from the baseline combustor indicate the expected flow acceleration caused by the combustor's area increase in the streamwise direction. The pressure drop from the rapid expansion at the aft top wall section is also clearly evident from the pressure data. The measured wall static pressure data agree closely with the inviscid prediction. Figure 81 is a shadowgraph of the baseline combustor showing the forward section near the aft isolator exit. The flow entering the combustor appears to be very well behaved. There are no strong shocks or disturbances that would indicate misalignment of hardware or obstructions in the stream.

The injector/cavity/ramp was installed in the bottom wall of the forward combustor section. For preliminary tests, provisions were made to introduce nitrogen through the four injector holes. In tests with no injection (see Fig. 82), wall pressure traces on the top and bottom walls indicated pressure rise due to a shock (generated by the cavity) impinging on the top wall, and then reflecting and impinging on the bottom wall downstream. The shadowgraph from this case (Fig. 83) captures a relatively weak shock generated from the fuel injectors (starting at the far left lower corner of the image) and another feature generated by the backward-facing step of the cavity (emanating from approximately the bottom center of the photo).

Figure 84 shows the wall static pressure trace with nitrogen injection through the injector array. The four injection port static pressures were monitored and were found to be fairly uniform ( $p_{jet} = 87$  psia). The strong pressure rise on the upper wall at approximately 52 inches downstream of the nozzle entrance corresponds to the bow shocks generated by the jets.

The other features in the pressure profile are similar to those observed in Fig. 82. The shadowgraph photo corresponding to this case appears in Fig. 85. The strong bow shocks can be clearly seen and their impingement on and reflection from the upper wall are also quite apparent. A qualitative estimate of injectant penetration and mixing can be obtained from Fig. 85, which clearly shows the nitrogen jets and associated features.

The combustor side-walls have been instrumented with thermocouples to monitor wall temperatures and heat fluxes. Their performance will be evaluated during thermal cycling tests using the furnace and the SUE vitiator. Equations for real-time on-line heat flux calculations based on the thermocouple measurements have been integrated into the data acquisition code.

## 8.0 Related Follow-On Contract Work

Following the aforementioned calibrations and flow visualizations, combustion studies using both ambient and partially-heated ethylene have been performed. With the Mach 1.8 facility nozzle, successful ignition of the cavity and main combustor has been accomplished over the entire range of simulation conditions. Data and results from these tests have been published and presented in Refs. 4 and 5. Calibration of the Mach 2.2 facility nozzle has been completed using a modified probe that measures total temperatures in addition to Pitot pressures. Preliminary combustion tests with the Mach 2.2 facility nozzle have also been very successful.

Detailed pre-combustor shock train studies have been initiated in a non-reacting test facility (Test Cell 19), where optical access and high frequency pressure instrumentation are available along the entire length of the isolator. Results from these experiments, along with preliminary analyses of the isolator back-pressure static pressure distributions presented above in Figs. 44 through 85, have been published in Ref. 5.

Gas sampling techniques are currently being evaluated and the use of an array of sampling bottles for collection of gas samples is currently being explored. Numerical and experimental studies are currently underway to investigate alternative fuel injection/flameholding/piloting concepts. The most promising of these concepts will then be explored in high-enthalpy reacting flows in the scramjet test facility. Other plans include refining measurement and data analysis procedures for various parameters, including heat transfer, calorimetry, and thrust, and real-time on-line data reduction and display. Unique ignition sources, such as a plasma torch, are also scheduled for testing in the combustion rig.

Liquid and gaseous fuel heat exchangers with the ability to heat hydrocarbon fuels to over 1460°R at 1000 psia are currently under design and are expected to be available in early 1999.

All of the test hardware in Test Cell 22 is water-cooled (except the heat-sink combustor), and the cooling water inlet and outlet temperatures and flowrates are monitored to perform a precise energy balance. An equilibrium chemistry code can use these measurements, along with measurements from the calorimeter, to compute combustion efficiency. Independently, thrust and wall static pressure measurements can be used in conjunction with an RJPA-generated carpet plot to estimate skin friction and combustion efficiency.<sup>6</sup> Experimental and analytical efforts could then be refined, after a comparison of the two separately obtained values of combustion efficiency.



## 9.0 Expert Consultant Services

To provide technical direction and expertise in the area of scramjet propulsion system research, Taitech, Inc. obtained the services of Dr. Frederick S. Billig. Dr. Billig retired from the position of Associate Supervisor and Chief Scientist at the Aeronautics Department of The Johns Hopkins University, Applied Physics Laboratory (JHU/APL), Laurel, Maryland. He was the program manager of the National Aerospace Plane (NASP) Project at JHU/APL. Dr. Billig brings to the present project pioneering analytical and experimental contributions to the understanding and development of supersonic combustion ramjet engines. Dr. Billig's nearly 40 years of research has focused on airbreathing propulsion, external burning, and supersonic combustion.

In support of this contract, Dr. Billig assisted in the technical management of experimental and analytical portions of the HyTech program and other high-speed propulsion activities. He has advised on instrumentation, the design and fabrication of test items, the planning and conducting of experiments, and data acquisition and reduction. Dr. Billig also participated in systems studies and analyses, and in the modeling of the fundamental physical processes involved in high-speed flowfields with chemical reactions. Dr. Billig further prepared and presented a lecture series to Air Force personnel covering a broad range of subjects in high-speed propulsion.

## 10.0 Future Plans

Following the recently completed calibration and flow visualizations, combustion studies using both ambient and heated ethylene will be performed. Gas sampling techniques are currently being evaluated and explored. An array of gas sampling bottles for the collection of gas samples is being assembled. Numerical and experimental studies are currently underway to investigate alternative fuel injection/flameholding/piloting concepts, the most promising of which will then be explored in high-enthalpy reacting flows. Other plans include refining measurement and data analysis procedures, including heat transfer, calorimetry, thrust, and real-time on-line data reduction and display. Calibration of other facility nozzles (Mach 2.2, 2.6, 3.0; pressure and temperature profiles with and without back pressure) will proceed as required, depending on the combustor inlet Mach number required for accurate simulation. Innovative ignition sources, such as a plasma torch, are also scheduled for testing in the combustion rig. Liquid and gaseous fuel heat exchangers with the ability to heat hydrocarbon fuels to over 1460°R at 1000 psia are currently under design and will be available mid-year. Detailed pre-combustor shock train studies are also planned in a non-reacting test facility (Test Cell 19), where optical access and high frequency pressure instrumentation will be available along the entire length of the isolator (Ref. 5).

### References

1. Pandolfini, P. P., Billig, F. S., Corpening, G. P., Corda, S., and Friedman, M. A., "Analyzing Hypersonic Engines Using the Ramjet Performance Analysis Code," *APL Technical Review*, Vol. 2, No. 1, 1990, pp. 68-79.
2. Pandolfini, P. P., and Friedman, M. A., "Instructions for Using Ramjet Performance Analysis (RJPA) - IBM-PC Version 1.24," JHU/APL, AL-92-P175, 1992.
3. Thompson, M. W., "Equilibrium Chemistry Stream Calorimetry Data Analysis Procedure Using the Ramjet Performance Analysis Code," JHU/APL, RTDC-TPS-028, 1997.
4. Gruber, M., Jackson, K., Donaldson, W., Donbar, J., Jackson, T., Mathur, T., Streby, G., Smith, C., and Billig, F., "A Cavity-Based Fuel Injector/Flameholder for Scramjet Applications," JANNAF Paper 2C-06, 1998.
5. Gruber, M., Jackson, K., Jackson, T., Mathur, T., and Hsu, K.-Y., "Investigations of Shock Trains in Rectangular Ducts," JANNAF Paper 4D-03, December 1998.
6. Gruber, M., Jackson, K., Mathur, T., and Streby, G., "Calibration of a Newly Developed Direct-Connect High-Enthalpy Supersonic Combustion Research Facility," AIAA Paper 98-1510, 1998.
7. Carroll, B. F., Dutton, J. C., and Addy, A. L., "NOZCS2: A Computer Program for the Design of Continuous Slope Supersonic Nozzles." Dept. of Mechanical and Industrial Engineering, University of Illinois at Urbana-Champaign, UILU ENG 86-4007, 1986

## **APPENDIX A**

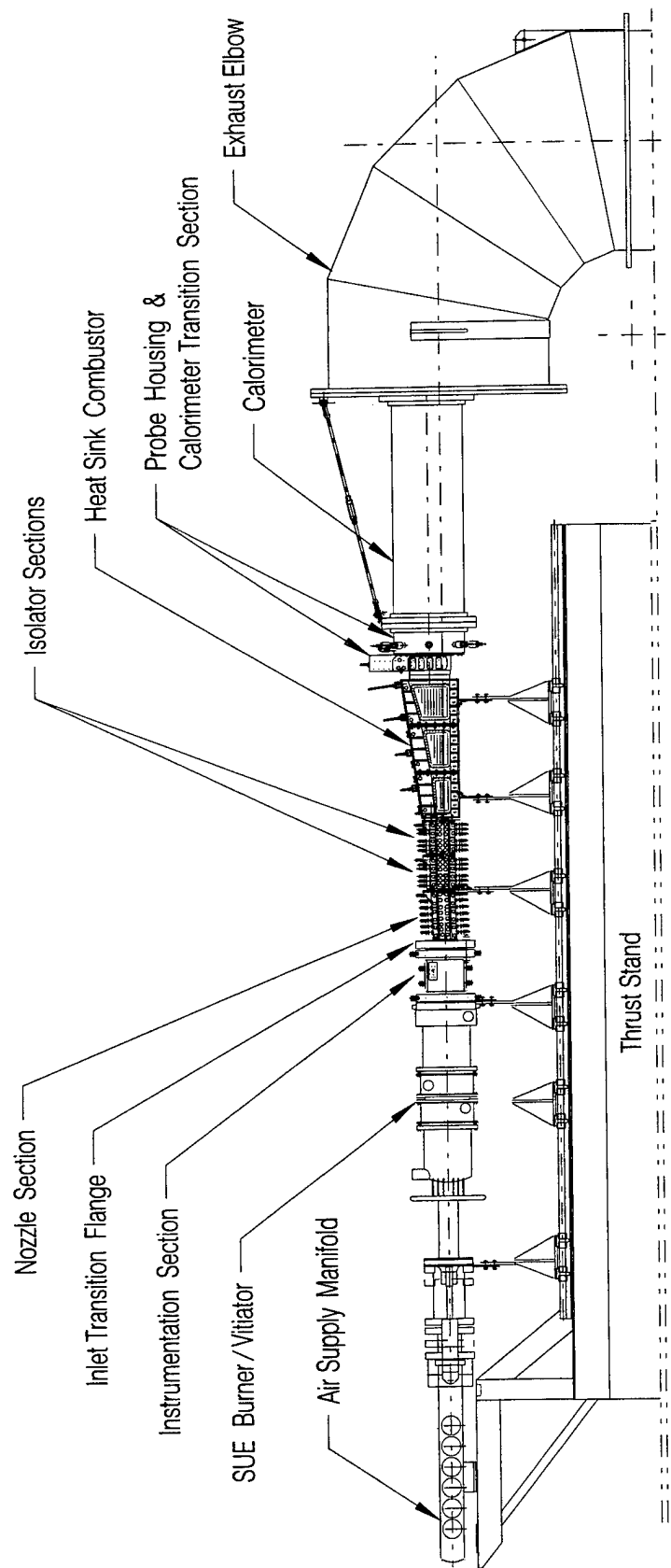


Figure 1. Test Cell 22 Scramjet Facility Schematic

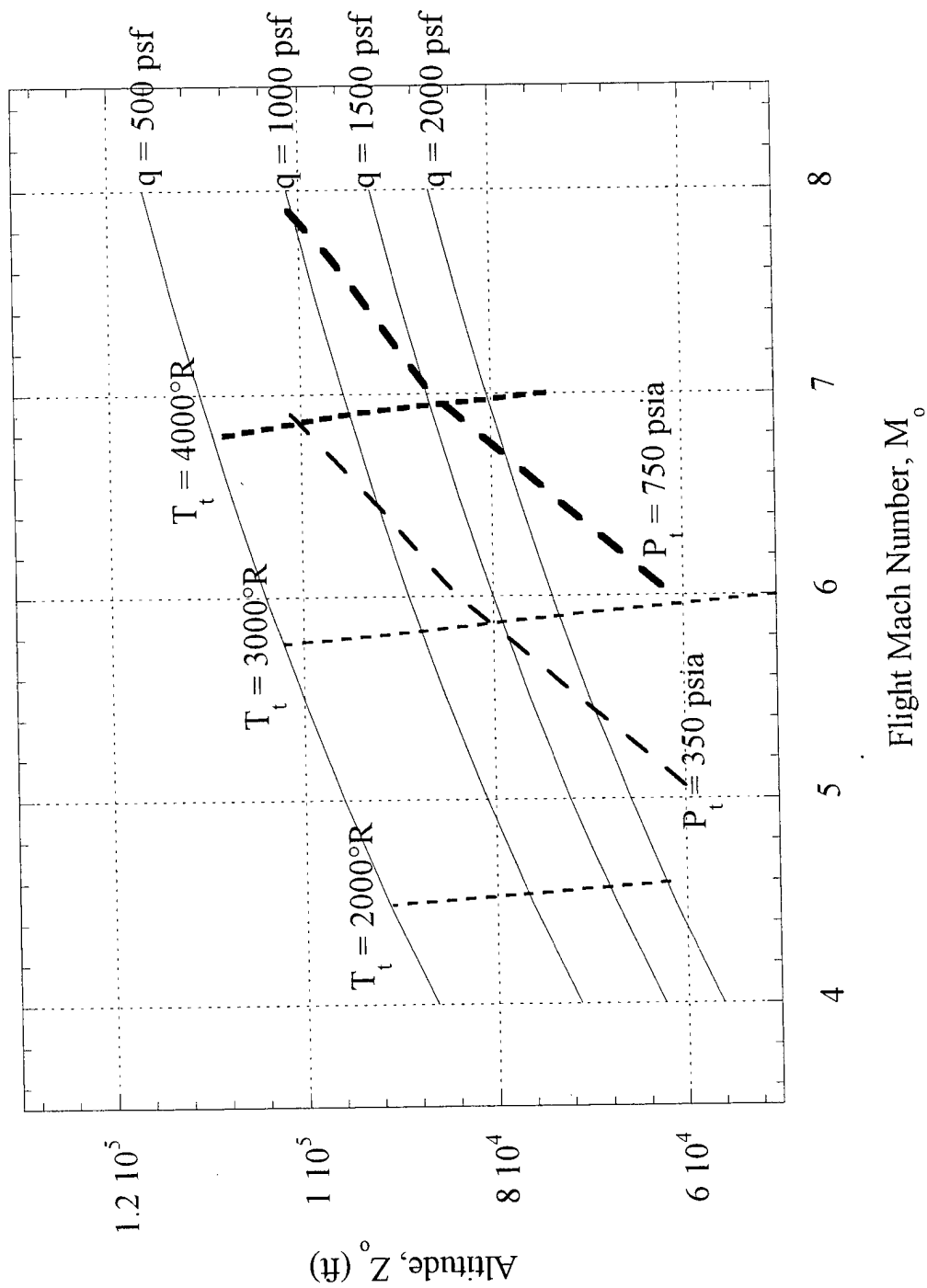


Figure 2. Scramjet Test Rig Facility Map

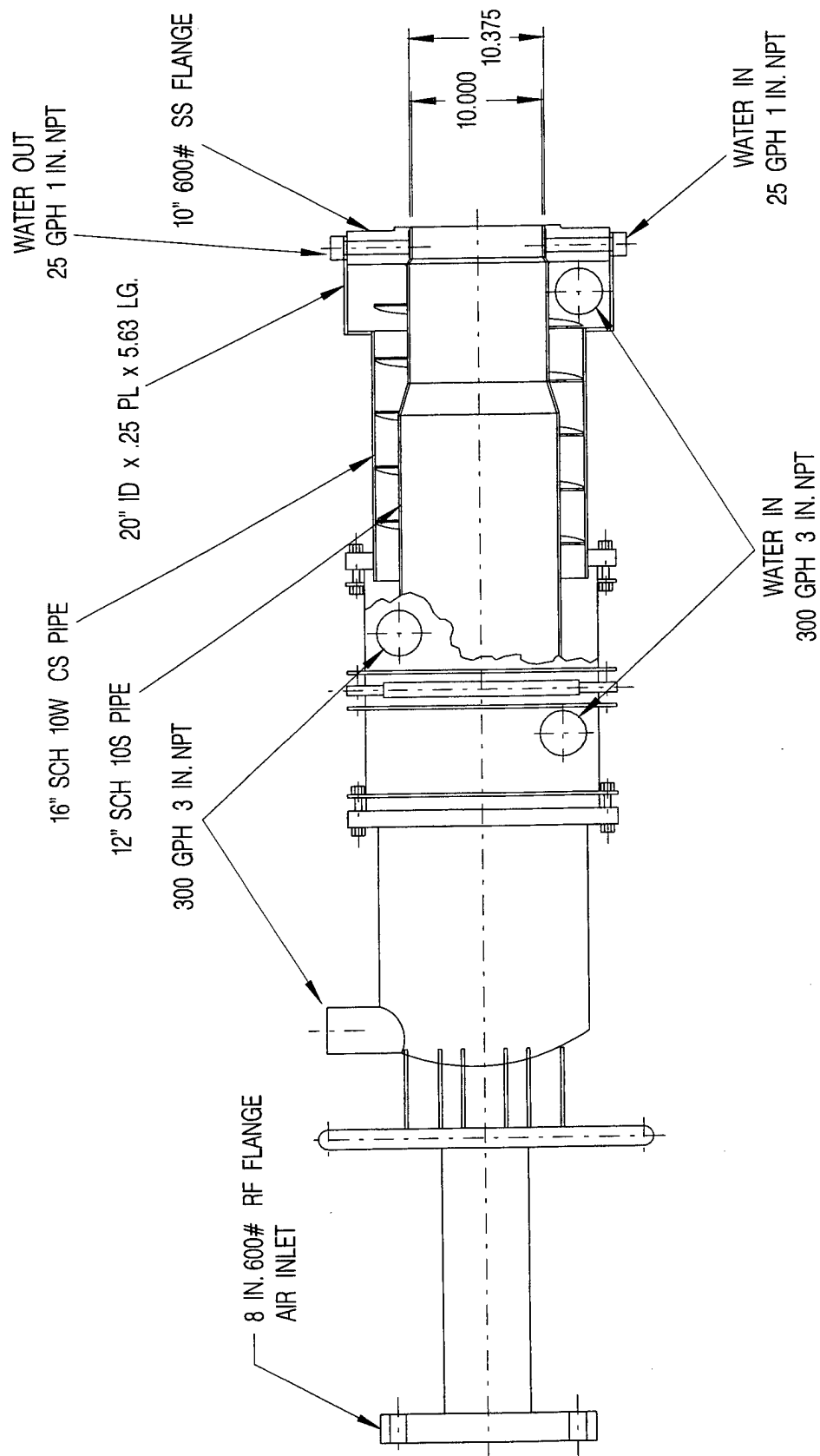


Figure 3. Kaiser-Marquardt SUE® Burner/Vitator Schematic Diagram

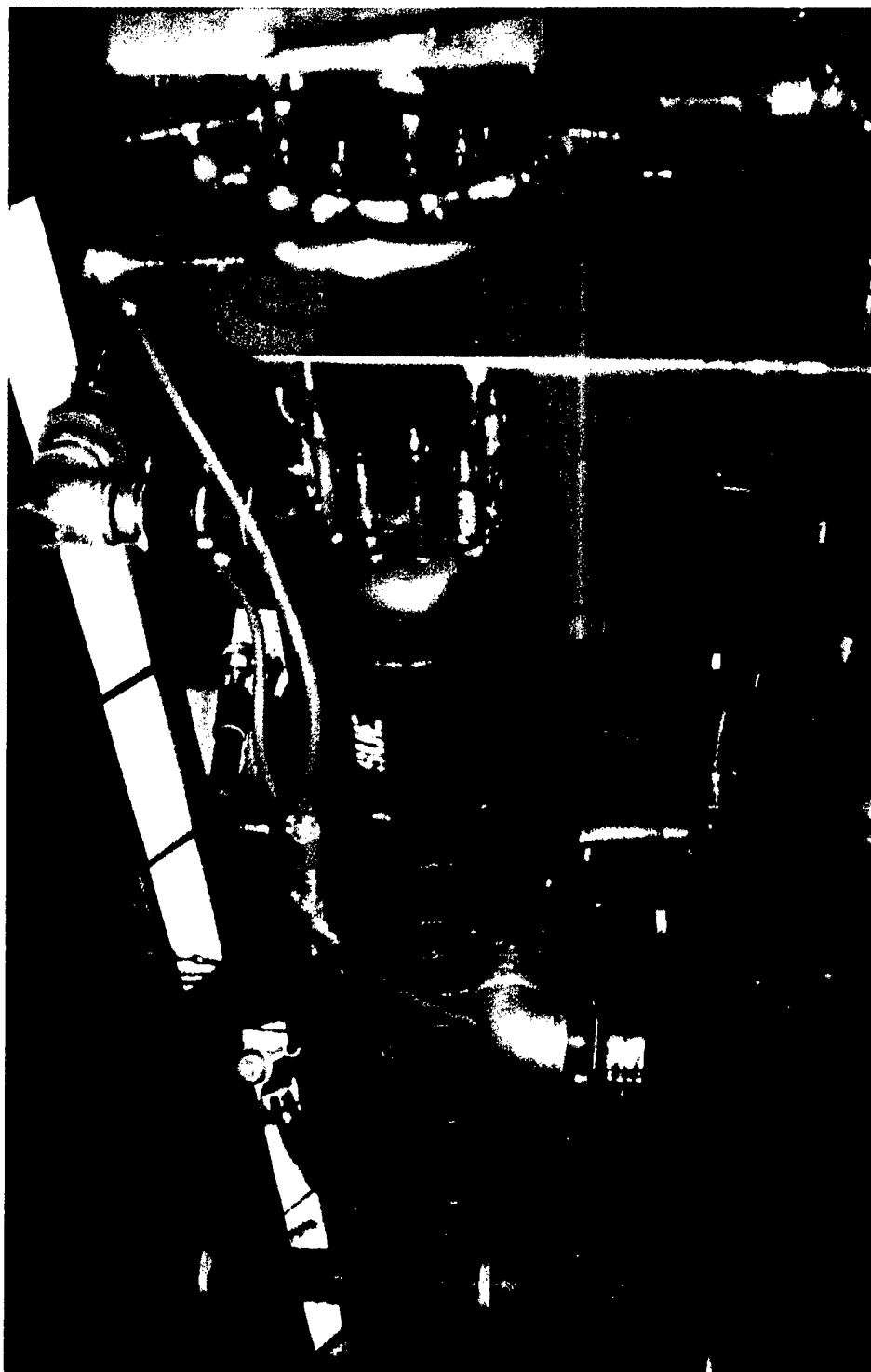


Figure 4. Kaiser-Marquardt SUE® Burner/Vitiator Mounted on Test Cell 22 Thrust Stand



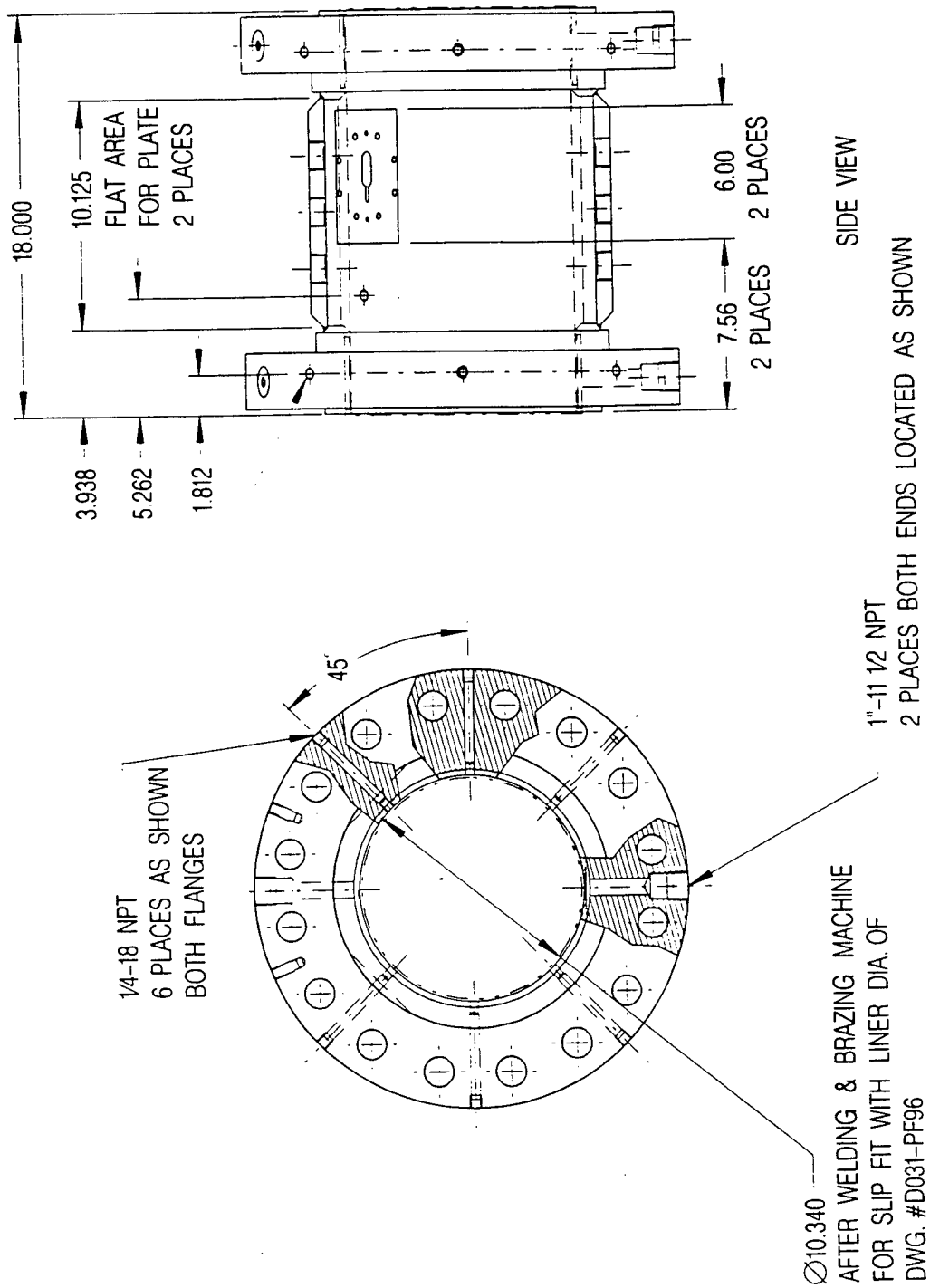


Figure 5. Schematic Diagram of Instrumentation Section

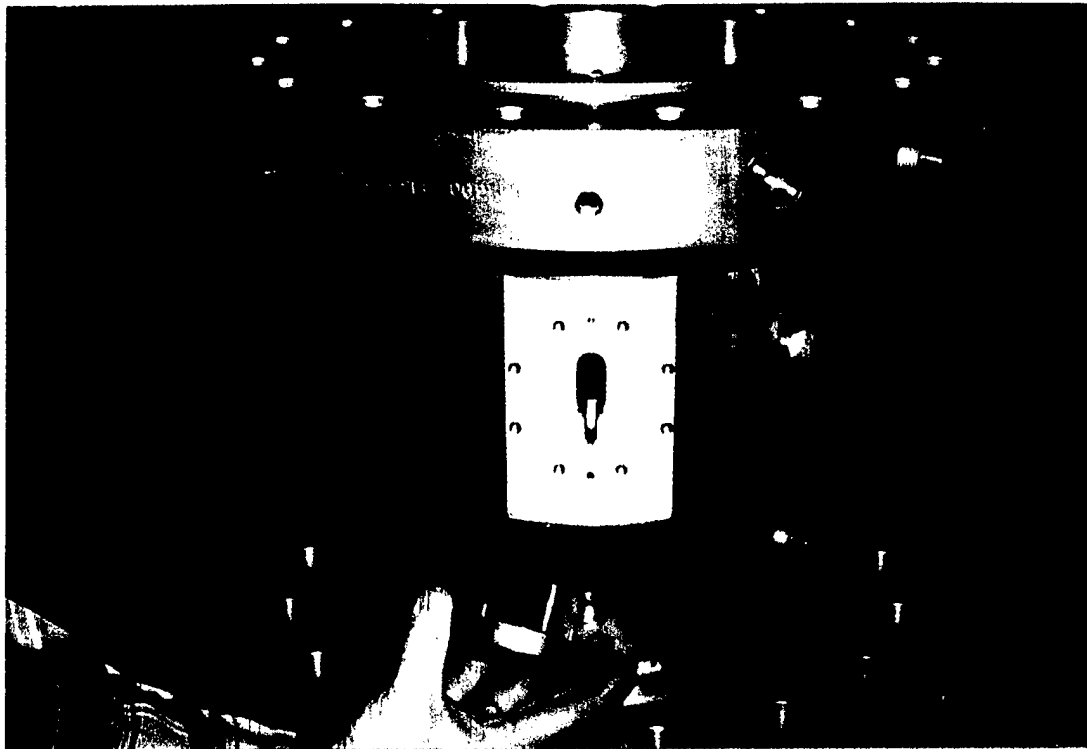


Figure 6. Photograph of Instrumentation Section Showing Traversing Probe Port and Plug

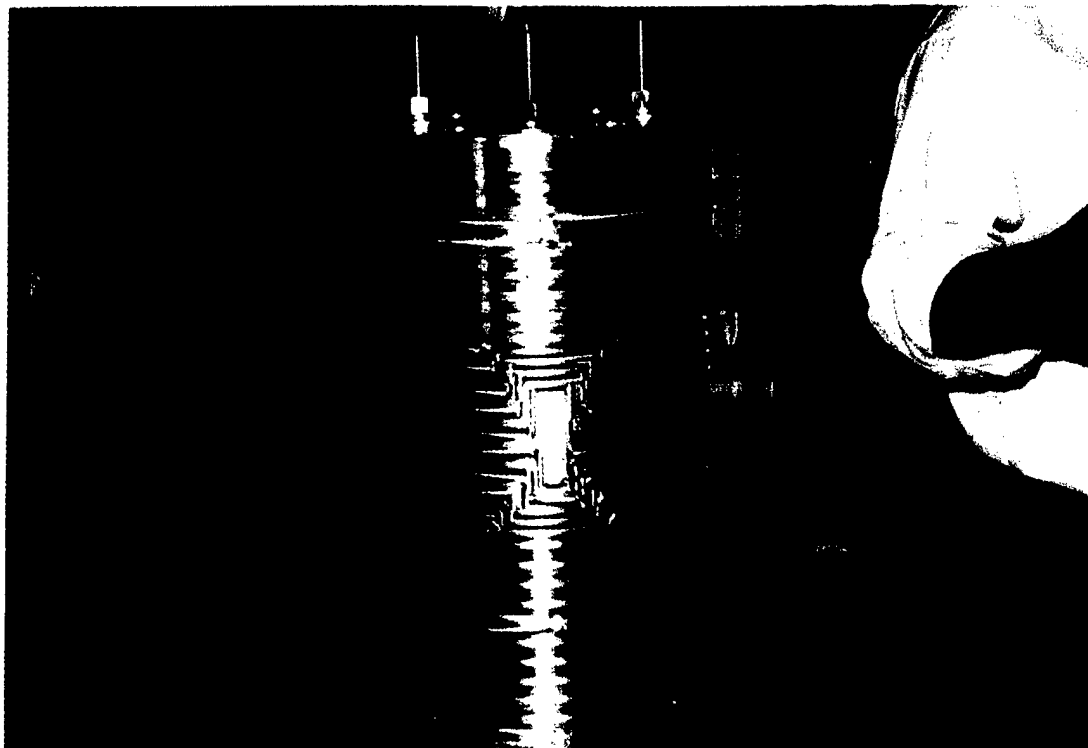


Figure 7. Instrumentation Section Inner Oxygen-Free Copper Liner with Milled Passages

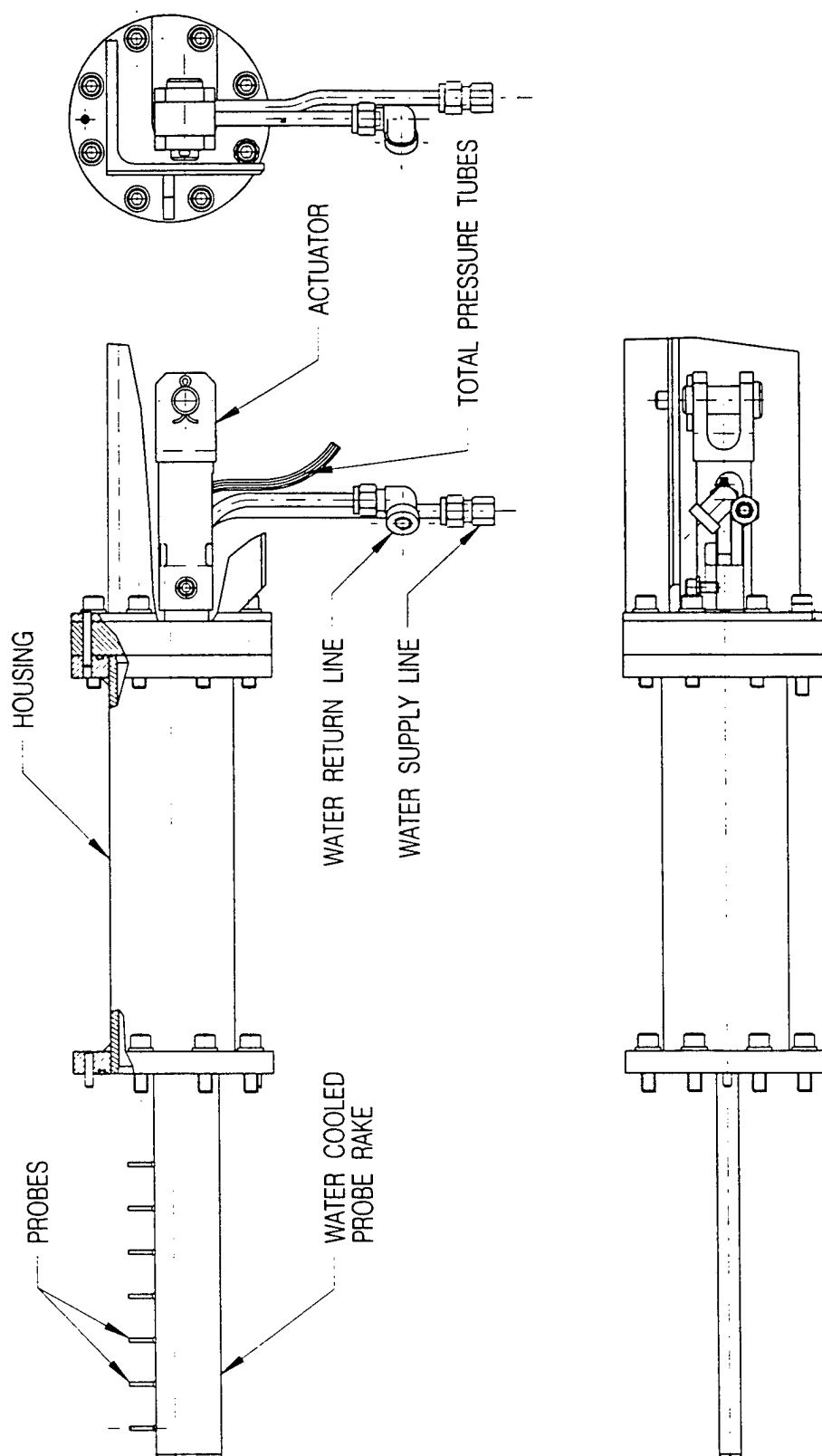


Figure 8. Schematic Diagram of Water Cooled Traversing Probe and Housing

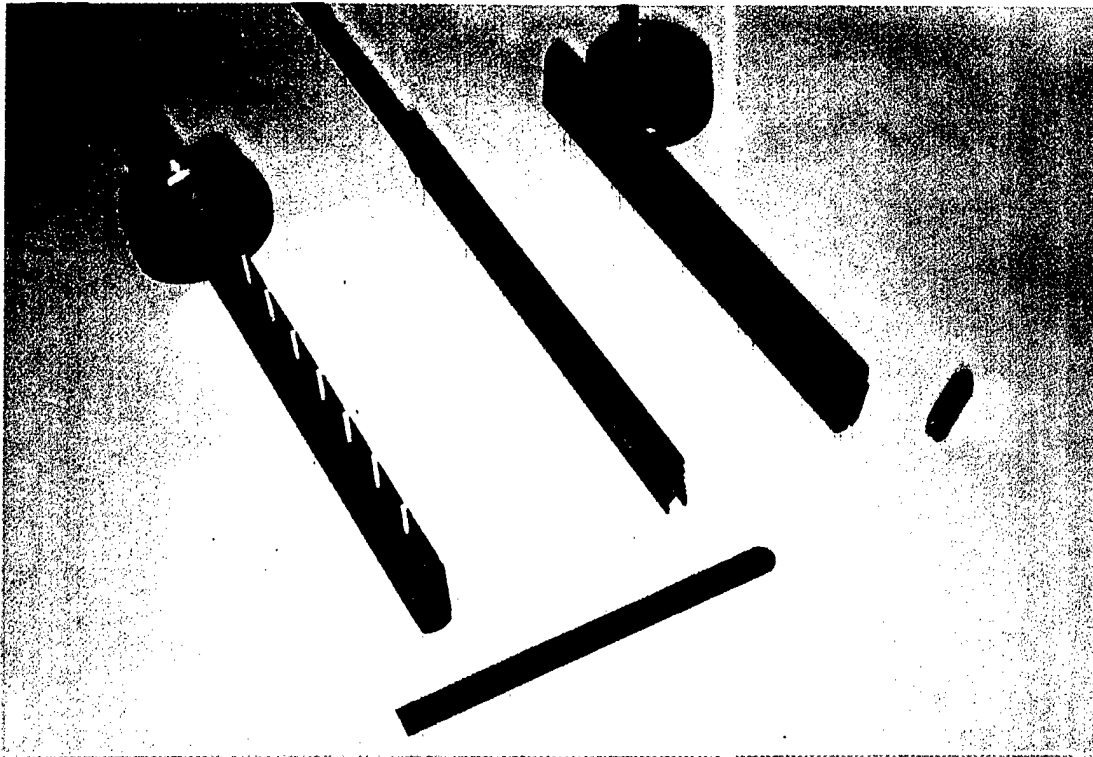


Figure 9. Photographs of Traversing Probe Internal and External Components

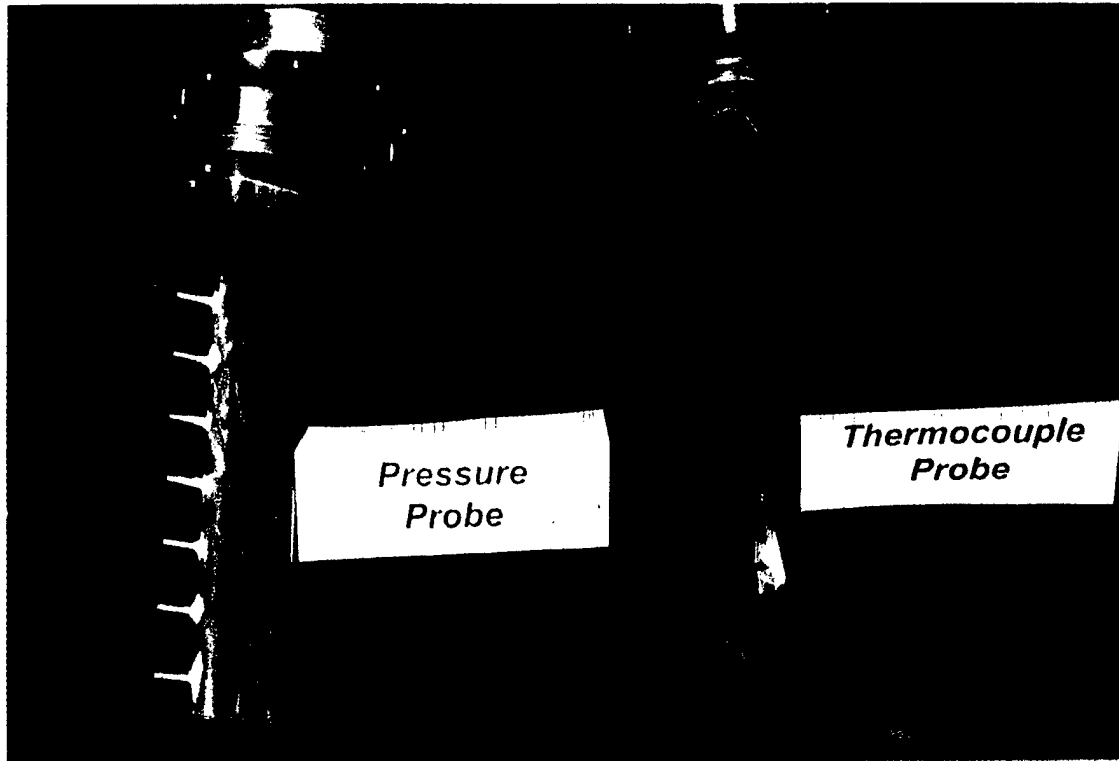


Figure 10. Photographs of Traversing Probes Showing Instrumentation Tips

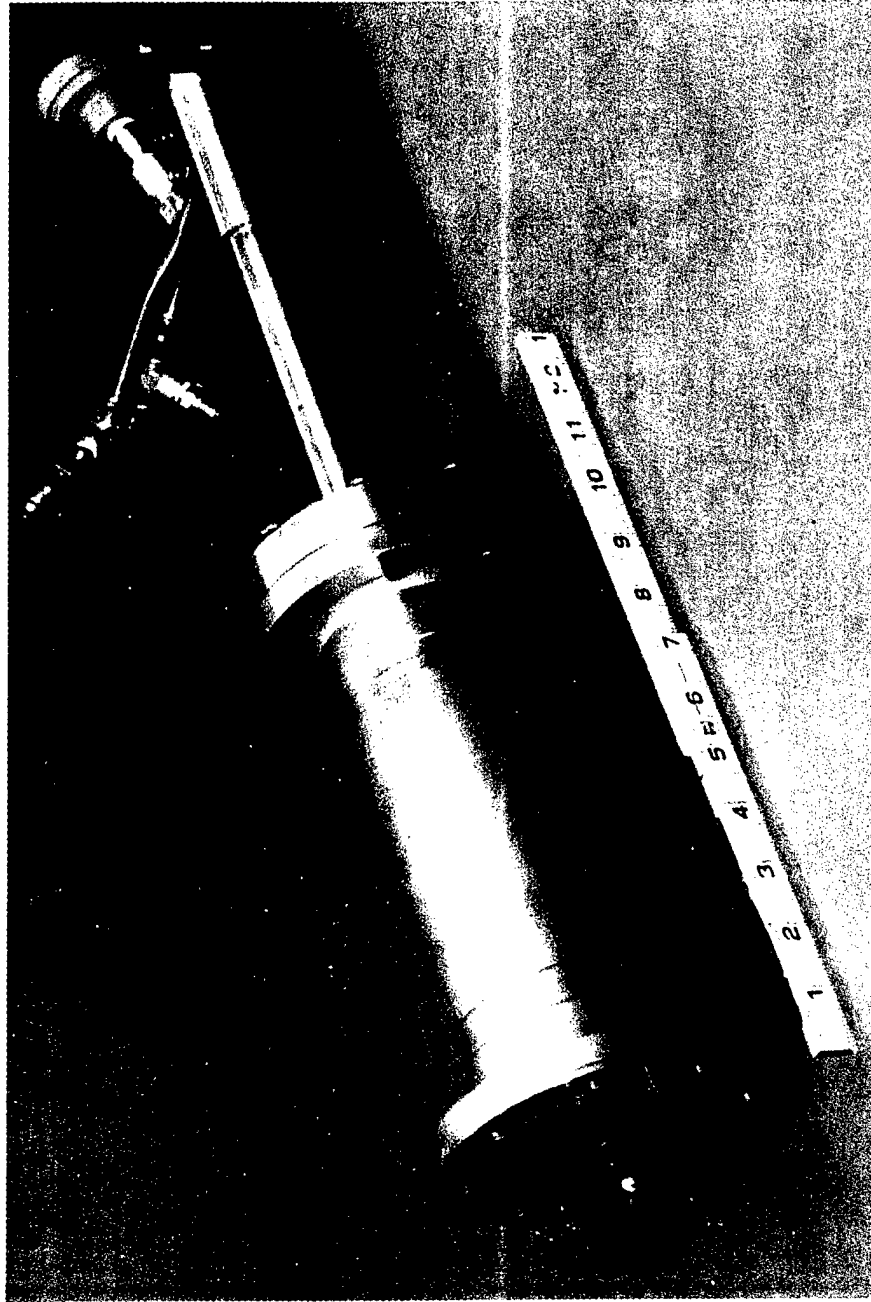


Figure 11. Traversing Probe Housing Assembly

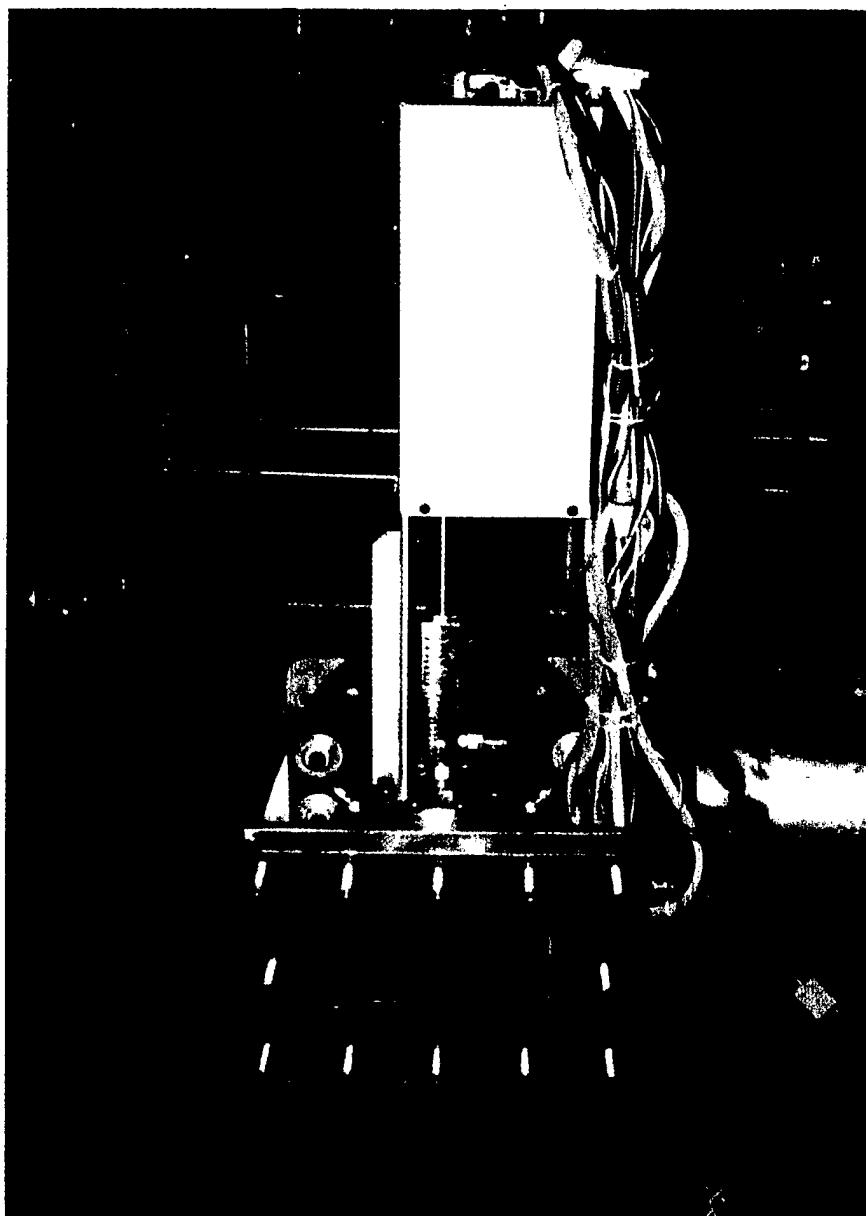


Figure 12. Traversing Probe Assembly Mounted on Calibration Section

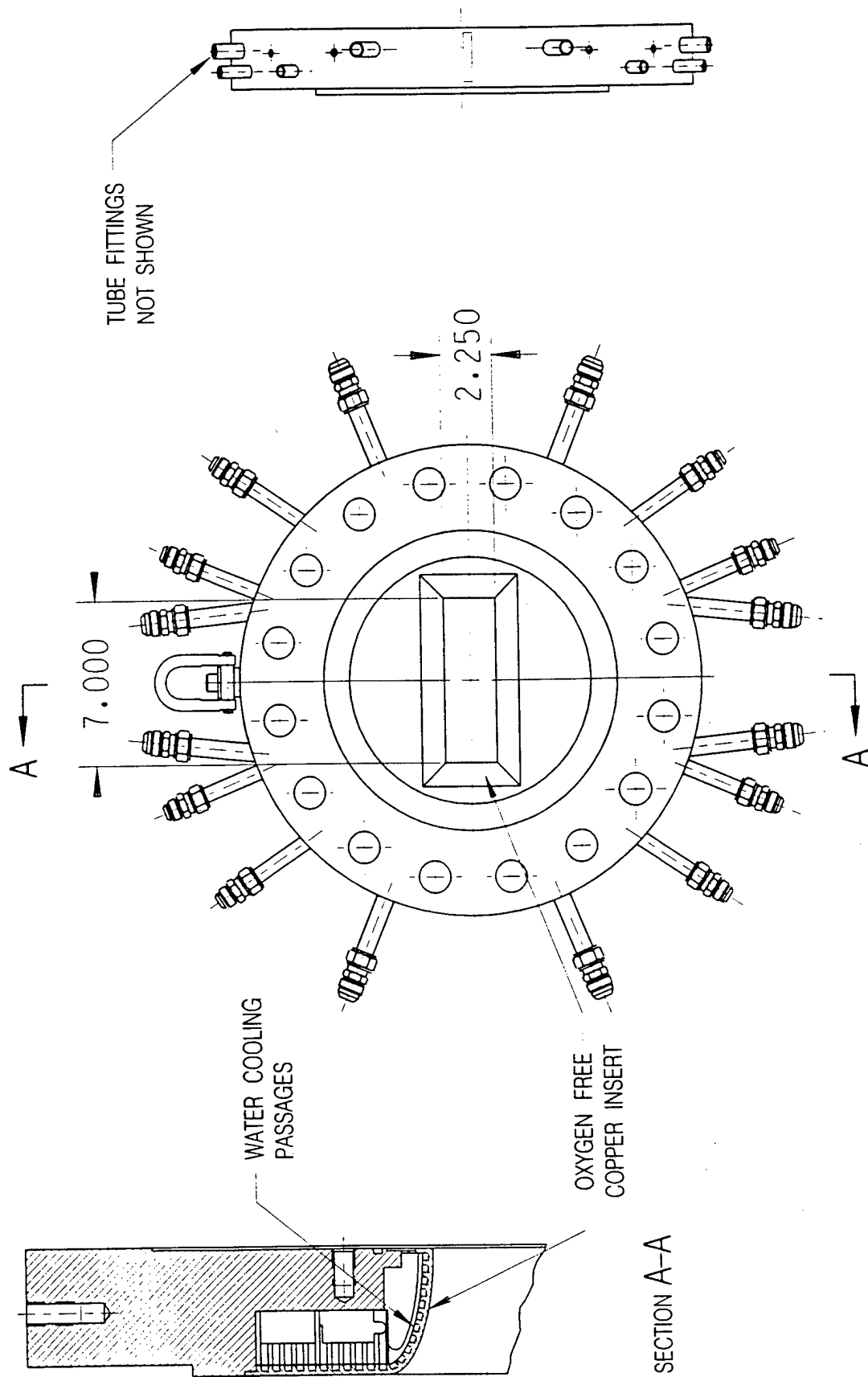


Figure 13. Schematic Diagram of Inlet Transition Flange

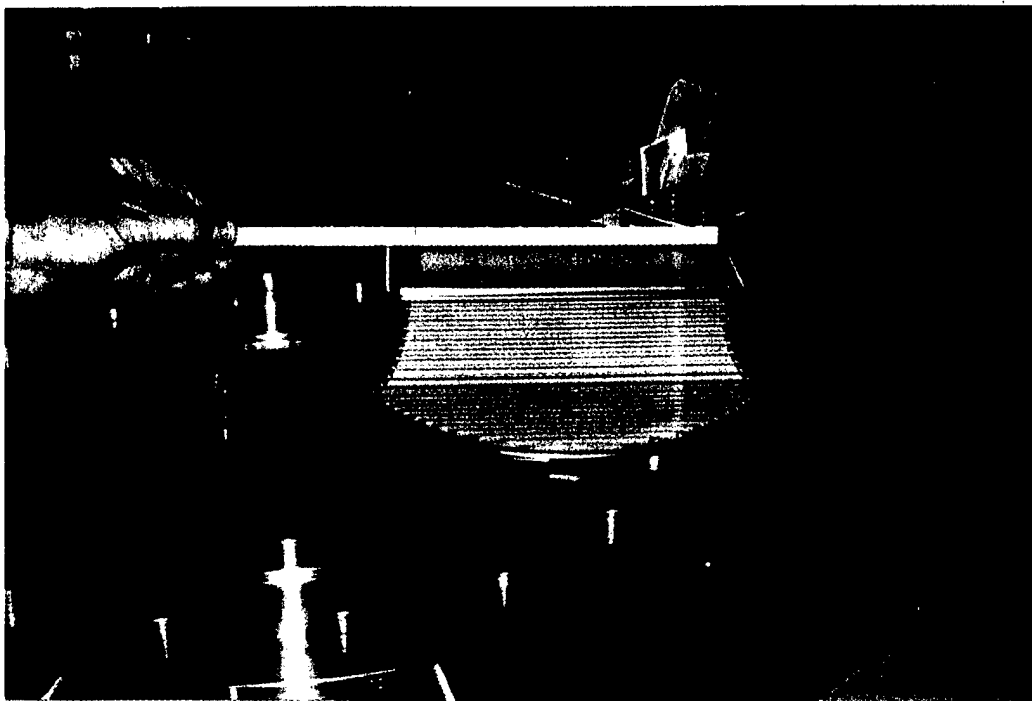


Figure 14. Photograph of Inlet Transition Flange Oxygen-Free Copper Machined Insert

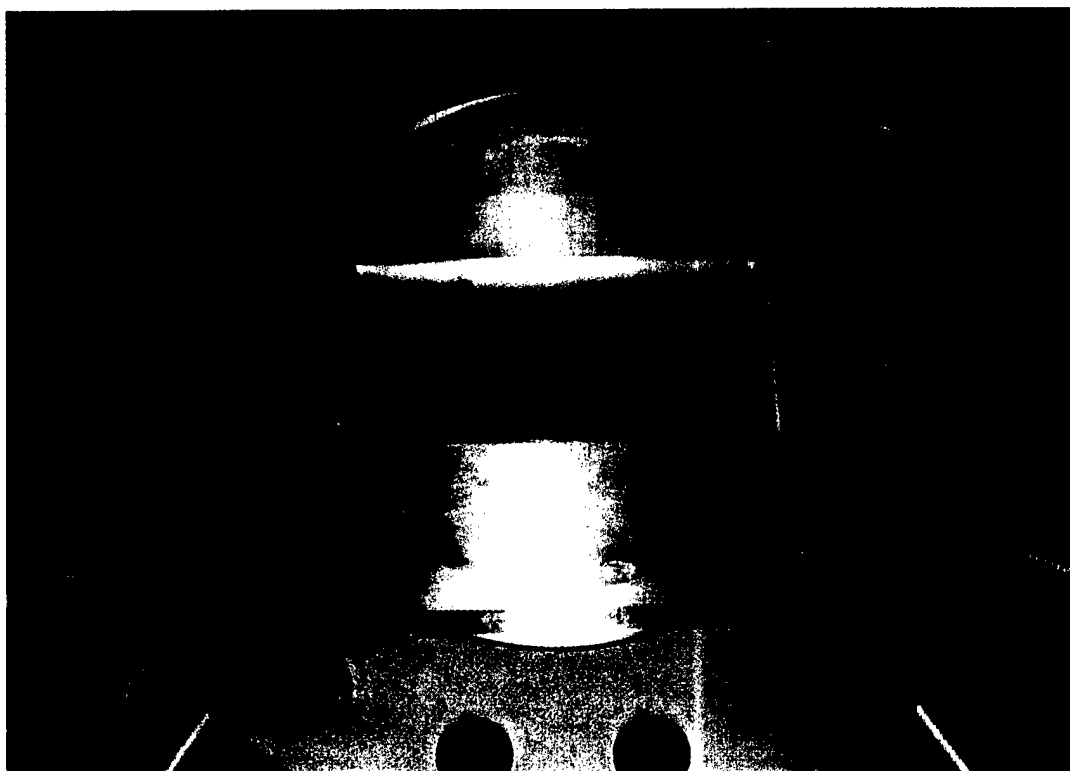


Figure 15. Photograph of Assembled Inlet Transition Flange



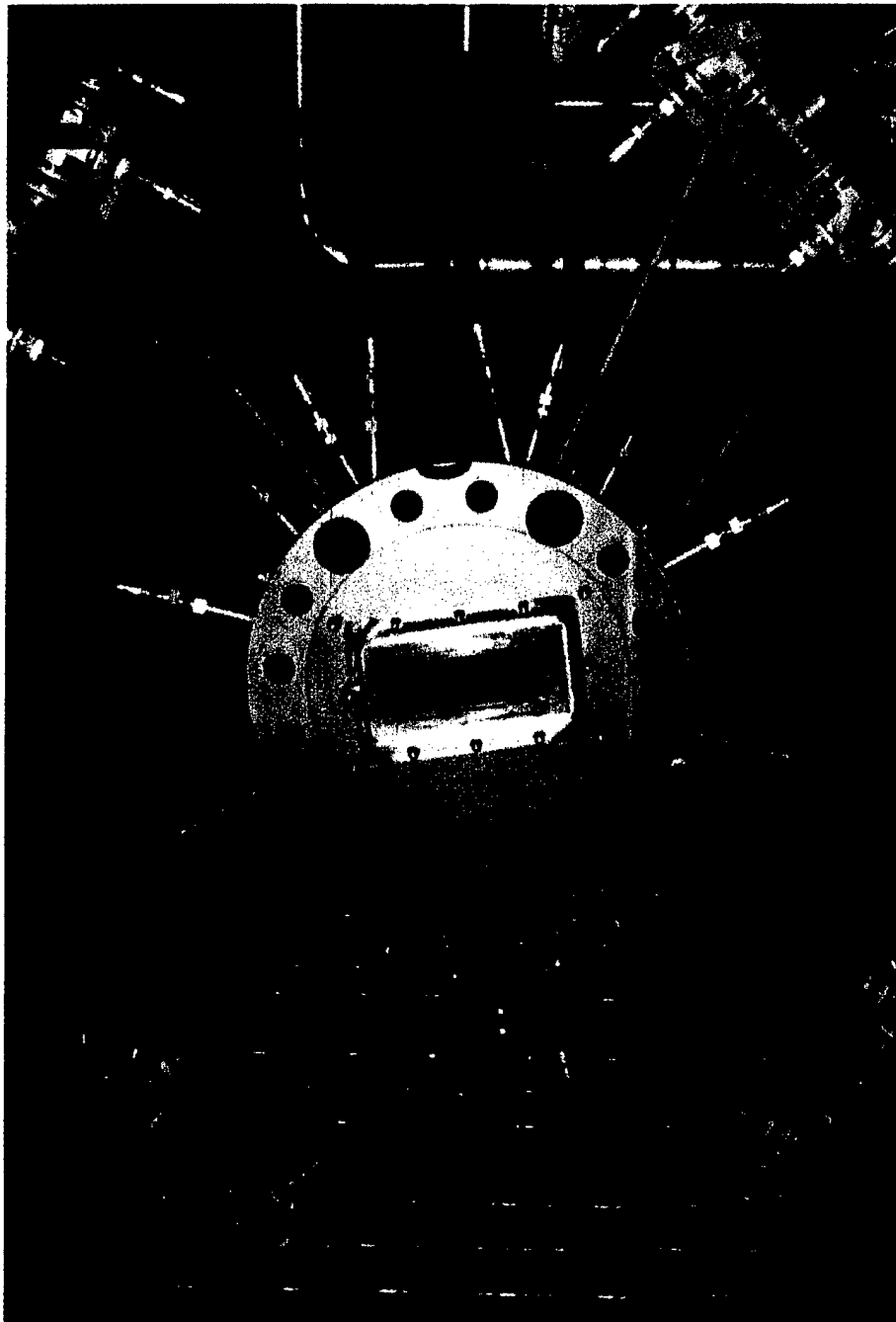


Figure 16. Inlet Transition Flange Assembly Showing Water Cooling Lines and Manifolds

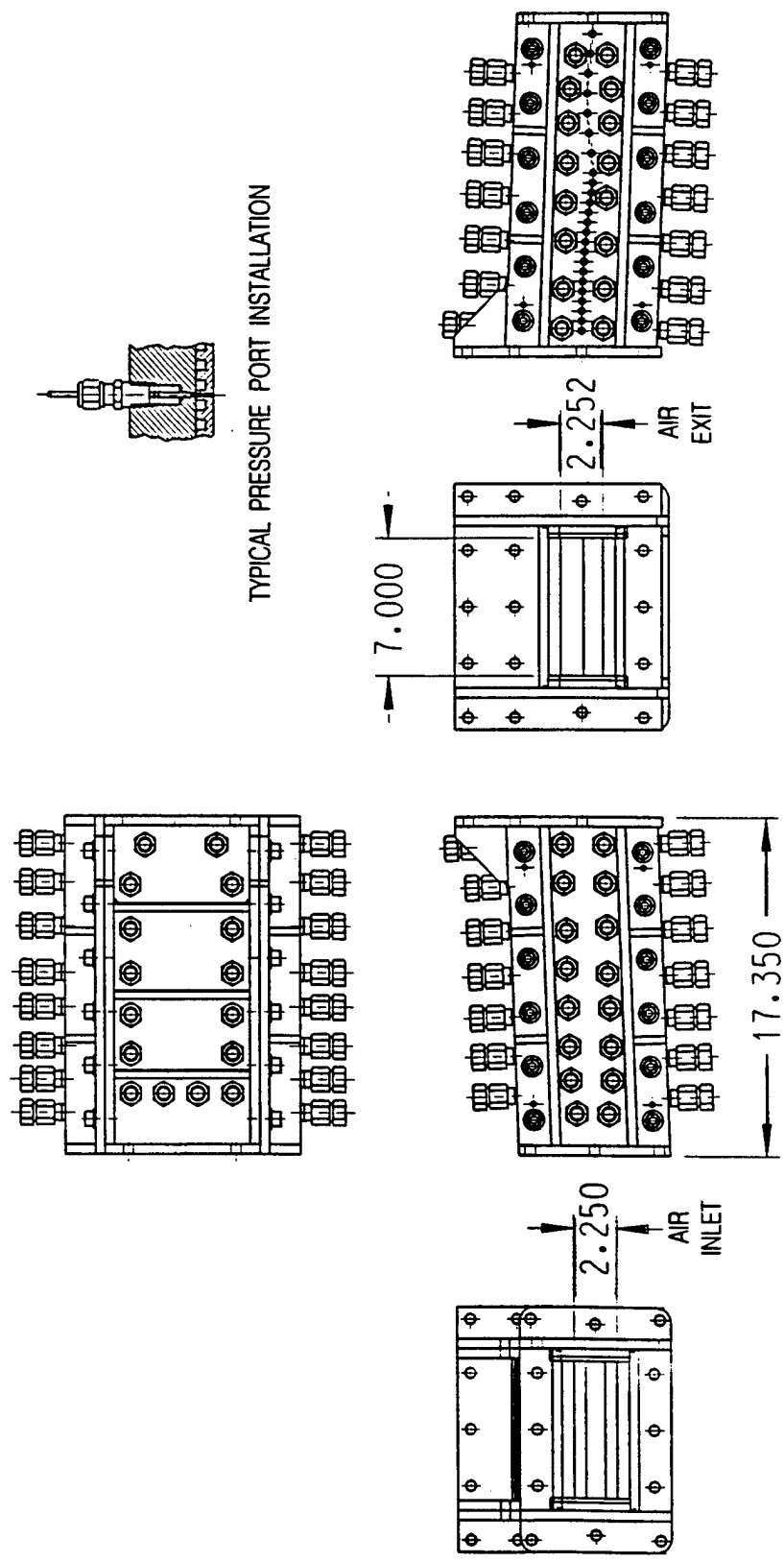


Figure 17. Schematic Diagram of Nozzle Section Showing Flow Channel Dimensions

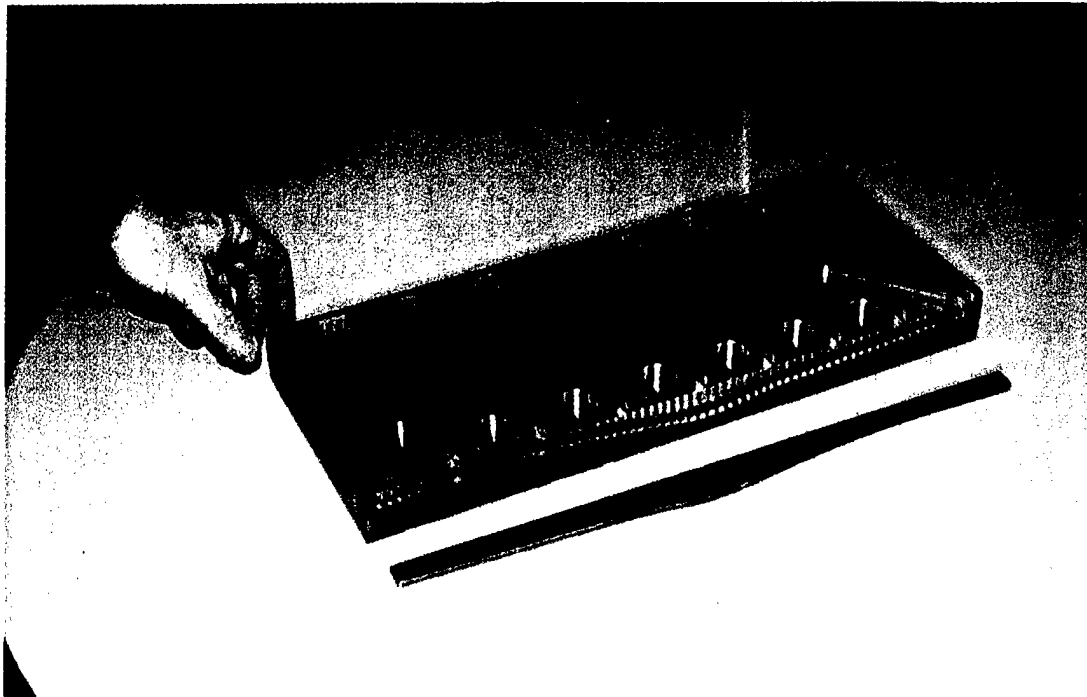


Figure 18. Mach 1.8 Nozzle Section Beryllium Copper Top Wall Showing Coolant Passages and Side Plate

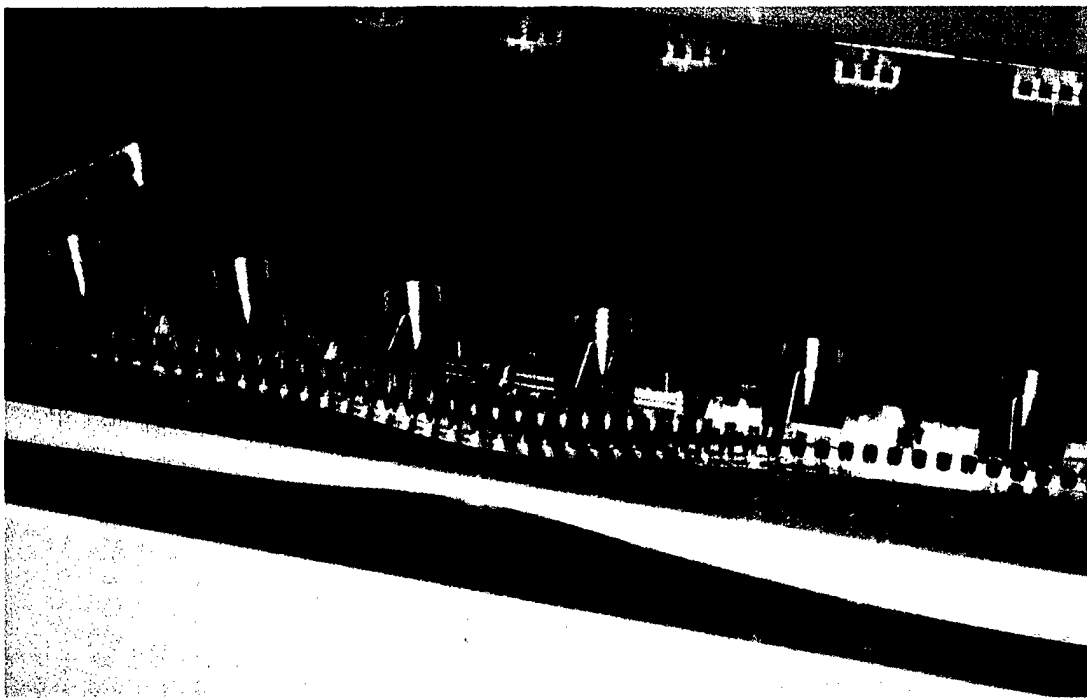


Figure 19. Mach 1.8 Nozzle Section Beryllium Copper Top Wall Showing Coolant Passages and Side Plate

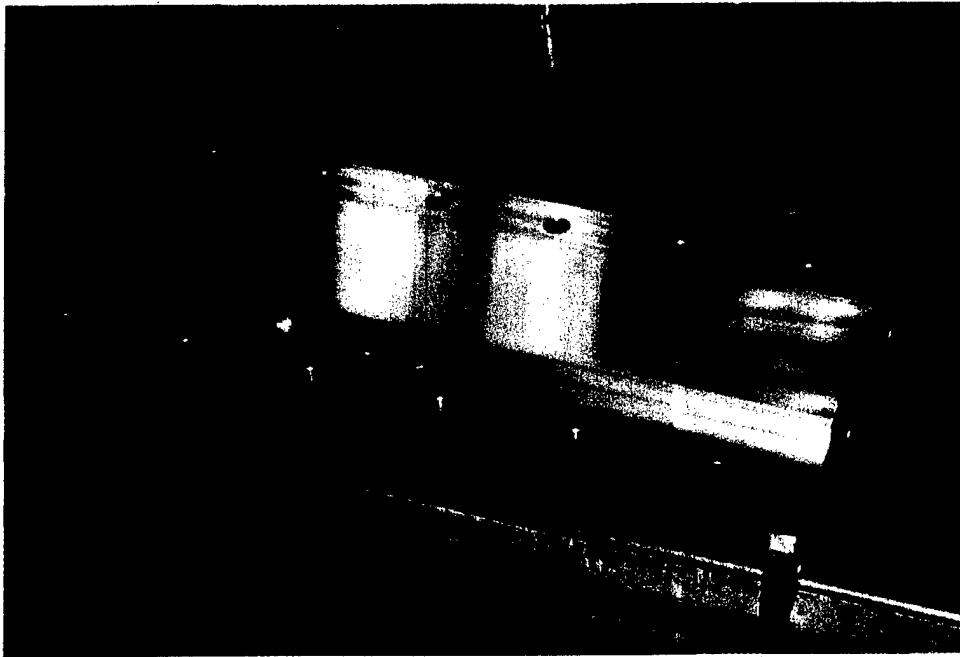


Figure 20. Nozzle Section Side Wall

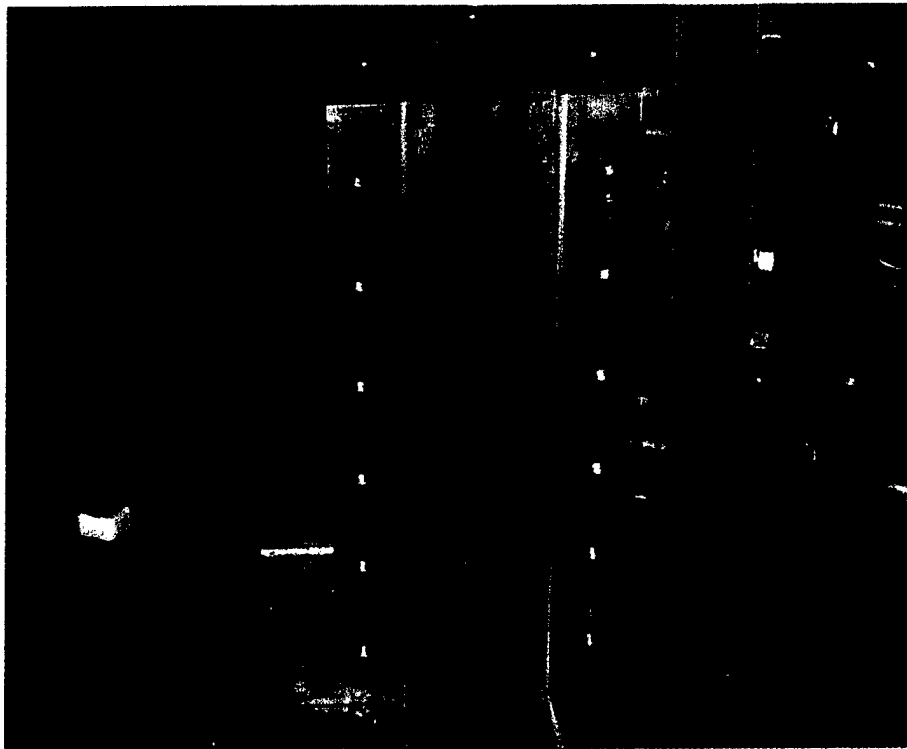


Figure 21. Mach 1.8 Nozzle Section Showing Top and Bottom Wall

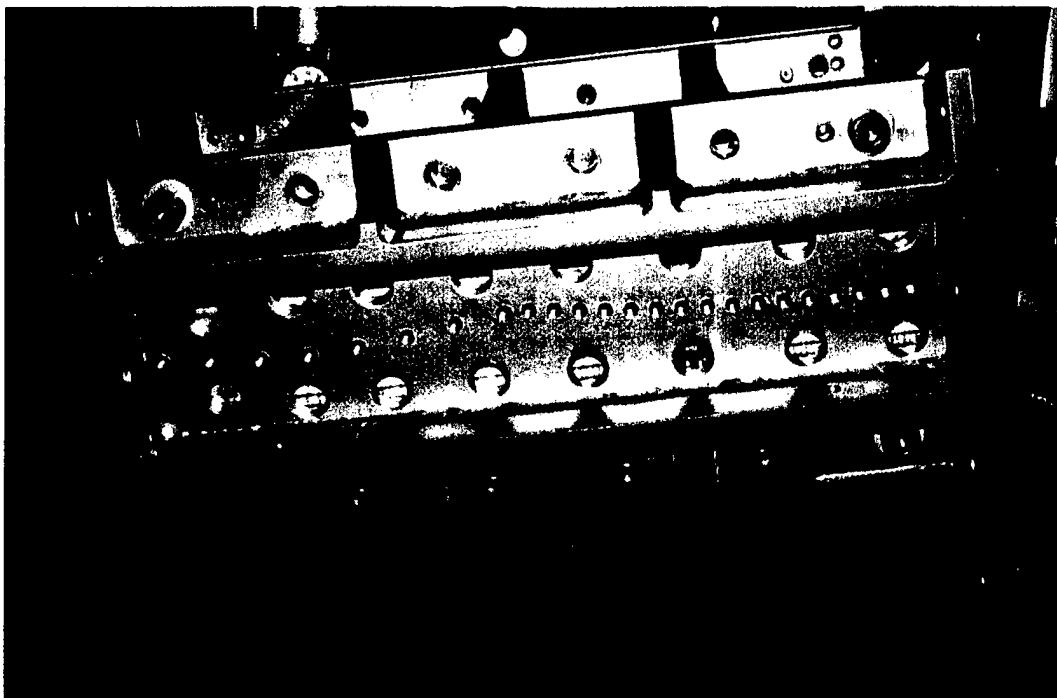


Figure 22. Nozzle Section Showing Side Wall Instrumentation Ports

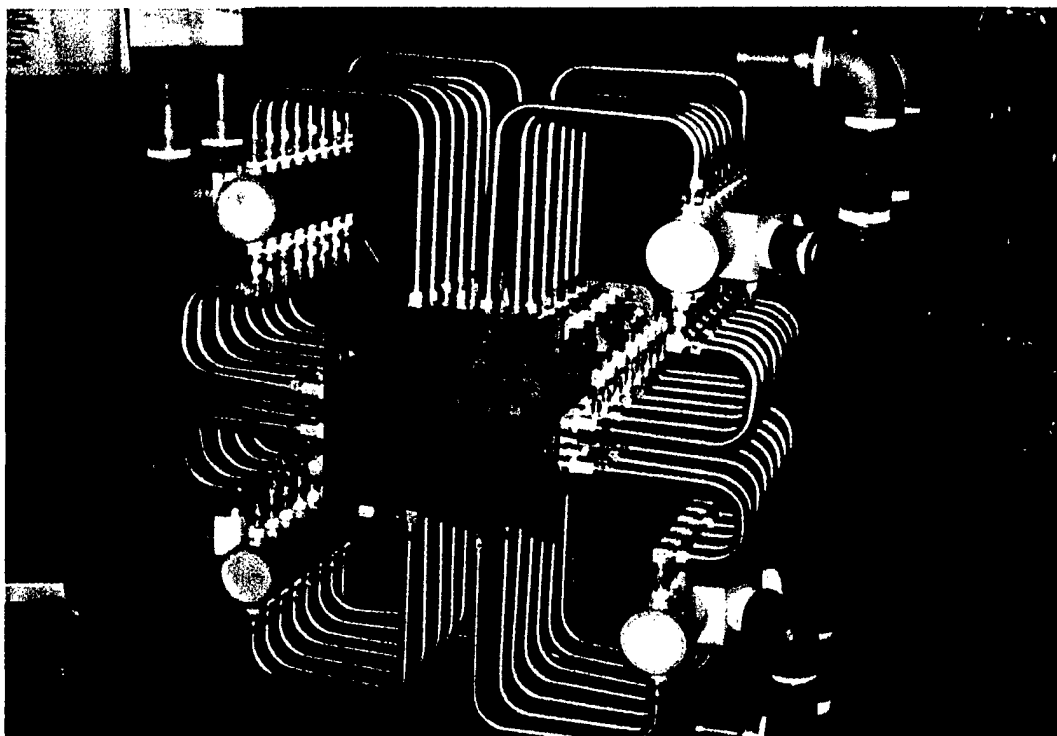


Figure 23. Mach 1.8 Nozzle Section Showing Water Cooling Lines and Manifolds

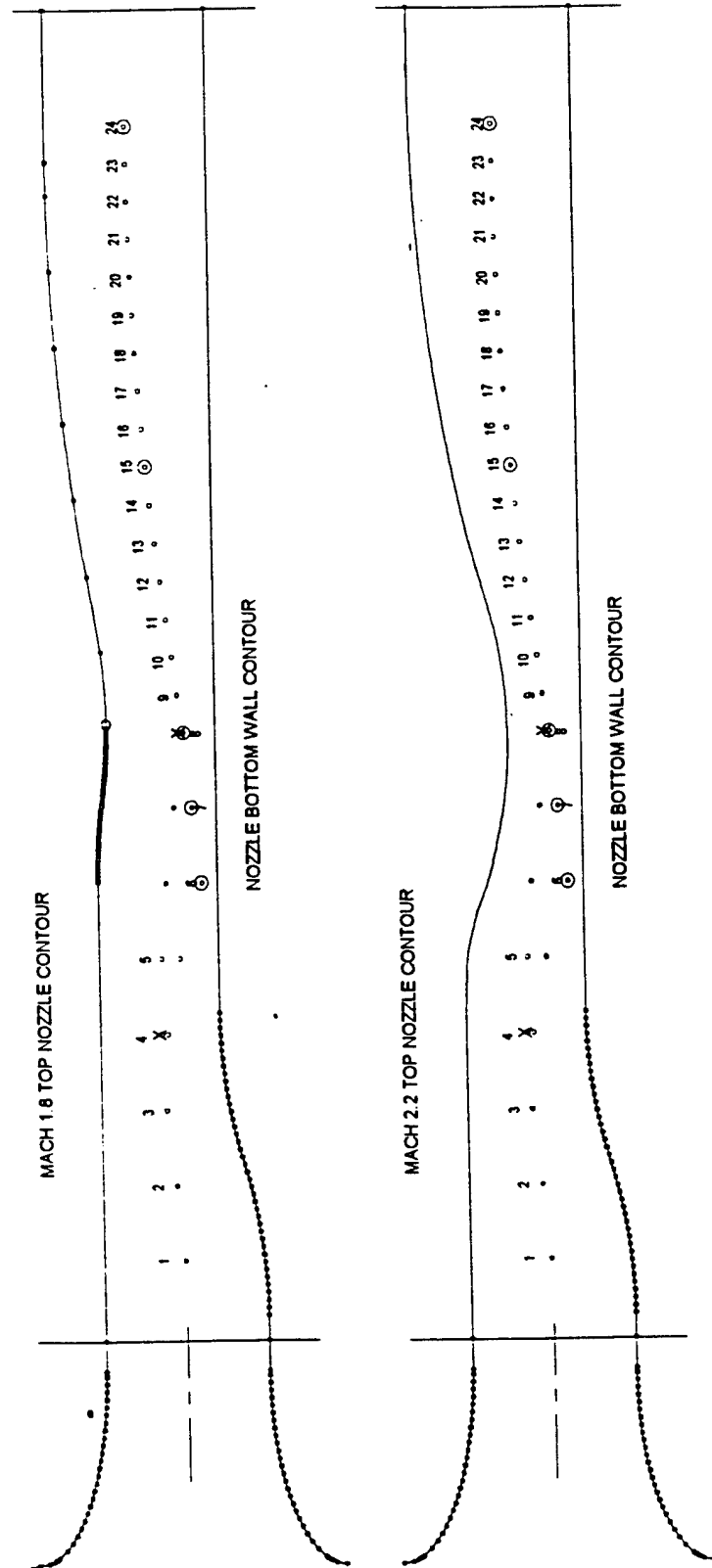


Figure 24. Mach 1.8 and 2.2 Nozzle Contours

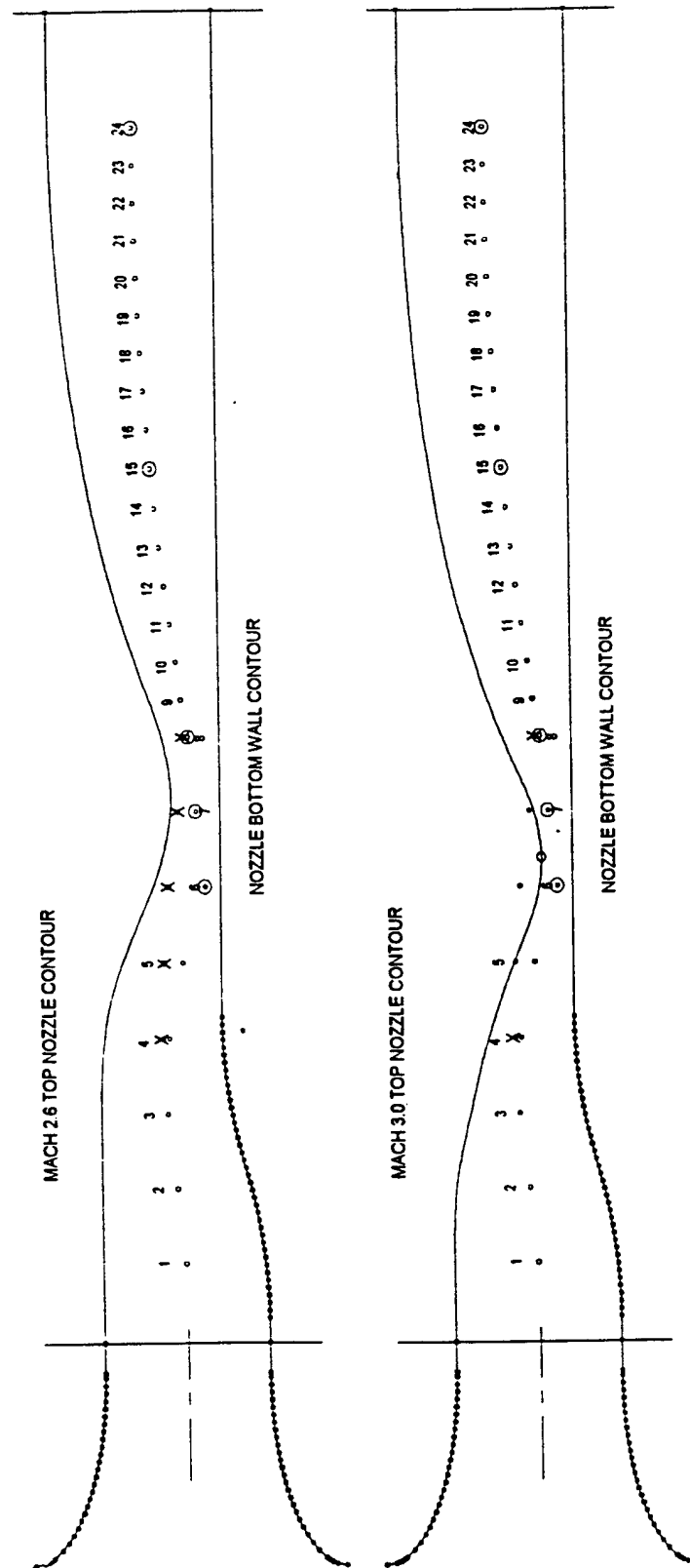
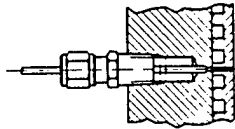
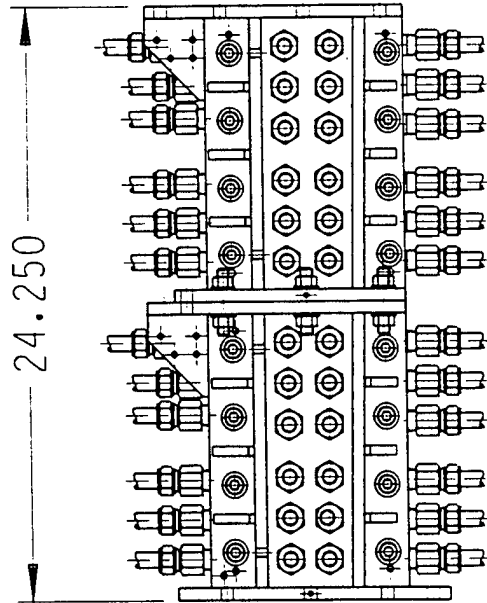
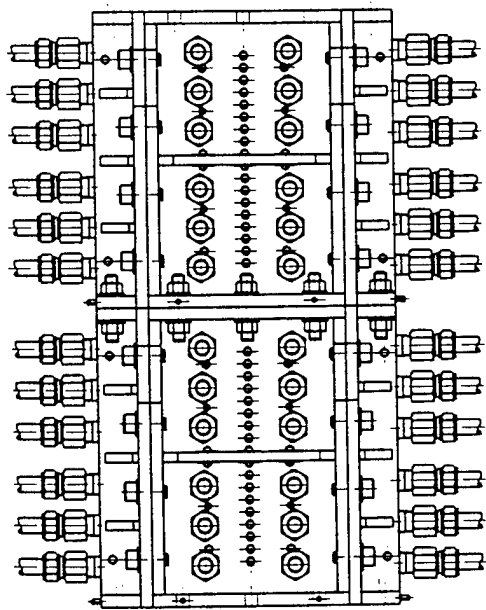


Figure 25. Mach 2.6 and 3.0 Nozzle Contours



TYPICAL PRESSURE PORT INSTALLATION

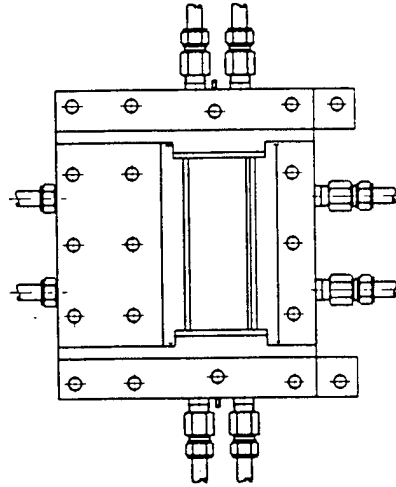


Figure 26. Schematic Diagram of Isolator Sections



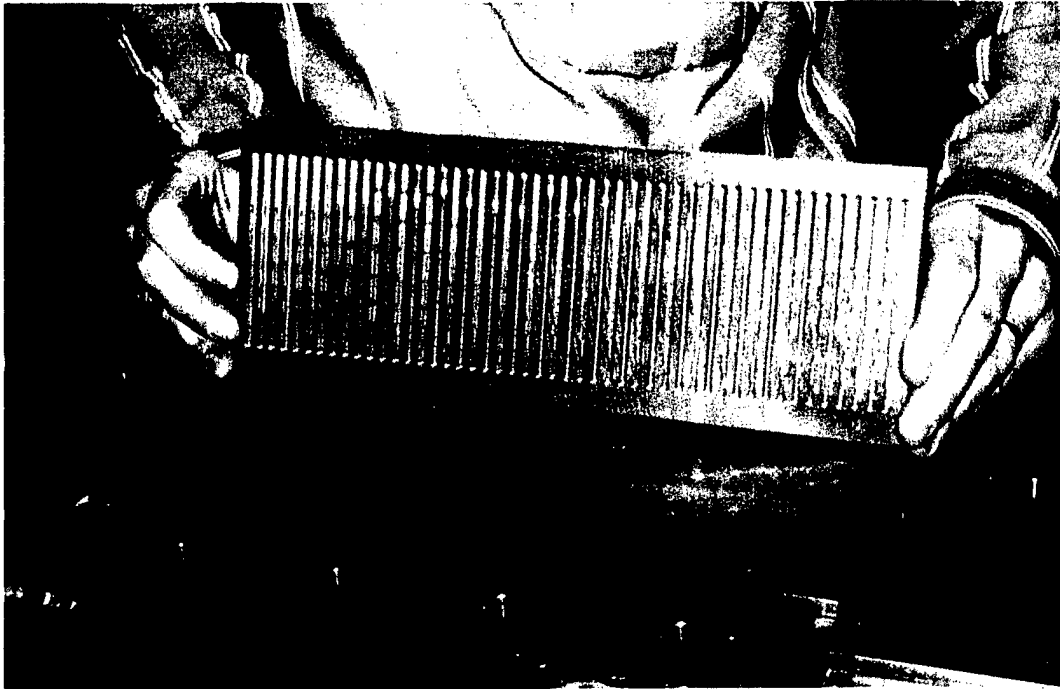


Figure 27. Photograph of Isolator Section Side Wall Oxygen-Free Copper Inner Wall Plate

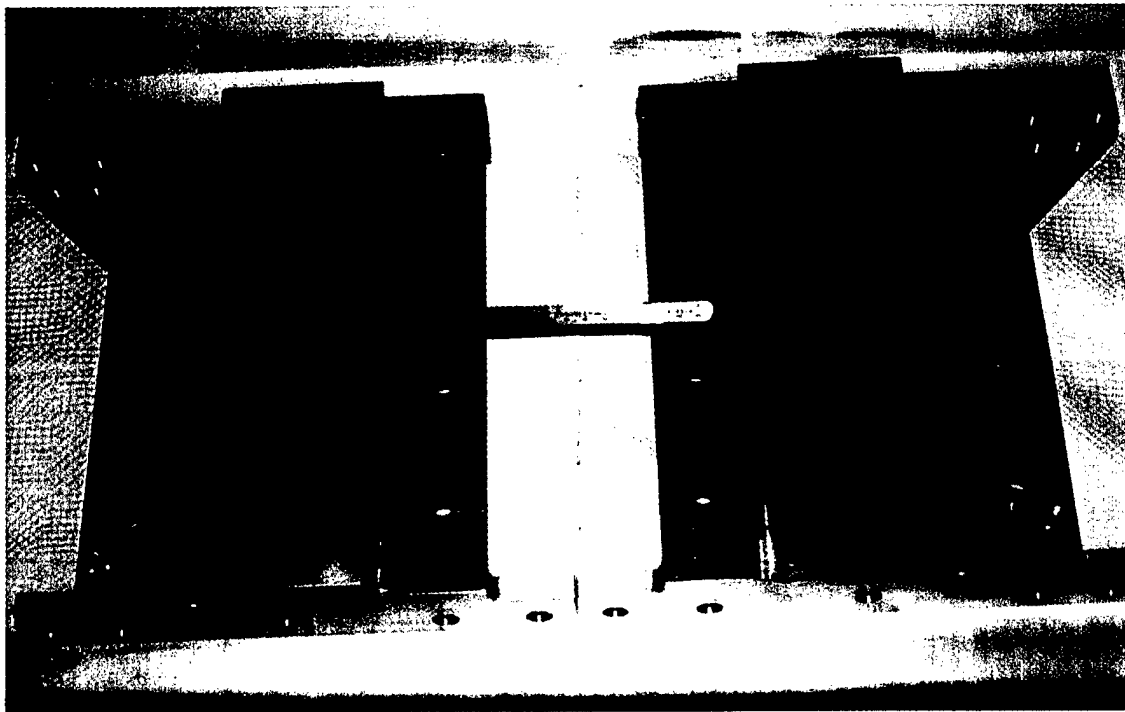


Figure 28. Photograph of Finished Isolator Section Side Walls

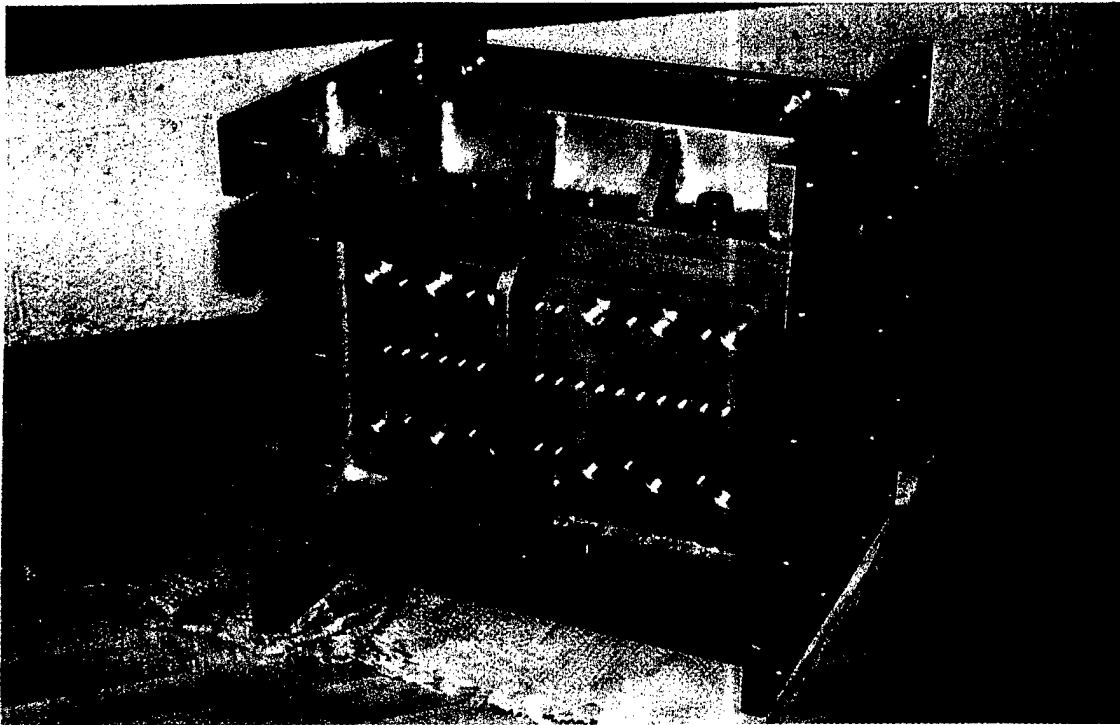


Figure 29. Assembled Isolator Section Showing Pressure Instrumentation Ports

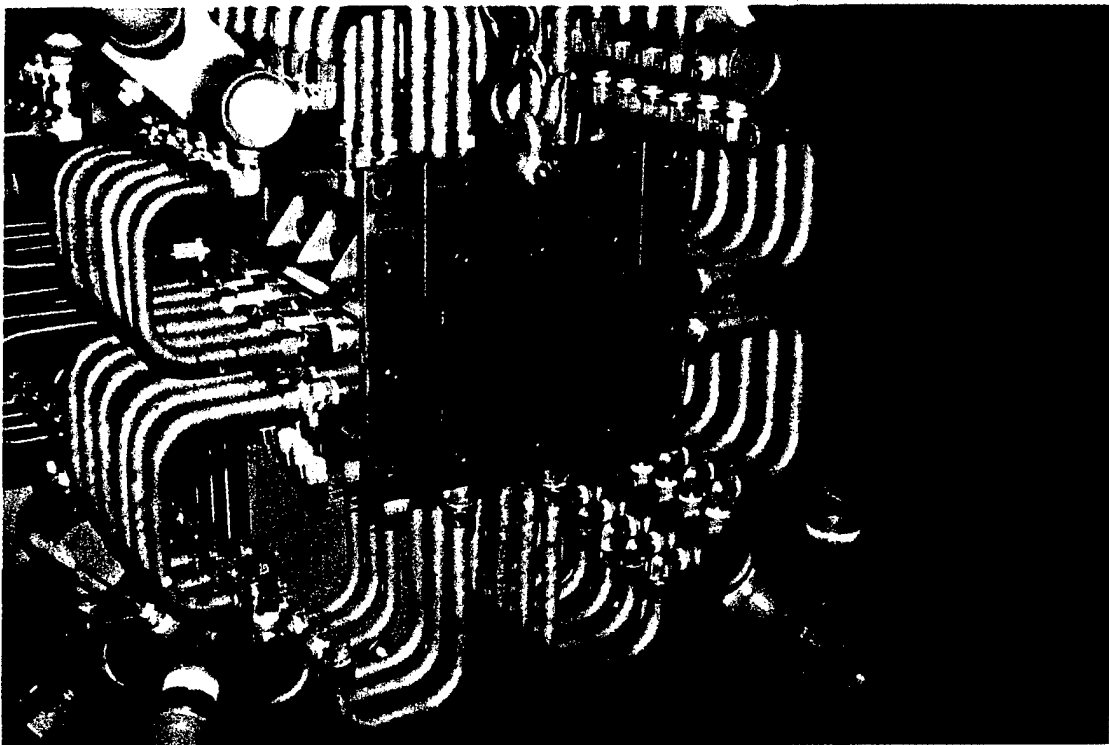


Figure 30. Isolator Section with Water Cooling Lines and Manifolds

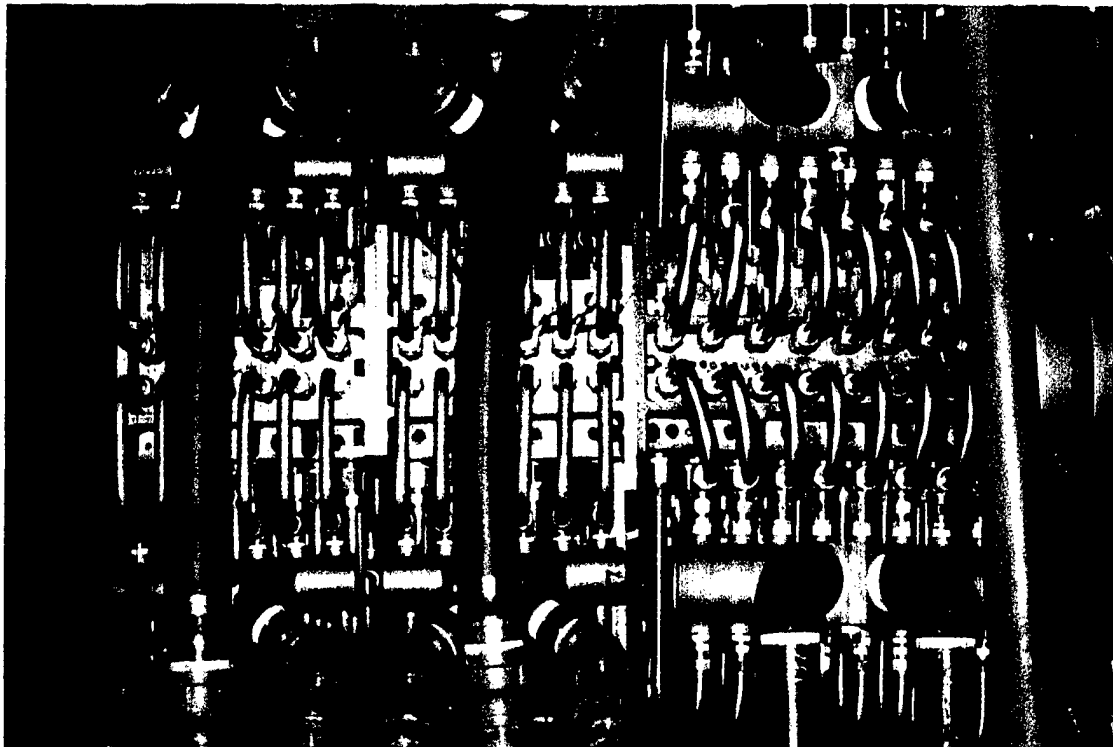


Figure 31. Photograph of Mach 1.8 Nozzle Section and Two Isolator Sections Mounted On Test Cell 22 Thrust Stand



Figure 32. Facility Calibration Section Showing Traversing Probe Mounting Bosses

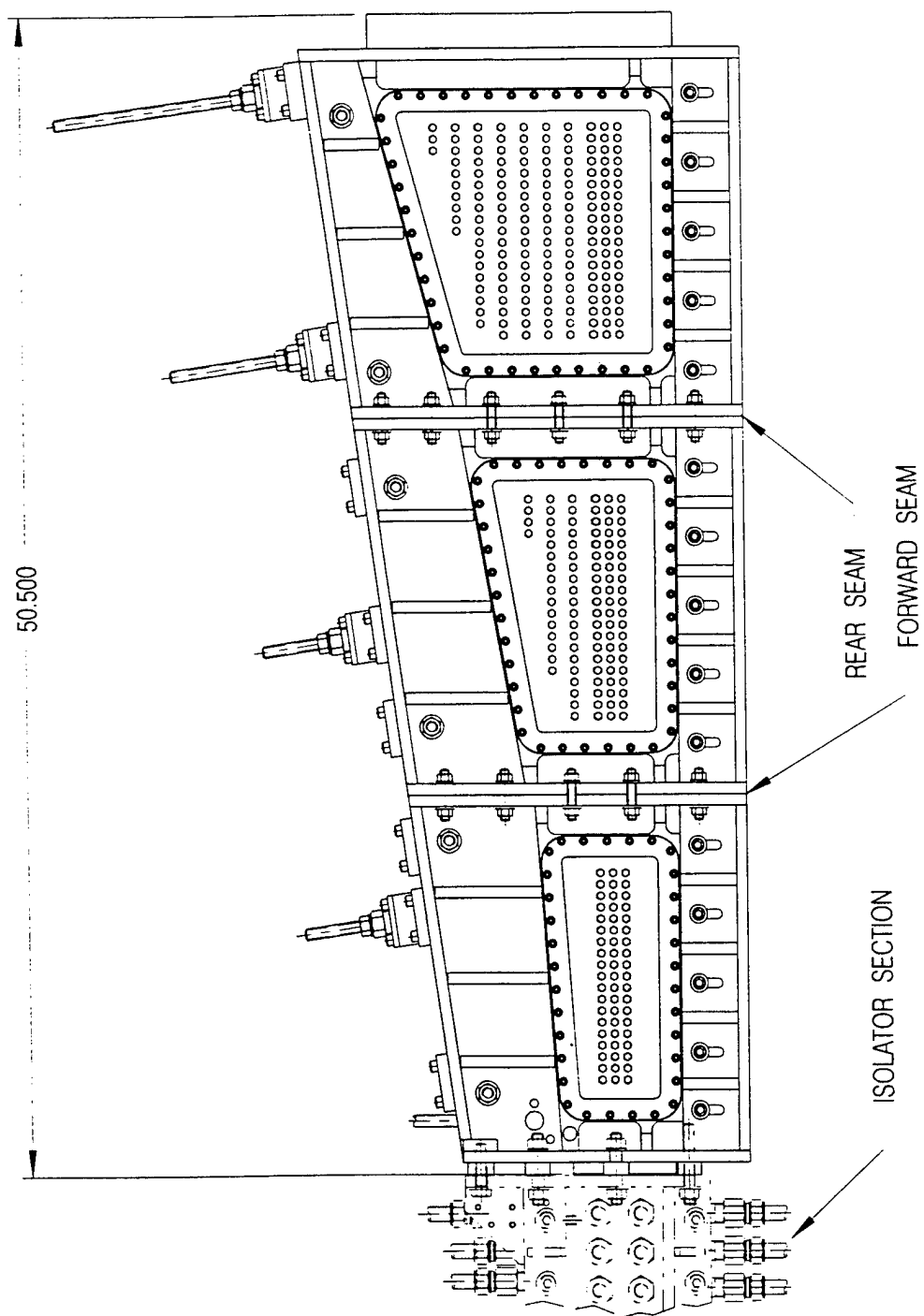


Figure 33. Schematic Diagram of Scramjet Test Rig Heat-Sink Combustor Section

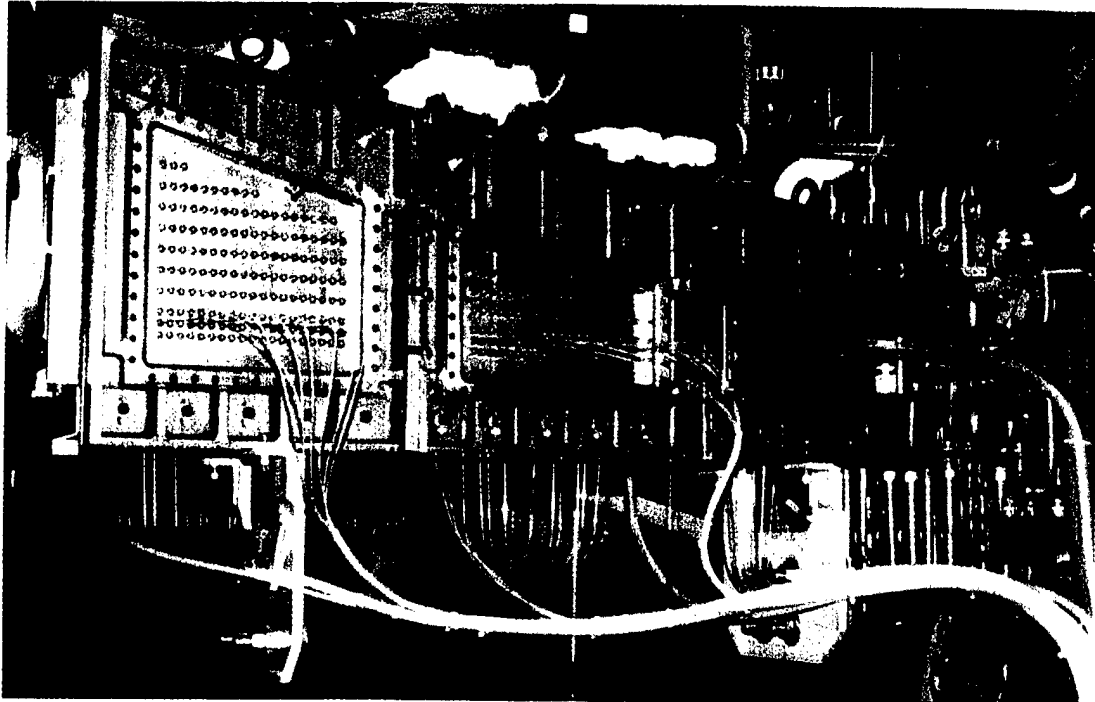


Figure 34. Photograph of Scramjet Heat-Sink Combustor Section (Flow from Right to Left) Showing the Three Side Wall Sections and Instrumentation Ports

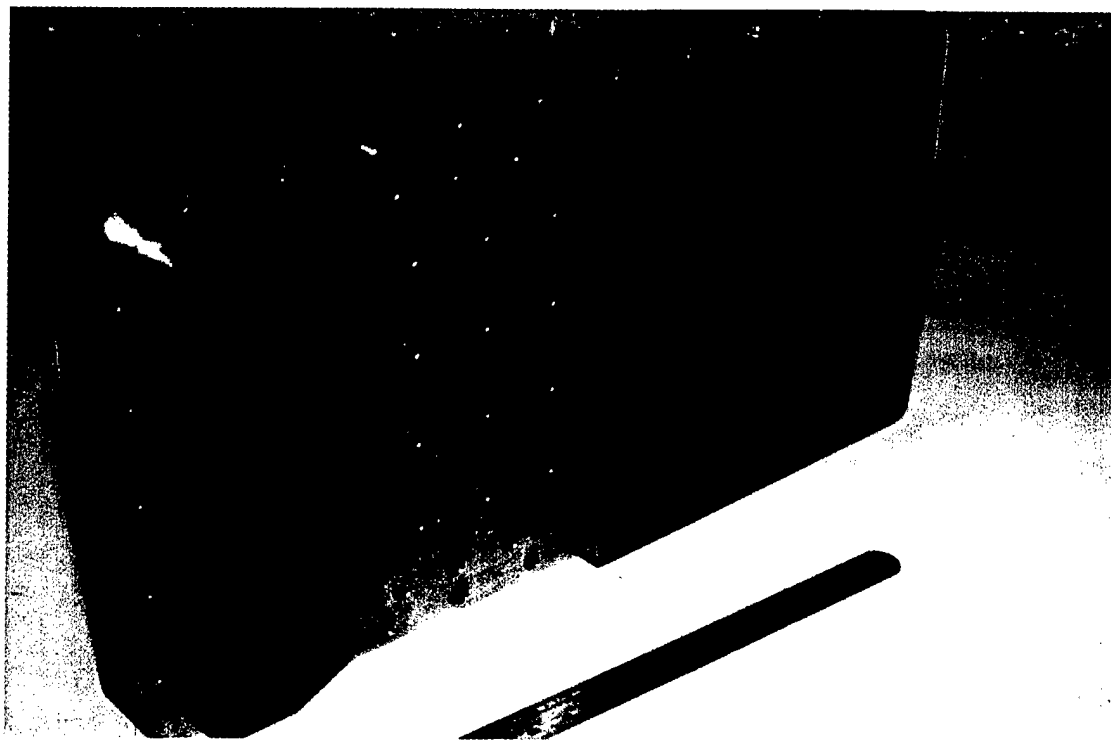


Figure 35. Fuel Injection/Flame-Holder Insert

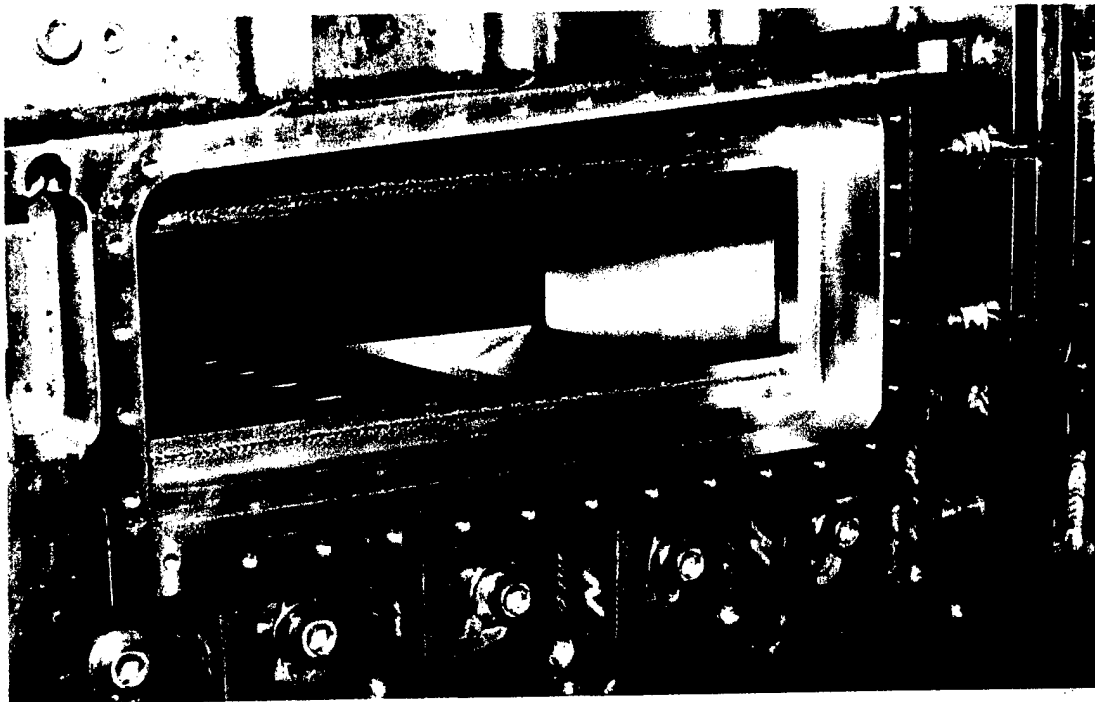


Figure 36. Fuel Injection/Flame-Holder Insert Mounted In Bottom Wall of the Heat-Sink Combustor Forward Section (Side Wall Insert Removed)

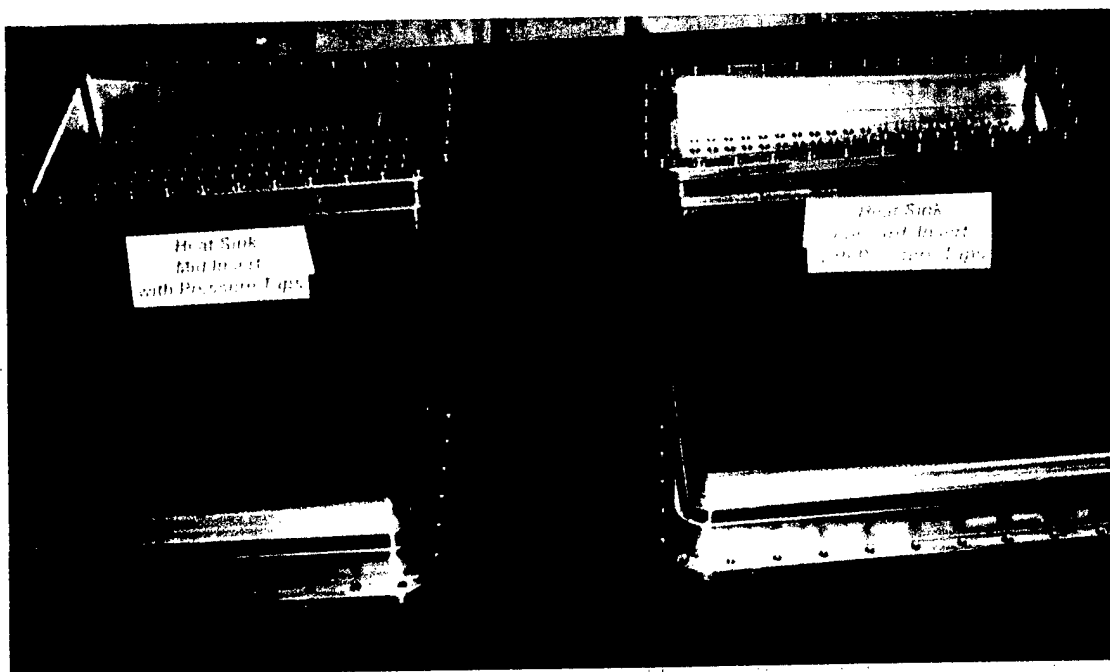


Figure 37. Heat-Sink Combustor side Wall frames and Inserts

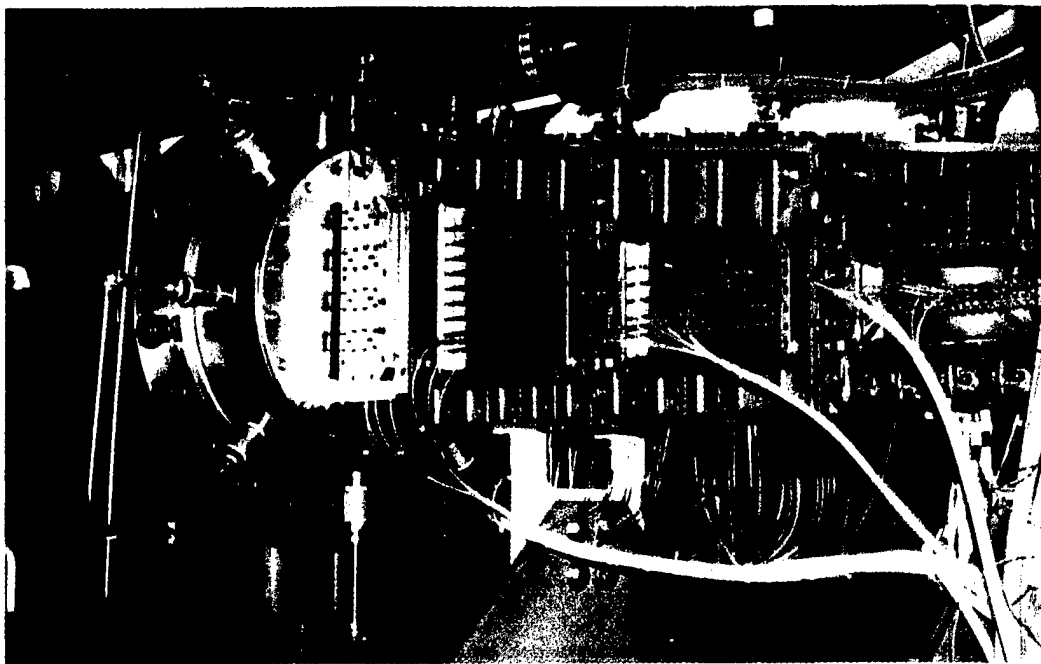


Figure 38. Heat-Sink Combustor/Calorimeter Transition Section

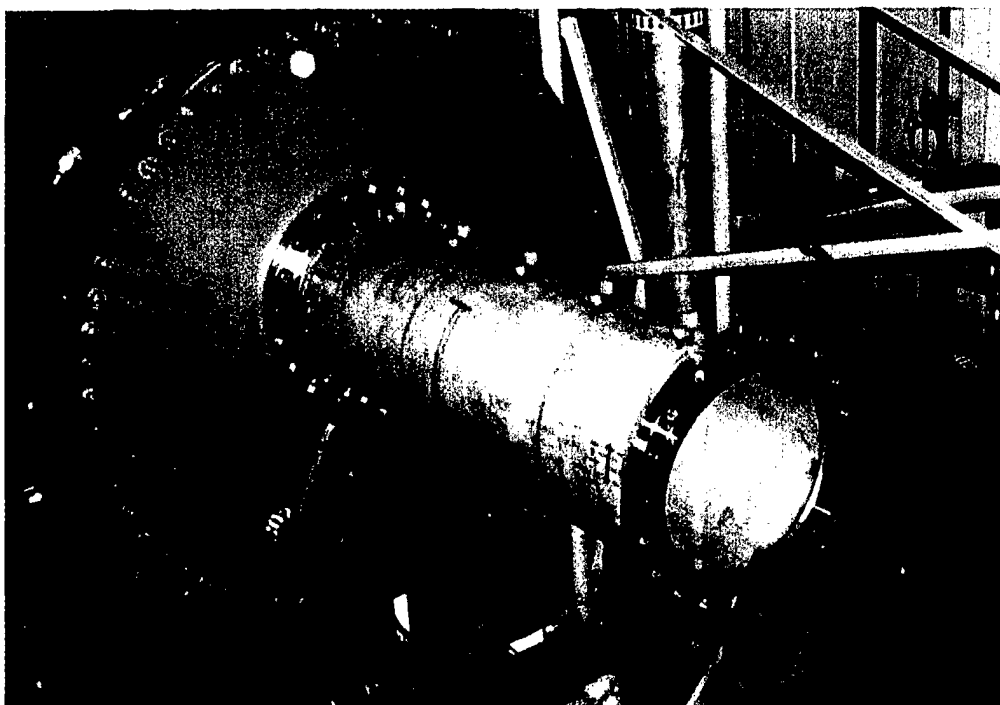


Figure 39. Facility Calorimeter Section Mounted on Exhaust Elbow

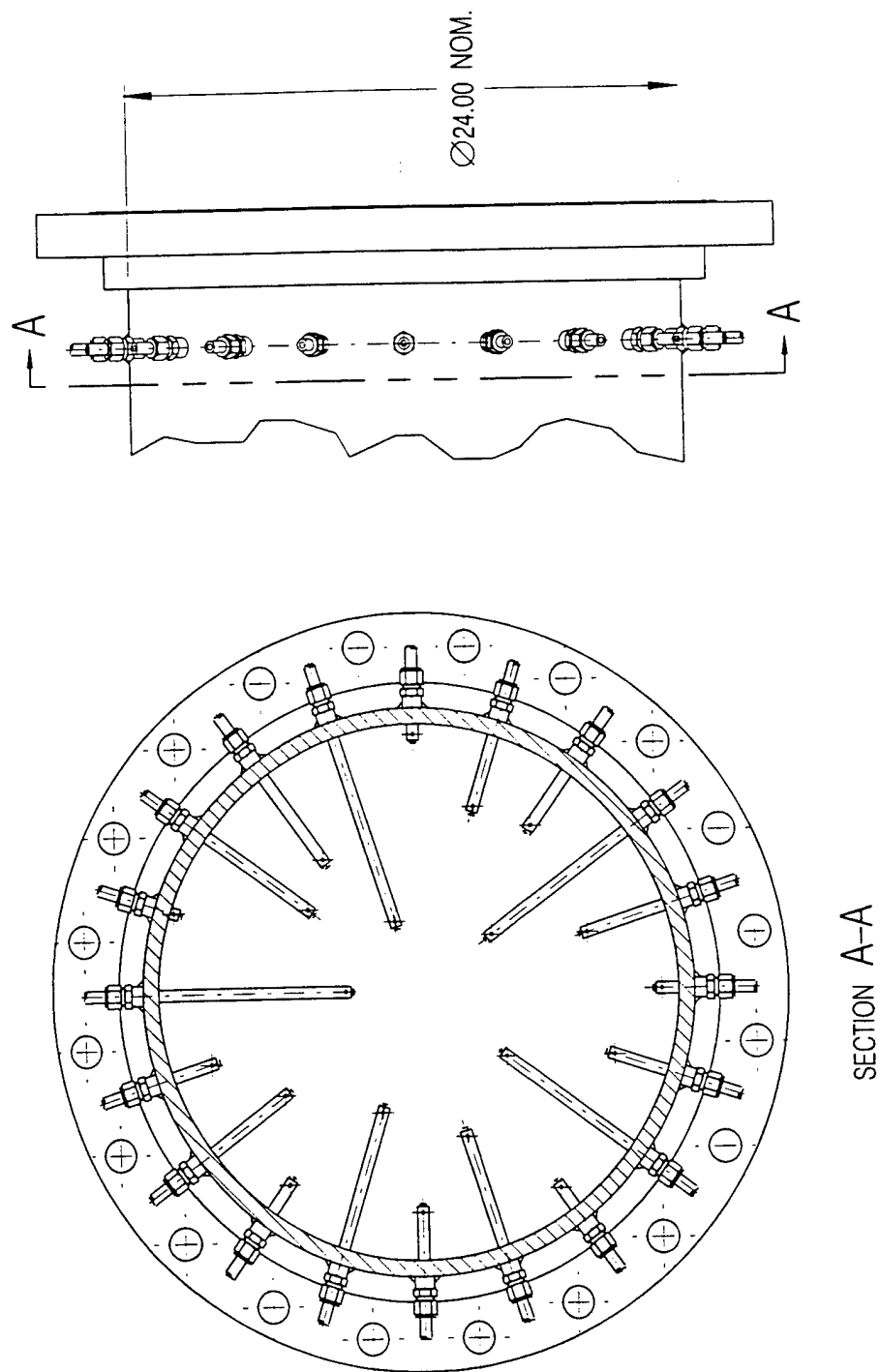


Figure 40. Calorimeter Thermocouple Array



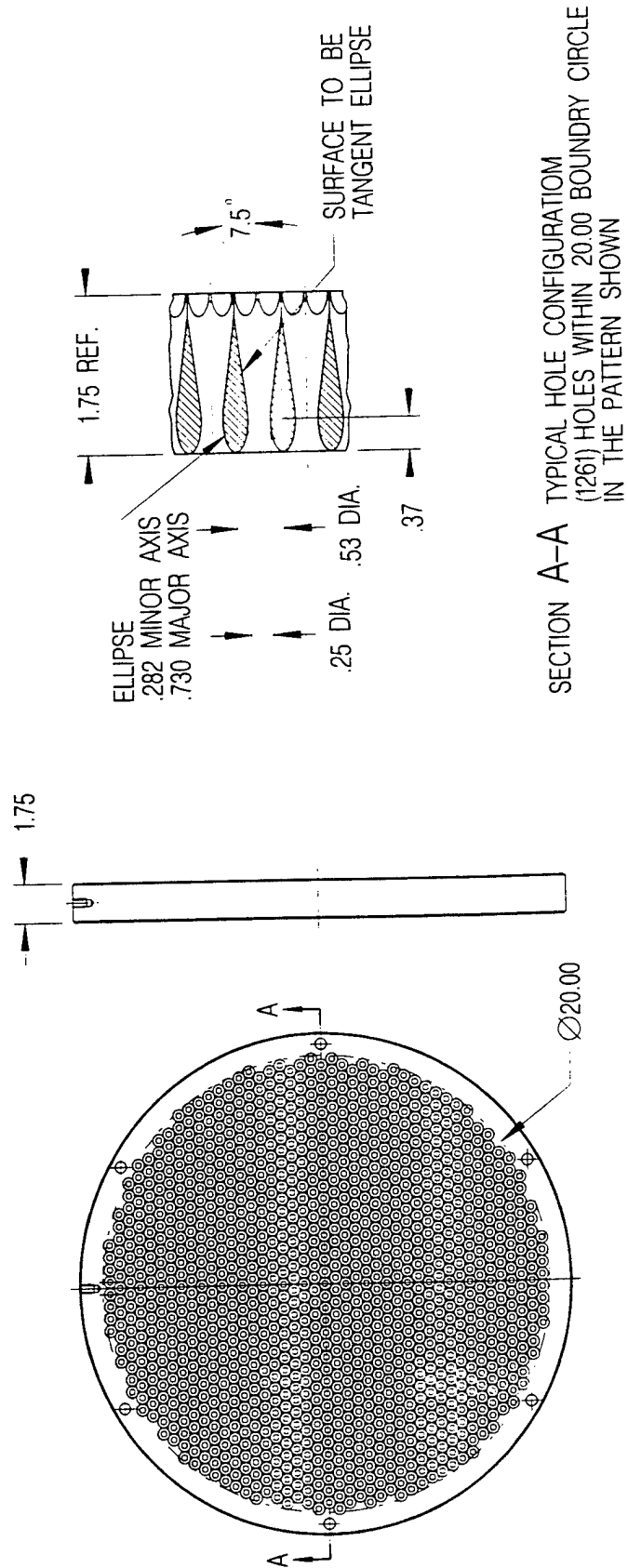


Figure 41. Calorimeter Aero-Grid

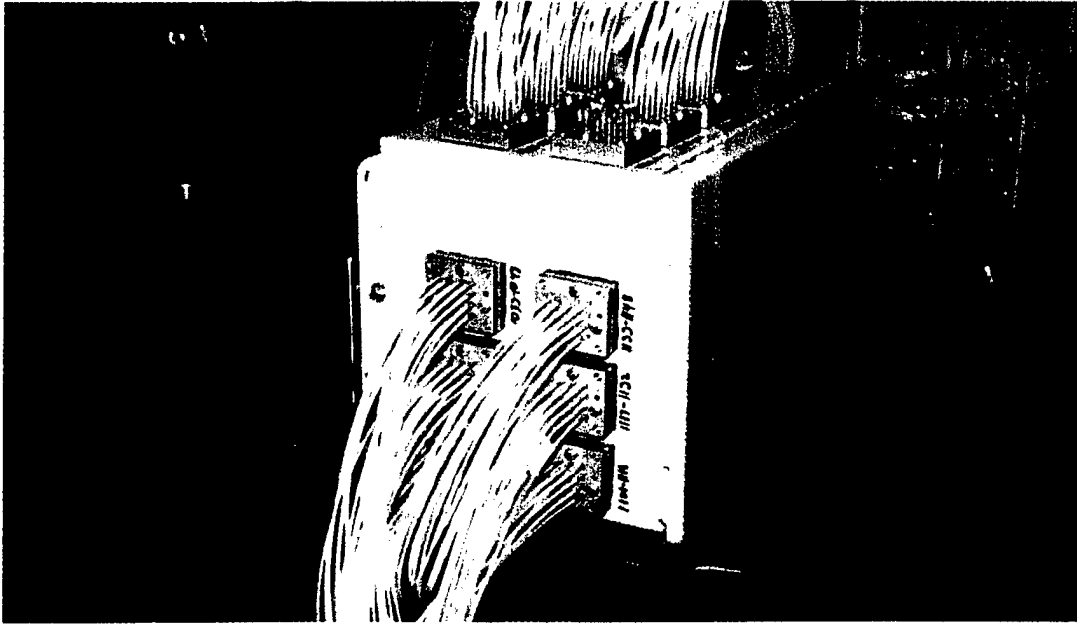


Figure 42. PSI Pressure Measurement Terminal Box

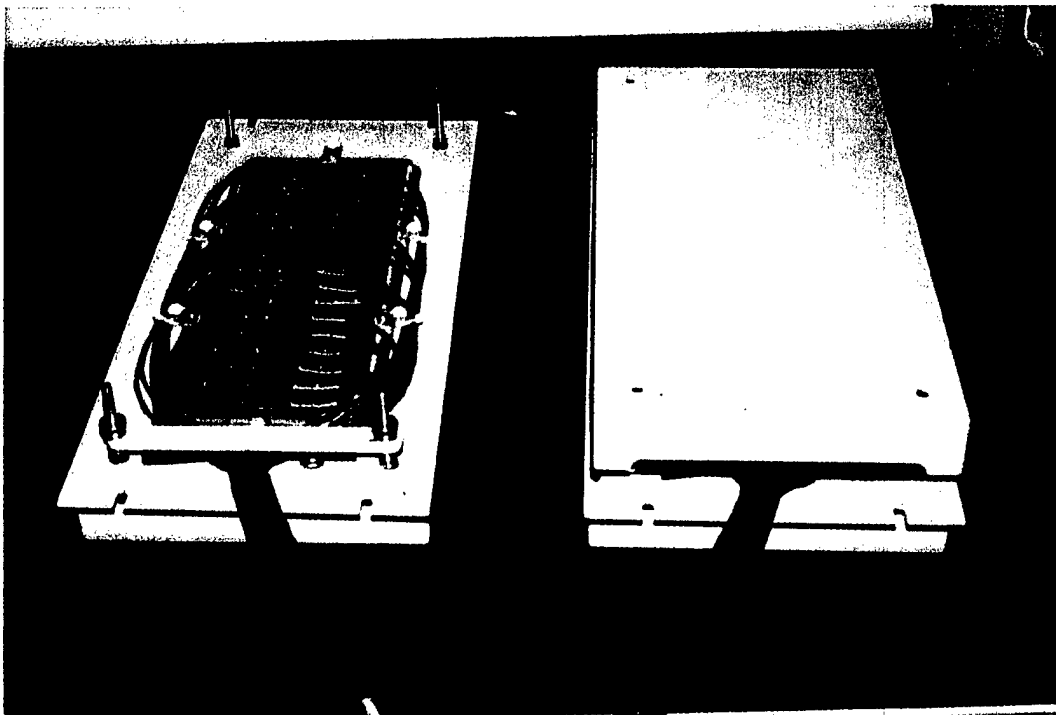


Figure 43. Thermocouple Reference Junction Boxes

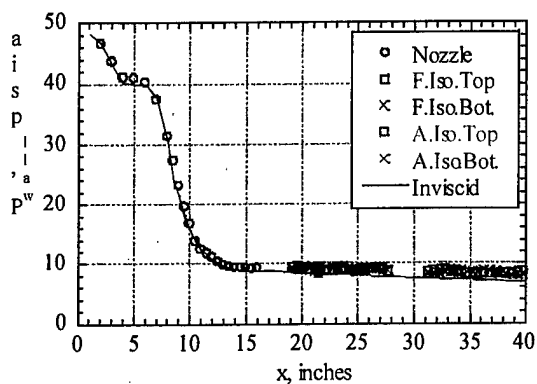


Figure 44 Nozzle-Isolator Pressure Distributions at  $M_0 = 4$ ,  $Q_0 = 1000$  psf ( $p_e/p_i = 0.88$ )

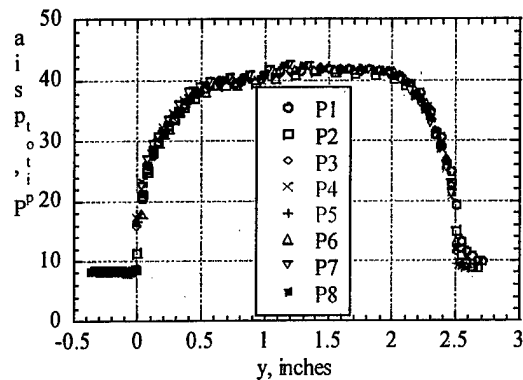


Figure 45 Isolator Exit Pitot Pressure Distribution at  $M_0 = 4$ ,  $Q_0 = 1000$  psf ( $p_e/p_i = 0.88$ )

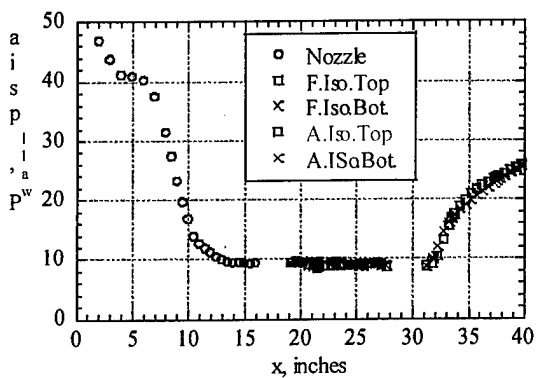


Figure 46 Nozzle-Isolator Pressure Distributions at  $M_0 = 4$ ,  $Q_0 = 1000$  psf ( $p_e/p_i = 2.74$ )

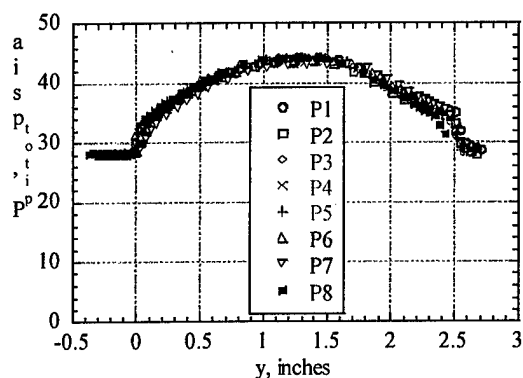


Figure 47 Isolator Exit Pitot Pressure Distribution at  $M_0 = 4$ ,  $Q_0 = 1000$  psf ( $p_e/p_i = 2.74$ )

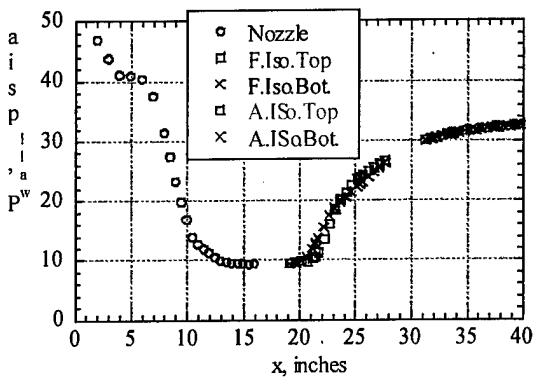


Figure 48 Nozzle-Isolator Pressure Distributions at  $M_0 = 4$ ,  $Q_0 = 1000$  psf ( $p_e/p_i = 3.46$ )

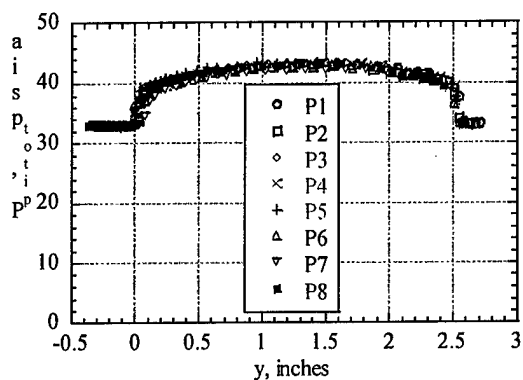


Figure 49 Isolator Exit Pitot Pressure Distribution at  $M_0 = 4$ ,  $Q_0 = 1000$  psf ( $p_e/p_i = 3.46$ )

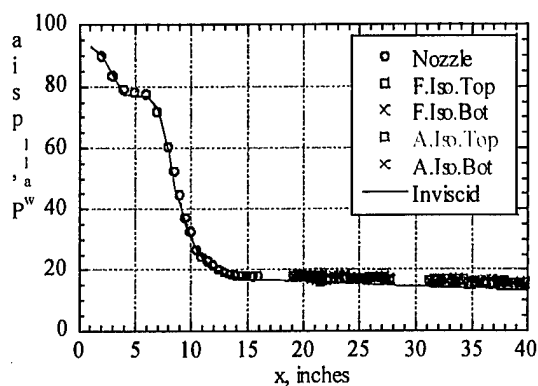


Figure 50 Nozzle-Isolator Pressure Distributions at  $M_0 = 4$ ,  $Q_0 = 2000$  psf ( $p_e/p_i = 0.86$ )

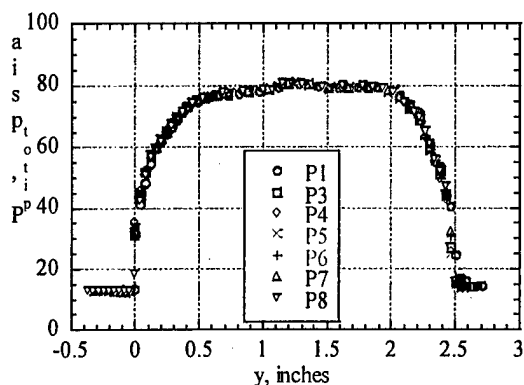


Figure 51 Isolator Exit Pitot Pressure Distribution at  $M_0 = 4$ ,  $Q_0 = 2000$  psf ( $p_e/p_i = 0.86$ )

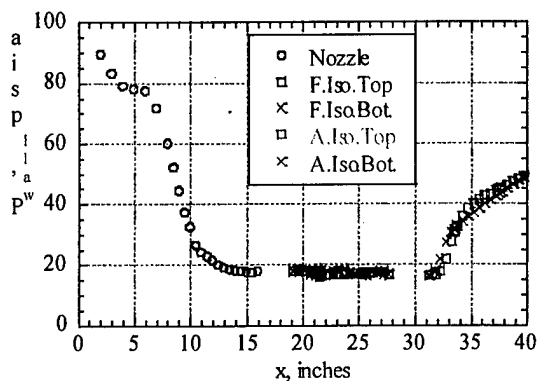


Figure 52 Nozzle-Isolator Pressure Distributions at  $M_0 = 4$ ,  $Q_0 = 2000$  psf ( $p_e/p_i = 2.72$ )

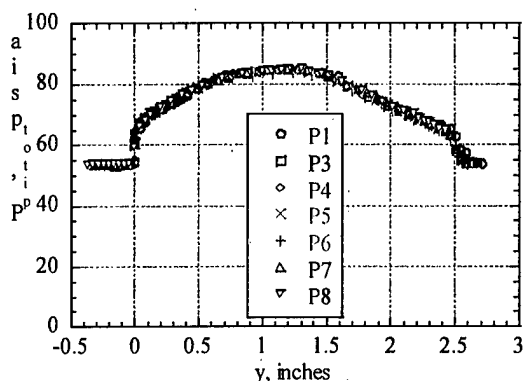


Figure 53 Isolator Exit Pitot Pressure Distribution at  $M_0 = 4$ ,  $Q_0 = 2000$  psf ( $p_e/p_i = 2.72$ )

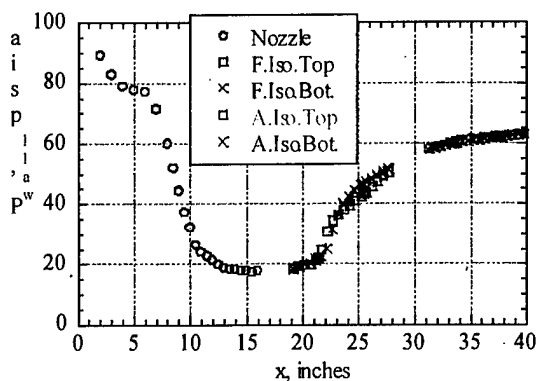


Figure 54 Nozzle-Isolator Pressure Distributions at  $M_0 = 4$ ,  $Q_0 = 2000$  psf ( $p_e/p_i = 3.40$ )

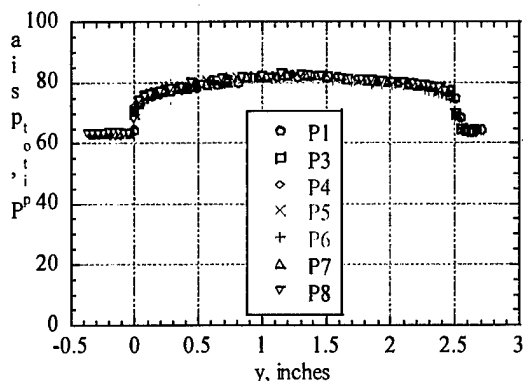


Figure 55 Isolator Exit Pitot Pressure Distribution at  $M_0 = 4$ ,  $Q_0 = 2000$  psf ( $p_e/p_i = 3.40$ )

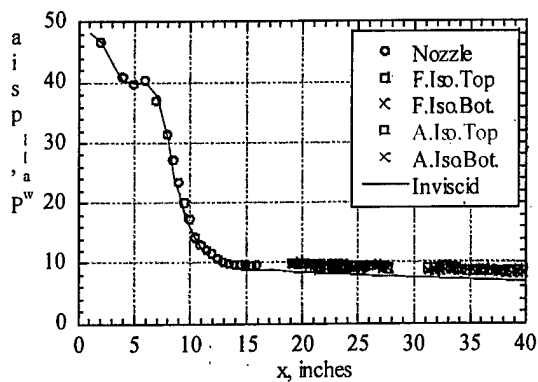


Figure 56 Nozzle-Isolator Pressure Distributions at  $M_0 = 5$ ,  $Q_0 = 1000$  psf ( $p_e/p_i = 0.87$ )

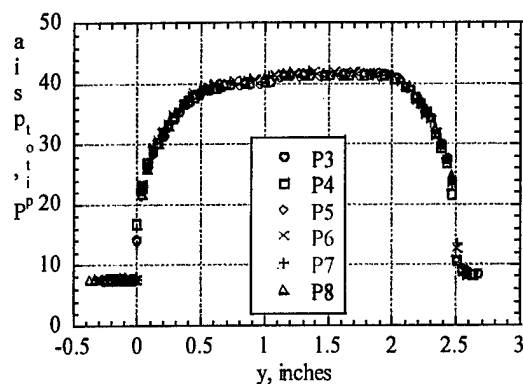


Figure 57 Isolator Exit Pitot Pressure Distribution at  $M_0 = 5$ ,  $Q_0 = 1000$  psf ( $p_e/p_i = 0.87$ )

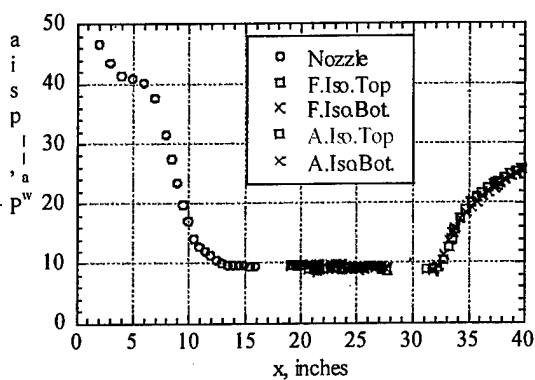


Figure 58 Nozzle-Isolator Pressure Distributions at  $M_0 = 5$ ,  $Q_0 = 1000$  psf ( $p_e/p_i = 2.68$ )

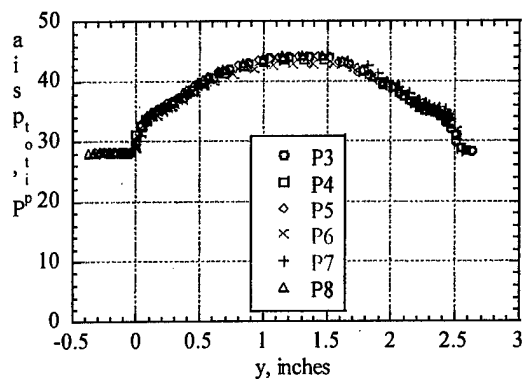


Figure 59 Isolator Exit Pitot Pressure Distribution at  $M_0 = 5$ ,  $Q_0 = 1000$  psf ( $p_e/p_i = 2.68$ )

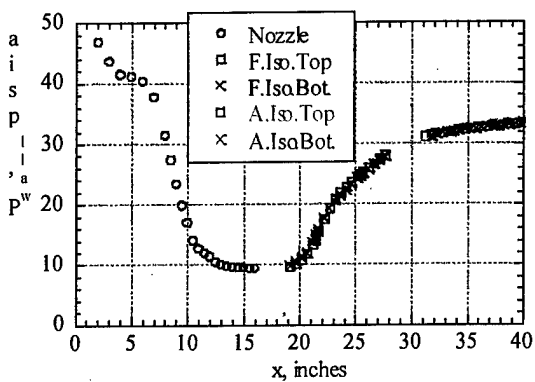


Figure 60 Nozzle-Isolator Pressure Distributions at  $M_0 = 5$ ,  $Q_0 = 1000$  psf ( $p_e/p_i = 3.39$ )

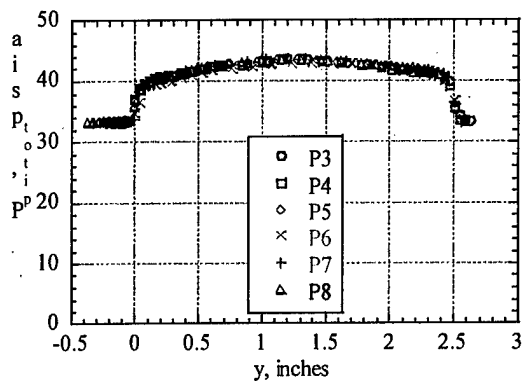


Figure 61 Isolator Exit Pitot Pressure Distribution at  $M_0 = 5$ ,  $Q_0 = 1000$  psf ( $p_e/p_i = 3.39$ )

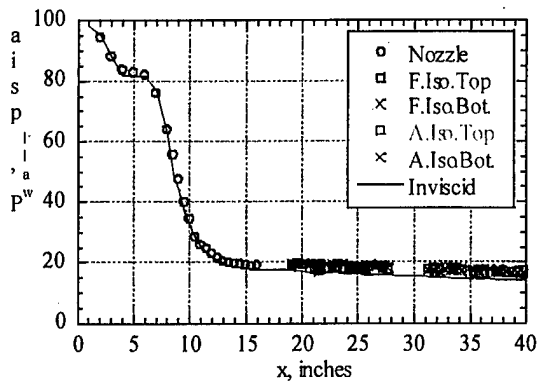


Figure 62 Nozzle-Isolator Pressure Distributions at  $M_0 = 5$ ,  $Q_0 = 2000$  psf ( $p_e/p_i = 0.87$ )

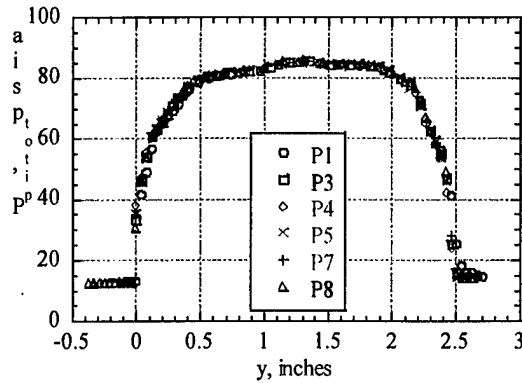


Figure 63 Isolator Exit Pitot Pressure Distribution at  $M_0 = 5$ ,  $Q_0 = 2000$  psf ( $p_e/p_i = 0.87$ )

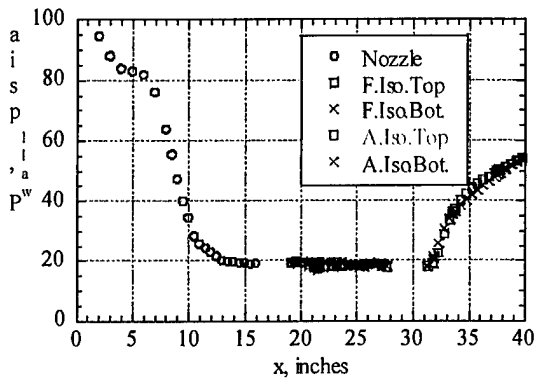


Figure 64 Nozzle-Isolator Pressure Distributions at  $M_0 = 5$ ,  $Q_0 = 2000$  psf ( $p_e/p_i = 2.80$ )

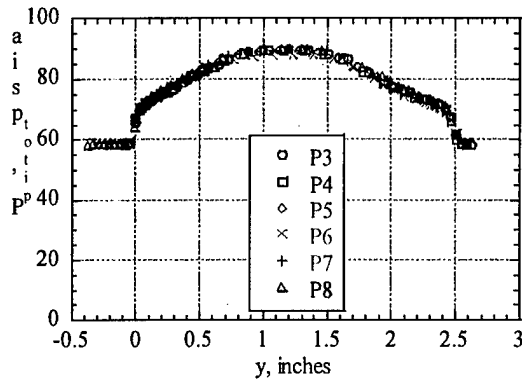


Figure 65 Isolator Exit Pitot Pressure Distribution at  $M_0 = 5$ ,  $Q_0 = 2000$  psf ( $p_e/p_i = 2.80$ )

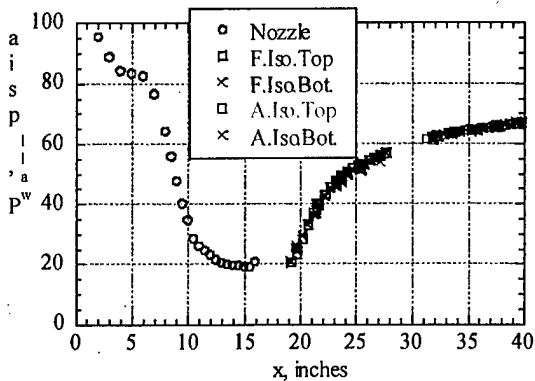


Figure 66 Nozzle-Isolator Pressure Distributions at  $M_0 = 5$ ,  $Q_0 = 2000$  psf ( $p_e/p_i = 3.22$ )

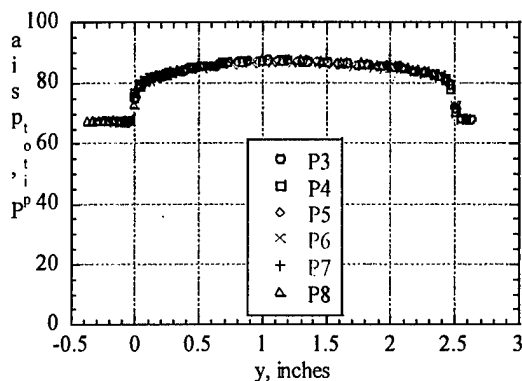


Figure 67 Isolator Exit Pitot Pressure Distribution at  $M_0 = 5$ ,  $Q_0 = 2000$  psf ( $p_e/p_i = 3.22$ )

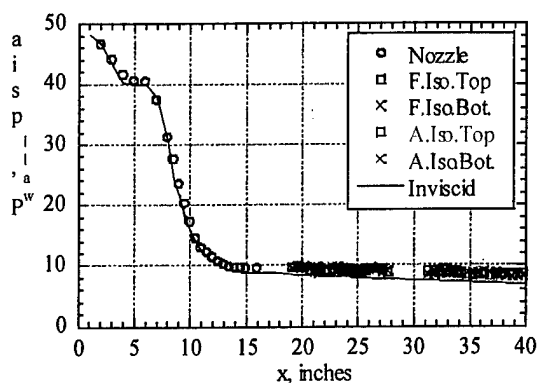


Figure 68 Nozzle-Isolator Pressure Distributions at  $M_0 = 6$ ,  $Q_0 = 1000$  psf ( $p_e/p_i = 0.88$ )

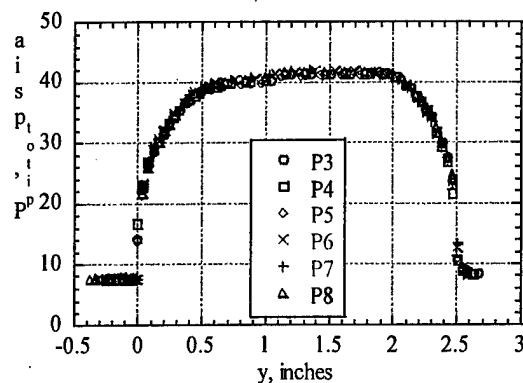


Figure 69 Isolator Exit Pitot Pressure Distribution at  $M_0 = 6$ ,  $Q_0 = 1000$  psf ( $p_e/p_i = 0.88$ )

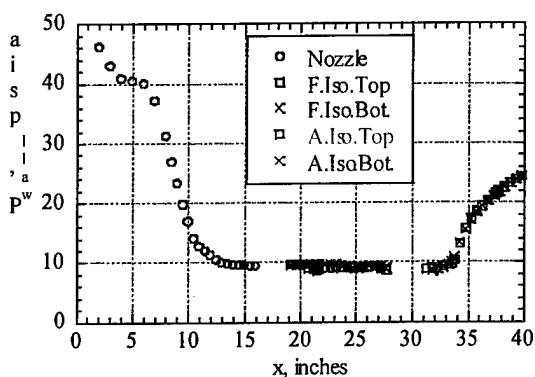


Figure 70 Nozzle-Isolator Pressure Distributions at  $M_0 = 6$ ,  $Q_0 = 1000$  psf ( $p_e/p_i = 2.55$ )

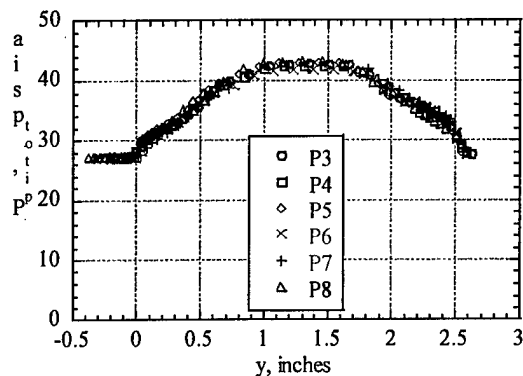


Figure 71 Isolator Exit Pitot Pressure Distribution at  $M_0 = 6$ ,  $Q_0 = 1000$  psf ( $p_e/p_i = 2.55$ )

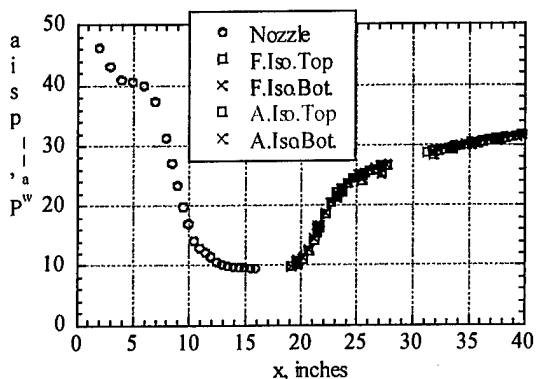


Figure 72 Nozzle-Isolator Pressure Distributions at  $M_0 = 6$ ,  $Q_0 = 1000$  psf ( $p_e/p_i = 3.24$ )

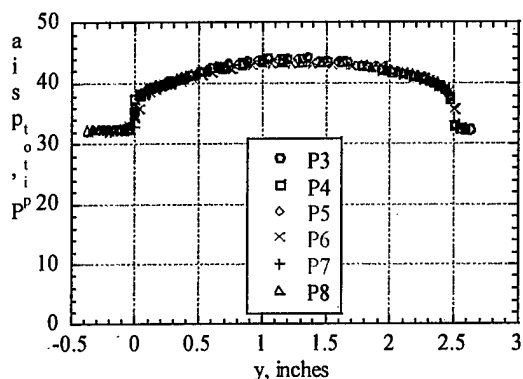


Figure 73 Isolator Exit Pitot Pressure Distribution at  $M_0 = 6$ ,  $Q_0 = 1000$  psf ( $p_e/p_i = 3.24$ )

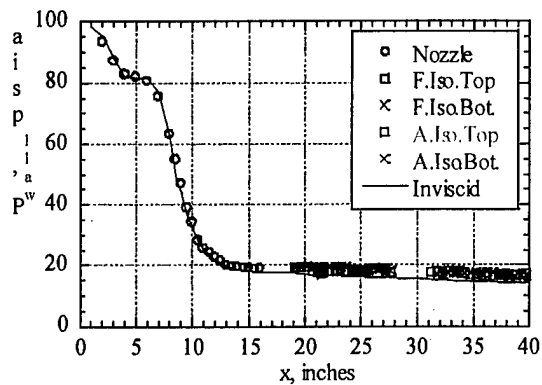


Figure 74 Nozzle-Isolator Pressure Distributions at  $M_0 = 6$ ,  $Q_0 = 2000$  psf ( $p_e/p_i = 0.87$ )

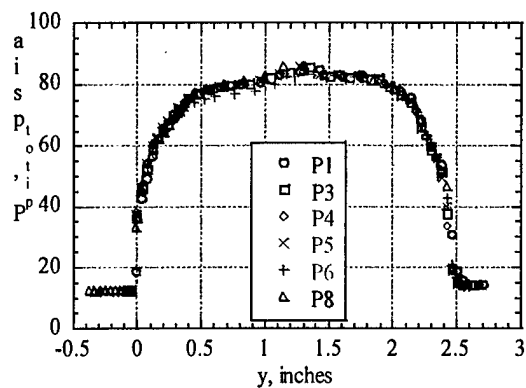


Figure 75 Isolator Exit Pitot Pressure Distribution at  $M_0 = 6$ ,  $Q_0 = 2000$  psf ( $p_e/p_i = 0.87$ )

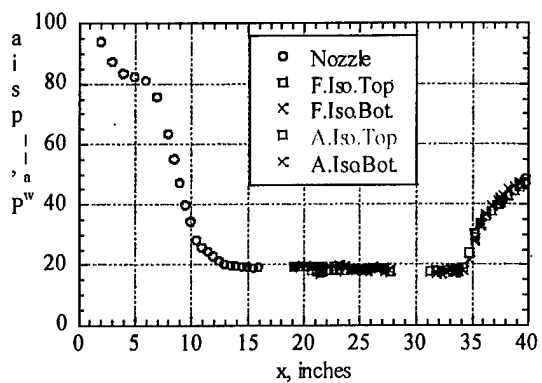


Figure 76 Nozzle-Isolator Pressure Distributions at  $M_0 = 6$ ,  $Q_0 = 2000$  psf ( $p_e/p_i = 2.48$ )

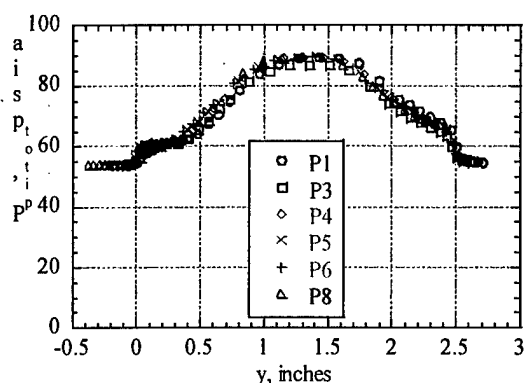


Figure 77 Isolator Exit Pitot Pressure Distribution at  $M_0 = 6$ ,  $Q_0 = 2000$  psf ( $p_e/p_i = 2.48$ )

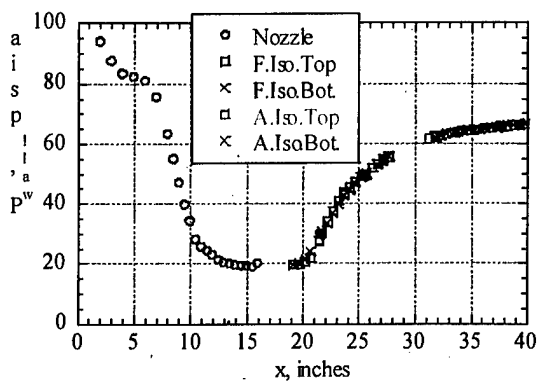


Figure 78 Nozzle-Isolator Pressure Distributions at  $M_0 = 6$ ,  $Q_0 = 2000$  psf ( $p_e/p_i = 3.40$ )

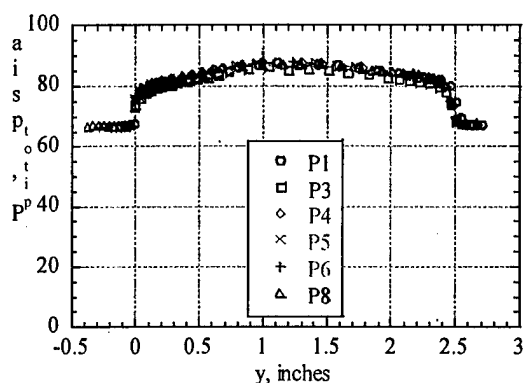


Figure 79 Isolator Exit Pitot Pressure Distribution at  $M_0 = 6$ ,  $Q_0 = 2000$  psf ( $p_e/p_i = 3.40$ )



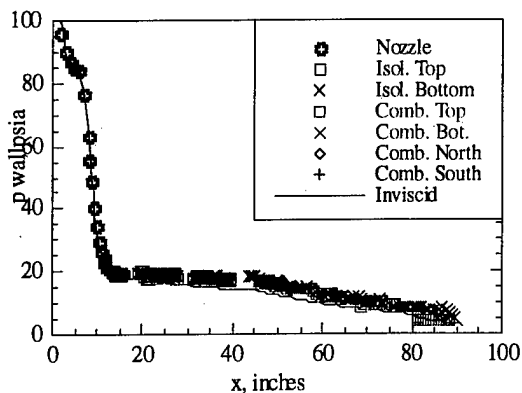


Figure 80 Baseline Combustor - Pressure Distribution at  $p_o = 112$  psia,  $T_o = 540^\circ\text{R}$

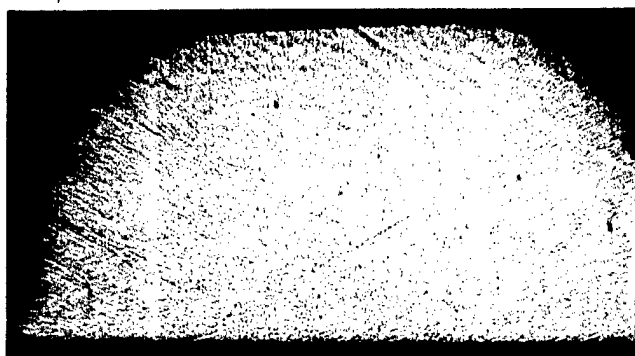


Figure 81 Baseline Combustor - Shadowgraph at  $p_o = 112$  psia,  $T_o = 540^\circ\text{R}$

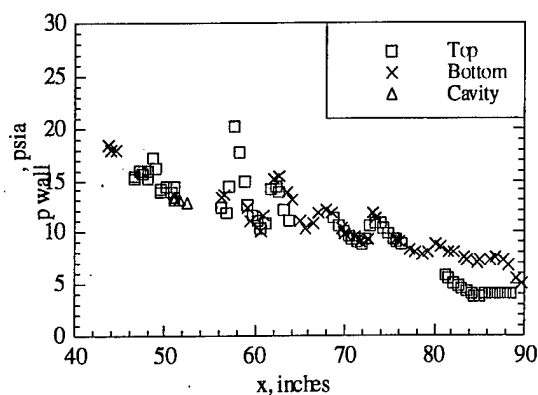


Figure 82 Combustor with Cavity - Pressure Distribution at  $p_o = 112$  psia,  $T_o = 540^\circ\text{R}$

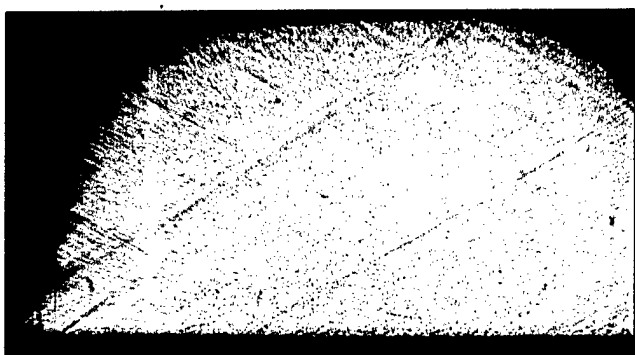


Figure 83 Combustor with Cavity - Shadowgraph at  $p_o = 112$  psia,  $T_o = 540^\circ\text{R}$

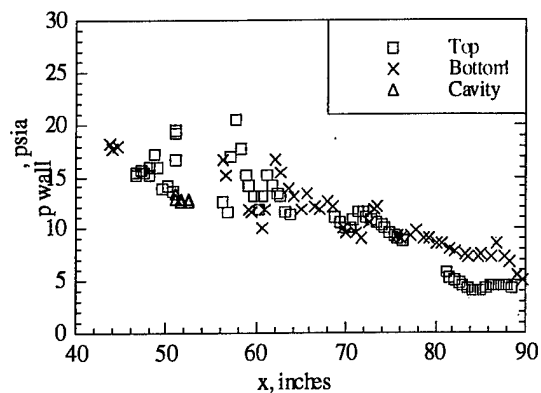


Figure 84 Combustor with Cavity ( $\text{N}_2$  Injection,  $p_{\text{jet}} = 87$  psia) - Pressure Distribution at  $p_o = 112$  psia,  $T_o = 540^\circ\text{R}$

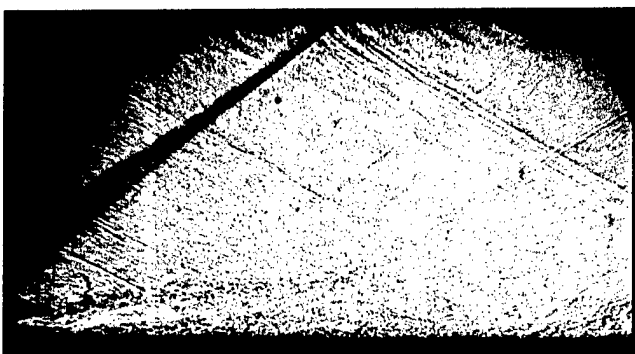


Figure 85 Combustor with Cavity ( $\text{N}_2$  Injection,  $p_{\text{jet}} = 87$  psia) - Shadowgraph at  $p_o = 112$  psia,  $T_o = 540^\circ\text{R}$